2015

CFD MODELING OF MULTIPHASE COUNTER-CURRENT FLOW IN PACKED BED REACTOR FOR CARBON CAPTURE

Li Yang
University of Kentucky, lya226@g.uky.edu

STUDENT AGREEMENT:

I represent that my thesis or dissertation and abstract are my original work. Proper attribution has been given to all outside sources. I understand that I am solely responsible for obtaining any needed copyright permissions. I have obtained needed written permission statement(s) from the owner(s) of each third-party copyrighted matter to be included in my work, allowing electronic distribution (if such use is not permitted by the fair use doctrine) which will be submitted to UKnowledge as Additional File.

I hereby grant to The University of Kentucky and its agents the irrevocable, non-exclusive, and royalty-free license to archive and make accessible my work in whole or in part in all forms of media, now or hereafter known. I agree that the document mentioned above may be made available immediately for worldwide access unless an embargo applies.

I retain all other ownership rights to the copyright of my work. I also retain the right to use in future works (such as articles or books) all or part of my work. I understand that I am free to register the copyright to my work.

REVIEW, APPROVAL AND ACCEPTANCE

The document mentioned above has been reviewed and accepted by the student's advisor, on behalf of the advisory committee, and by the Director of Graduate Studies (DGS), on behalf of the program; we verify that this is the final, approved version of the student's thesis including all changes required by the advisory committee. The undersigned agree to abide by the statements above.

Li Yang, Student

Dr. Kozo Saito, Major Professor

Dr. Haluk E. Karaca, Director of Graduate Studies

CFD MODELING OF MULTIPHASE COUNTER-CURRENT FLOW IN PACKED BED REACTOR FOR CARBON CAPTURE

DISSERTATION

A dissertation submitted in partial fulfillment of the
requirements for the degree of Doctor of Philosophy in
the College of Engineering
at the University of Kentucky

By
Li Yang
Lexington, Kentucky
Director: Dr. Kozo Saito, Professor of Mechanical Engineering
Lexington, Kentucky
2015

ABSTRACT OF DISSERTATION

CFD MODELING OF MULTIPHASE COUNTER-CURRENT FLOW IN PACKED BED REACTOR FOR CARBON CAPTURE

Packed bed reactors with counter-current, gas-liquid flows have been considered to be applicable in CO_2 capture systems for post-combustion processing from fossil-fueled power production units. However, the hydrodynamics within the packing used in these reactors under counter-current flow has not been assessed to provide insight into design and operational parameters that may impact reactor and reaction efficiencies. Hence, experimental testing of a laboratory-scale spherical ball, packed bed with two-phase flow was accomplished and then a meso-scale 3D CFD model was developed to numerically simulate the conditions and outcomes of the experimental tests. Also, the hydrodynamics of two-phase flow in a packed bed with structured packing were simulated using a meso-scale, 3D CFD model and then validated using empirical models.

The CFD model successfully characterized the hydrodynamics inside the packing, with a focus on parameters such as the wetted surface areas, gas-liquid interactions, liquid distributions, pressure drops, liquid holdups, film thicknesses and flow regimes. The simulation results clearly demonstrated the development of and changes in liquid distributions, wetted areas and film thicknesses under various gas and liquid flow rates. Gas and liquid interactions were observed to occur at the interface of the gas and liquid through liquid entrainment and droplet formation, and it became more dominant as the Reynolds numbers increased. Liquid film thicknesses in the structured packing were much thinner than in the spherical ball packing, and increased with increasing liquid flow rates. Gas flow rates had no significant effect on film thicknesses. Film flow and trickle flow regimes were found in both the spherical ball and structured packing.

A macro-scale, porous model was also developed which was less computationally intensive than the meso-scale, 3D CFD model. The macro-scale model was used to study the spherical ball packing and to modify its closure equations. It was found that the Ergun equation, typically used in the porous model, was not suitable for multi-phase flow. Hence,

it was modified by replacing porosity with the actual pore volume within the liquid phase; this modification successfully accounted for liquid holdup which was predicted via a proposed equation.

KEYWORDS: Packed bed reactor, CFD modeling and scaling, gas-liquid counter current flow, hydrodynamics, modified Ergun equation

Li Yang

Student's Signature

August 05, 2015

Date

CFD MODELING OF MULTIPHASE COUNTER-CURRENT FLOW IN PACKED BED REACTOR FOR CARBON CAPTURE

By

Li Yang

Prof. Kozo Saito
Director of Dissertation

Prof. Haluk E. Karaca
Director of Graduate Studies

August 05, 2015

Acknowledgments

It has been a long journey to complete this dissertation, and fortunately a great many people have provided help. I wish to express my gratitude to all of them. I have greatly benefited from their kind help and support, and they have made my graduate study experience one that I will cherish forever.

First, I would like to thank my advisor Dr. Kozo Saito for enabling me to study and perform my PhD dissertation at the University of Kentucky. His patience, insightful instructions, encouragement and continued support helped me overcome many difficulties and provided guidance for completing this dissertation.

Second, I am grateful to Dr. Kunlei Liu for his instruction and financial support. He is a great person from whom I learned how to do quality research and the importance of having attitudes of seriousness and dedication that are necessary for accomplishing goals in research and life.

Third, I am thankful to Dr. John M. Stencel, who gave numerous comments and great technical sport for writing my dissertation.

Fourth, I would like to thank my committee members, Dr. Yang-Tse Cheng, Dr. Tim Wu, Dr. Keith Rouch and Dr. Rick Honaker for reviewing my dissertation, for their alternative ideas and explanations which have undoubtedly augmented this work, and for their timely flexibility.

Fifth, I am also grateful to people who have helped to make this dissertation better. Special thanks to Dr. Tianxiang Li, Dr. Zhengchang Song, Dr. Nelson K. Akafuah, Dr. Ahmad

Salaimeh, Dr. Liangyong Chen, Dr. Zhen Fan, Dr. Guojie Qi, Dr. Dazhi E, Dr. Harisawa and Dr. Fuchihata who gave insightful comments and constructive criticism on how to improve the dissertation.

Finally, and most importantly, I would like to thank my husband Fang Liu for his love, understanding and dedication to our family, and to my daughters Alice and Lucy. I am also indebted to my parents for their encouragement and support.

Table of Content

List of Tables

List of Figures

CHAPTER1. INTRODUCTION

1.1. Research Motivation

Scientific consensus exists on the primary driving mechanisms for global increases in atmospheric carbon dioxide (CO_2) concentrations – they are anthropogenic emissions from the use of fossil fuels and changes in land use. The use of coal alone accounted for 43% of the total global CO_2 emissions in 2010 (Yu 2013) and is a part of the reason that atmospheric CO_2 concentrations climbed to 403.7 ppm in May, 2015 (Pieter, NOAA/ESRL), a value 40 % above pre-industrial levels. Other greenhouse gases (GHG), including, methane (CH_4), water vapor (H_2O) and ozone (O_3) are also recognized as the main atmospheric constituents that affect global warming trends (Watson, Rodhe et al. 1990). Hence, if the deleterious effects of rising GHG concentrations are to be averted or avoided, an imperative need exists to reduce the extent to which they are emitted into the atmosphere (Liu 2013).

Currently, technologies are under development for capturing and sequestering CO_2, with a primary focus on power generation. Technologies for CO_2 capture include pre-combustion, post-combustion, oxy-fuel combustion and chemical looping combustion scenarios. Post-combustion capture is removing CO_2 from the flue gas, a stage when fuel is already combusted, solvent based CO_2 absorption is one of the most popular approaches (Chen, Yates et al. 2012, Mathias, Reddy et al. 2013). Pre-combustion capture is the removal of CO_2 from syngas prior to its combustion, usually in application with Integrated Gasification Combined Cycle (IGCC) (Spliethoff 2010, Padurean, Cormos et al. 2012). Oxy-fuel combustion uses pure oxygen to combust fuels instead of

air, so nitrogen is not involved in the combustion process, thus CO_2 in the flue gas is in high concentration (Figueroa, Fout et al. 2008, Jones, Bhattacharyya et al. 2011). Chemical looping combustion belongs to the category of oxy-fuel combustion, it uses oxygen carriers to provides oxygen instead of a costly air separation unit (ASU), thus the energy penalty is low (Liu, Li et al. 2012, Liu 2013, Liu, Zhang et al. 2013, Zhang, Liu et al. 2013, Chen, Liu et al. 2014, Liu, Chen et al. 2014, Chen, Zhang et al. 2015, Fan, Chen et al. 2015, Liu, Kozo et al. 2015). Of these carbon capture technologies, post combustion CO_2 capture is the most technologically mature, and may be implemented at the large-scale needed for application to power production in the near future.

1.1.1 Amine-based Post Combustion CO_2 Capture

A process diagram of a post-combustion CO_2 capture using a packed bed reactor is presented in Figure 1.1 (Feron 2010, Chung, Patiño-Echeverri et al. 2011); it includes two reactors, one of which is called an absorber and the other is a stripper. An aqueous solution that is usually amine based is circulated between the two reactors in which one absorbs CO_2 (absorber) and the other releases CO_2 (stripper) to produce a flow of highly concentrated CO_2. In the absorber, the CO_2 and solvent are in counter-current flow where CO_2 is absorbed by the amine based solvent, thereby producing a gas outlet product that is CO_2-depleted; simultaneously, the CO_2 enriched amine exits the column from the bottom of the absorber and flows into the top of the stripper. In the stripper, the CO_2 enriched amine solution is heated up to a temperature exceeding 100 °C to release CO_2 and generate a high purity CO_2 stream that is ready for sequestration. The regenerated amine (without CO_2) is pumped back to the top of the absorber for a next

cycle. Because the amine from the stripper is at a relatively high temperature, a heat exchanger (HEX) is typically applied for improving overall process efficiency.

The absorber is a packed bed reactor which is filled with packing materials. The main objective of using a packed bed is to improve the effective contact between the gas and liquid phase reactants (Ranade, Chaudhari et al.).

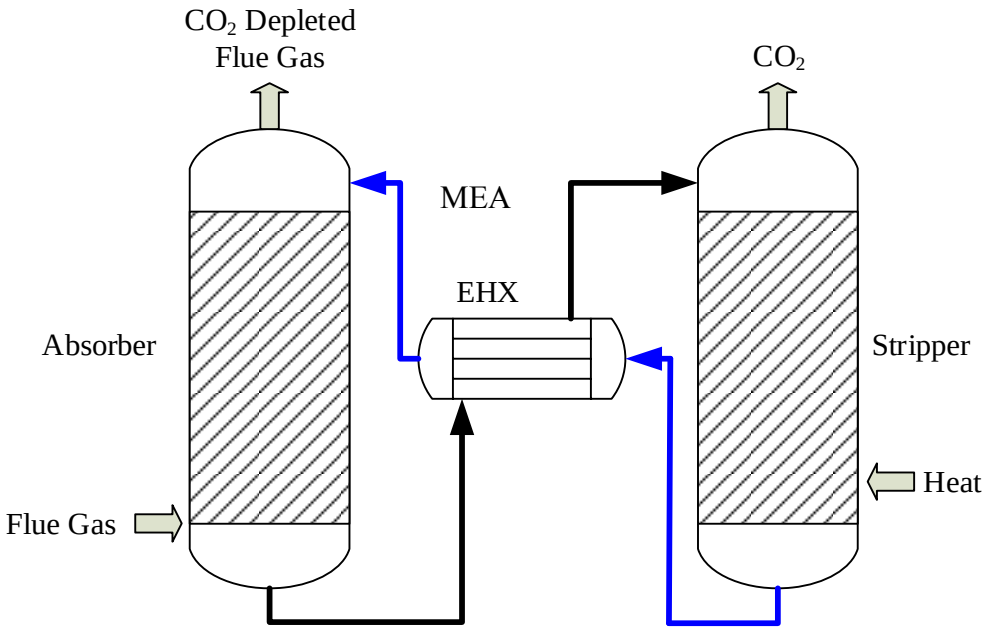

Figure 1.1 Post combustion solvent based CO_2 capture process (Ranade, Chaudhari et al.).

1.1.2. Packed Bed Reactors

The packed bed reactor, also called a trickle bed reactor, was originally designed for wastewater treatment but has become very useful in diverse industries in which two-phase flow and chemical reactions are prevalent. In general, a packed bed is a hollow tube, pipe or other vessel that is filled with packing materials (Henley, Seader et al. 2011). The packing materials can be small objects like spherical balls, rings or specifically designed, structured packing materials; arranged in random or structured

orientations; a random packing consists of randomly distributed packing material within the bed while structured packing consists of uniformly arranged material in the bed. Figure 1.2 shows some examples for random packing and structured packing.

(a) Random packing materials (http://www.amacs.com/packing/random/).

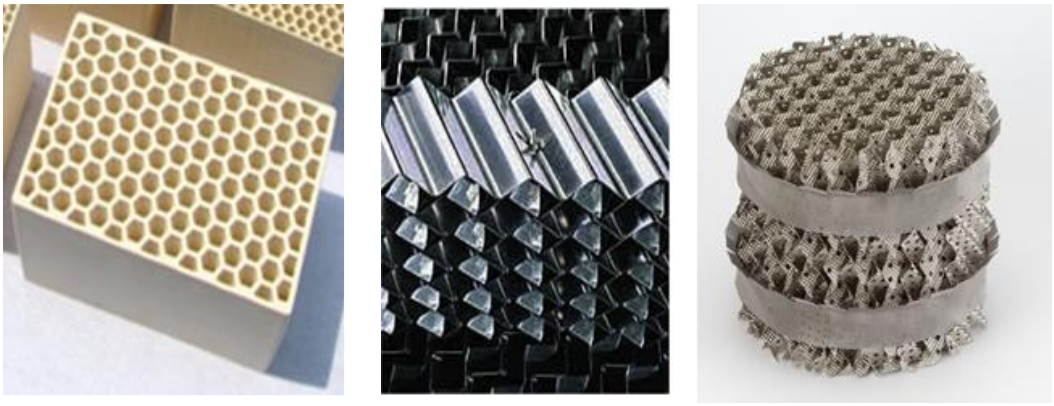

(b) Structured packing materials (Ranade, Chaudhari et al. 2011)

Figure 1.2 Packed beds with (a) random and (b) structured packing materials.

Packing materials improve the contact area at which chemical or physical reactions take place and, thereby, can increase markedly the efficiency by using a packed bed reactor. As an example, for gas-liquid multi-phase flow in a packed bed the liquids will spread onto the packing materials and tend to wet its surface to form a liquid film layer; then

when a gas flows across the packing material, the gas-liquid contact area within the reactor will therefore be enhanced. This contact area is where mass transfer occurs (Mahr and Mewes 2007), and increasing contact area is one important pathway recognized to enhance mass transfer and chemical reactions. Therefore, the use of packing bed promotes reactor and reaction advantages such as high capacity, high efficiency and, if designed appropriately, low pressure drop.

Different-shaped packing materials provide possibilities to vary contact areas and void space between the packing. Both of these factors affect performance but typical selection of a packing material depends, to a large extent, on the application and the cost. In general, random packing is a lower cost approach as compared to structured packing, and this advantage leads random packed beds to be used most frequently during the next decades (Calis, Nijenhuis et al. 2001). However, structured packing can provide higher separation efficiency, higher capacity and better radial mixing than random packing. Due to these advantages, it has been estimated that 25% of all refinery vacuum towers are now equipped with structured packing (Mahr and Mewes 2007). Because both random and structured packing are used throughout industry but their assessment and application within CO_2 capture technological applications are only beginning, it is important to study the hydrodynamics like liquid distribution, hold-up and wetted area caused by the packing materials to enable more accurate and efficient reactor designs that will be needed to minimize investment and operation costs of the huge systems envisioned for the power industry (Kapteijn, Heiszwolf et al. 1999). For example, for a CO_2 absorber capable of handling emissions from only a 0.7MW power system, a height of approximately 19.5 m would be required with an inside packing material covering a

length at least 13.7 m. However, a commercial CO_2 capture capacity would be typically near and greater than 300 MW, a scale-up of greater than 300-to-1! Hence, improving CO_2 capture rates is a decisive way to limit the size of commercial reactors, and achieving this goal can be assisted by understanding the hydrodynamics inside a packed bed where gas-liquid interfaces control the important reactions.

Although the most mature technology for CO_2 capture is in a post combustion operational mode, all CO_2 capture technological options are still in their infancy because no full-scale commercial system on an actual fossil fuel power plant has ever been built. A schematic of a packed bed reactor with spherical ball packing materials is shown in Figure 1.3. The reactants, i.e. amine solution and CO_2-laden gas flow counter-currently the packing.

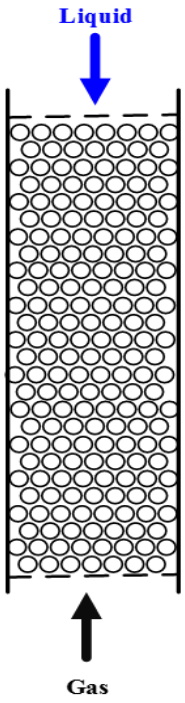

Figure 1.3 A schematic of a fixed bed reactor.

Since packed bed reactors are widely used for gas-liquid flow reactions, and the packing is one of the key factors affecting overall reaction rates. Therefore, understanding the hydrodynamics within packed beds is essential. Although extensive investigations have been performed on packed bed reactors over the years, the current understanding of flows within them is insufficient to enable optimization within the large scales needed for applications within power production (Kuzeljevic 2010, Kaskes, Vervloet et al. 2014). Furthermore, experimental studies of packed bed reactors and reactions are very time consuming and expensive, not only because of extensive scale-up needs for transitioning from a laboratory to a commercial system (Saito, Ito et al. 2014) but also because of the high number of options that are possible for the interior components, or packing, of the reactors. Also, experimentally it is very difficult to measure the very complex geometry of most packed bed materials and, especially when limited space exists between the packing, it is impractical to insert measuring devices which by themselves may disturb or alter liquid and gas flow patterns.

Hence, this dissertation focuses on packed bed reactors and packing for application to studying multiphase flow and hydrodynamics during post combustion CO_2 capture. Instead of an experimental approach, computational fluid dynamics (CFD) was the primary tool used during the research (Zhang, Weng et al. 2014, Yang, Akafuah et al. 2015)(Zhang 2015); when possible, the results of the CFD studies are compared to laboratory-scale experimentation. Scale modeling technique (Saito and Finney 2014, Saito and Williams 2015) offers basic concepts and methods to use scale model experiments to validate numerical modeling predictions. Figure 1.4, adopted from (Saito and Williams 2015) shows the concept of scale and numerical modeling methods. After

this validation is made, numerical modeling approach leverages the ever-increasing computational power of computers with sophisticated CFD software. Because the geometry of any one packing material can be very complex and the resulting flow patterns also demanding to simulate, a need existed to focus on a limited number of predetermined packing configurations that are described and discussed in the following chapters.

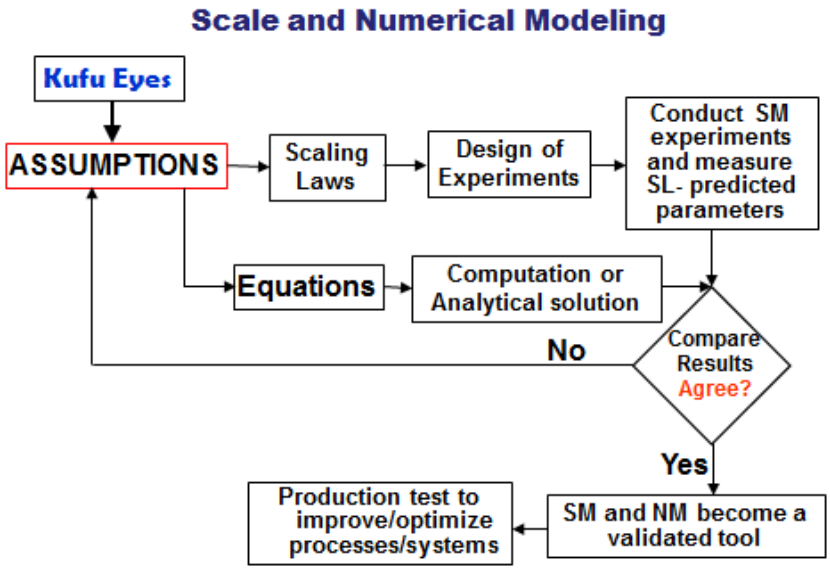

Figure 1.4 Basic concept of scale modeling and numerical simulation (Saito and Williams 2015).

Historically, the sizes reactors and the number of packing elements under assessment have been limited by computational constraints. It has been a challenge to simulate the whole domain of a reactor with its packing material but symmetry, selected arrangements of the packing structures and judicious meshing choices make CFD assessments more productive than pure experimentation. To date, some computational research has been performed based on a meso-scale model approach, however, these simulations have been

based on single phase, or gas-liquid phase in co-current flow (Attou and Ferschneider 1999, Propp, Colella et al. 2000, Souadnia and Latifi 2001, Van Baten, Ellenberger et al. 2001, van Baten and Krishna 2001, Gunjal, Ranade et al. 2003, Freund, Bauer et al. 2005, Atta, Roy et al. 2007, Bai, Theuerkauf et al. 2009, Gao, Zhang et al. 2011, Dixon 2012, Sachdev, Pareek et al. 2012, Heidari and Hashemabadi 2013, Owens, Perkins et al. 2013, Haroun, Raynal et al. 2014, Kaskes, Vervloet et al. 2014, Lu, Xu et al. 2014). What is missing is an accurate assessment on multiphase and counter-current flow system, a current trend in the packed bed reactors applied for post combustion CO_2 capture. This dissertation, therefore, focuses on this CO_2 capturing system.

1.2 Objectives

The overall goal of this dissertation is to develop: (1) a comprehensive three dimensional (3D) counter-current, multiphase meso-scale model, and (2) a macro-scale model for CO_2 absorber simulation. The meso-scale model, which does not require as much detailed information compared to the micro-scale model, still can provide sufficiently detailed results to bridge between the micro-scale and the macro-scale (actual industrial level). Therefore, the meso-scale model was chosen in this study to understand the fundamental aspects of liquid film formation, and predict flow distributions, pressure drops, liquid holdups, wetted areas and the interactions between gas and liquid phases. The meso-scale model also will be used to point out ways for enhancing the contact between gas and liquid phases. Using scale modeling theory (Saito and Finney 2014), the meso-scale model can be used to optimize the performance of macro-scale model.

Specific objectives to achieve the aforementioned goal are to:

(1) develop a comprehensive 3D CFD model for simulating liquid-gas counter-current multiphase flow while using both spherical ball and structured packing, and then to verify the model with experimental data;

(2) obtain insight into film formation, flow distributions, pressure drops, liquid holdups, wetted areas and the interactions between phases in both spherical ball and structured packing;

(3) assess the effects of operating conditions on film formation, flow distributions, pressure drops, liquid holdups, wetted areas and the interactions between phases and then to develop a working relationship between these parameters and the operating conditions;

(4) develop a fundamental understanding of controlling factors influencing gas-liquid interactions; and

(5) modify and optimize a macro-scale packed bed model for simulating the hydrodynamics in a CO_2 capture process using amine-based liquids.

However, this thesis does not offer detailed analysis and discussions on rigorous scaling relationships and scaling laws that can relate all three scales: mico-scale, meso-scale and macro-scale. This scaling study is important and interesting, but simply beyond the scope of this thesis and therefore leaves it as future study.

1.3 Overview of the Dissertation

The following is a summary of the remainder of this dissertation. Chapter 2 provides a comprehensive literature review on previous research in this field. The status of research for liquid flow regimes, distributions, holdups, and pressure drops are discussed; a status of understanding wetted surface areas of packing materials is given and a closure model

in different packed beds is presented that assess current experimental and CFD methods and results. Also identified are gaps in data and knowledge, and shortcomings are analyzed which may be overcome by the research carried out through this dissertation.

Chapter 3 introduces the hydrodynamic assessment on a meso-scale while using a spherical ball packed bed reactor. The outcome of the CFD model will be compared to data like pressure drops from experimentation that was accomplished while using various mass flow conditions. This hydrodynamic assessment also examines relationships between the flow regime, flow distributions, pressure drops, liquid holdups and wetted areas and the operating conditions.

Chapter 4 introduces the hydrodynamic study on a meso-scale model on a structured packed bed reactor. The numerical model is validated by comparing simulated and empirical pressure drop model from scientific literature. Also analyzed the relationships between flow regimes, flow distributions, pressure drops, liquid holdups and wetted areas and the operating conditions.

Chapter 5 presents the hydrodynamic study using a macro-scale model and a closure model from literature data. A new closure model was modified.

Chapter 6 Conclusion and future work.

CHAPTER 2. LITERATURE REVIEW

2.1 Introduction

Multiphase flow occurs when more than one phase (gas, liquid, solid) is present in a flow field. For the gas-liquid flow systems considered in this dissertation it is convenient to treat one phase as primary and the other as the secondary phase (ANSYS fluent help) in which the primary phase is characterized by continuous flow. The secondary phase can be distributed throughout the primary phase; each phase presented may be in either laminar or turbulent flow, which then leads to a variety of potential flow regimes. For gas-liquid systems, four types of flow regimes exist, including filming flow, trickle, sprayed and bubbling flow. These regimes are depicted in Figure 2.1, and a detailed explanation of them is presented in section 2.2

2.2 Hydrodynamic Characterizations

For a packed bed reactor, the packing is considered to be stationary and contributes to complex interactions between and flows of the gas and liquid phases (Gualito, Cerino et al. 1997). These interactions are manifested under different flow regimes and cause distinct gas and liquid distributions in a packed bed. Hence, for packed bed reactors, it is imperative to understand hydrodynamic characterizations like flow regimes, pressure drops, liquid holdups, wetted areas, liquid distributions and the packing arrangement if optimized reactor and reaction performance are to be realized (Gunjal, Kashid et al. 2005).

2.2.1 Flow Regime Studies

When gas and liquid flows are co-current or counter-current through a packed bed, several flow regimes are established depending on the operating and design parameters, as shown in Figure 2.1. With small gas and liquid flow rates, the liquid flows as a film moving over the solid surface; this regime is called film flow and the liquid is considered the continuous phase [see Figure 2.1 (a)]. In this regime, the solid surface is partially or fully wetted, depending on the liquid flow rates. If the gas flow rate is slowly increased with a fixed liquid flow rate under film flow conditions, then part of the liquid will begin to flow in the form of suspended droplets, like in Figure 2.1 (b).This transition is due to the increasing interactions of the gas with the liquid film, and is called the trickle regime. With further increases in both gas and liquid flow rates, all of the liquid will flow in the form of suspended droplets; this regime is called the spray regime, and is depicted in Figure 2.1 (c). If the gas flow rate is very small and the liquid flow rate is quickly increased, the gas will become a dispersed phase and the gas will flow in the form of bubbles, a regime known as the bubble regime and depicted in Figure 2.1 (d). Finally, at high liquid and gas flow rates, a flow transition occurs to what is called the pulse flow regime. In post combustion CO_2 capture technology using packed bed reactors, the best operational regime has been determined to be the pulse flow regime (Gunjal, Kashid et al. 2005).

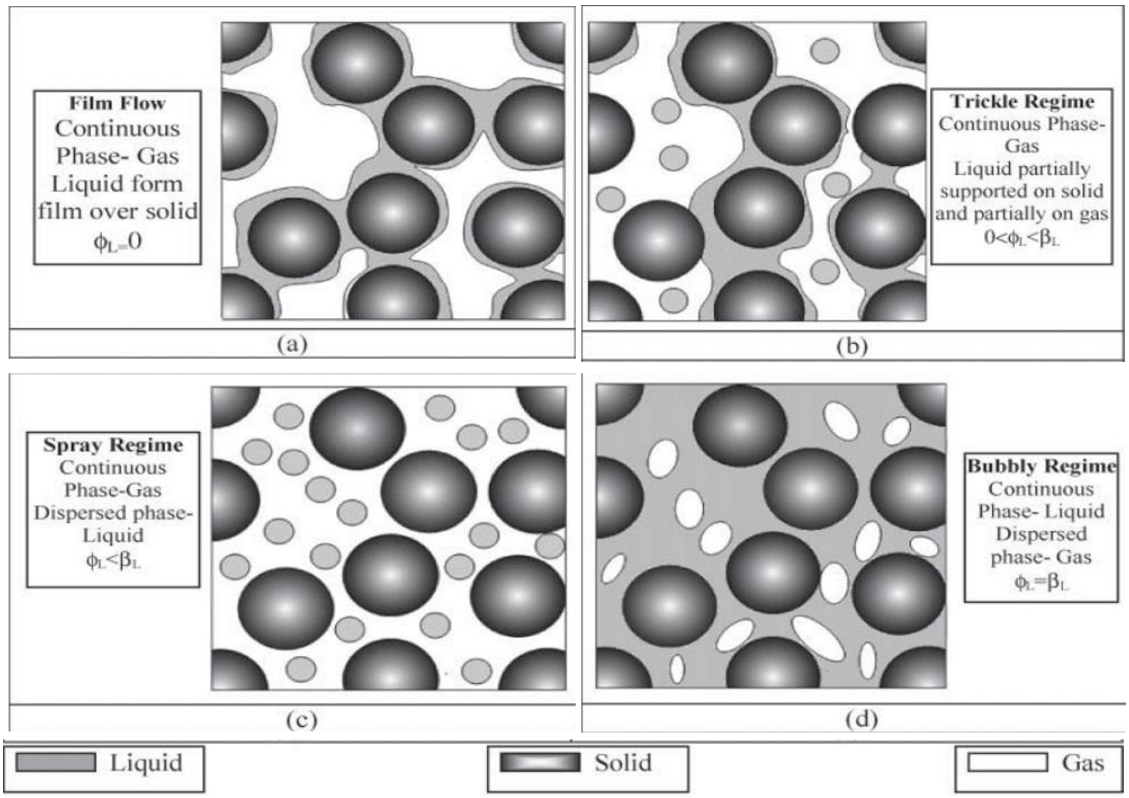

Figure 2.1 Physical picture of the flow in spherical packed bed reactors (Gunjal, Kashid et al. 2005).

It is relatively simple to experimentally identify trickle flow or bubbly flow, but not pulse flow (Latifi, Rode et al. 1992), because microelectrodes have to be embedded within a non-conducting wall of a reactor and they have to continuously irrigated if their signals provide assessments of flow regime transitions, particularly in the transition to pulse flow. The type of signal analysis is also of interest; for example, research on the use of nonlinear time series data analyses to determine flow regime transitions has been extensive (Drahoš, Zahradnik et al. 1991, Horowitz, Cukierman et al. 1997, Letzel, Schouten et al. 1997, Lin, Juang et al. 2001), with the conclusion that this method is not able to capture regime transitions accurately. In other flow transition measurement approaches, Krieg et al.(Krieg, Helwick et al. 1995, Urseanu, Boelhouwer et al. 2004)

used pressure fluctuations to characterize flow regimes but transitions between regimes were difficult to establish because no sharp boundaries between the regimes could be identified. Hence, no effective experimental method has yet been developed for the flow regime determinations. As a consequence, the mapping of flow regime transitions remains to a large extent mostly empirical (Kuzeljevic 2010).

Although it is very difficult to identify flow regime transitions in the packed bed reactor using experimental methods, several CFD method approaches have been identified. For example, Gualito, et al. (Gualito, Cerino et al. 1997, Gunjal, Kashid et al. 2005) used CFD modelling of wall pressure fluctuation measurements to identify prevailing flow regimes in trickle beds. Battista, et al. (Battista, Muzen et al. 2003) and Tong (Tong, Marek et al. 2013) described co-current, two-phase flow patterns within corrugated structures in detail by using a meso-scale model. However, no detailed examinations and delineations in 3D have been found within scientific literature that cover gas–liquid, counter-current flow regimes in a packed bed reactor.

2.2.3 Liquid Distribution Studies

Liquid flow distribution and the extent of mixing are also keys for designing and improving the performance of a packed bed reactor. Liquid distribution is influenced by phase properties, flow rates, operating pressures, packing sizes, shapes and the orientation of the packing in the bed.

Both experiments and CFD simulations have been performed to assess liquid distributions, but some of these have been based on single phase flow. For example, Sebastia-Saez, et al. (Sebastia-Saez, Gu et al. 2013) studied liquid flow distributions at

different Weber numbers, while Jiang, et al. (Jiang, Khadilkar et al. 2002) used a two dimensional (2D) discrete cell approach to study liquid distributions. Some simulation studies have studied co-current, two phase gas-liquid flows (Sundaresan 1994, Saroha, Nigam et al. 1998, Gunjal, Ranade et al. 2003, Lopes and Quinta-Ferreira 2007, Jafari, Zamankhan et al. 2008, Niegodajew, Asendrych et al. 2014). Gunjal, et al. (Gunjal, Ranade et al. 2003) found that the liquid distribution became more uniform when liquid was introduced through a port located within the central part of a reactor as compared to when it was introduced through an inlet on the wall of the reactor. Sundaresan (Sundaresan 1994), using 2D geometry, found that the liquid distribution in trickle bed reactors was in the form of rivulet and film flow and revealed that an injector at the top of a reactor could produce more uniform liquid distributions.

Experimental studies of liquid distributions have also been performed. Saroha, et al. (Saroha, Nigam et al. 1998), in experimental measurements on liquid distribution in a trickle-bed reactor, found that the radial liquid distribution during two-phase flow was affected by the liquid flux values. Gamma and X-ray tomography, magnetic resonance imaging, radioactive particle tracking, electrical capacitance tomography and positron emission tomography have also been used to investigate multiphase flows (Moslemian, Devanathan et al. 1992, Gladden and Alexander 1996, Boyer, Duquenne et al. 2002, Götz, Zick et al. 2002, Barigou 2004, Ismail, Gamio et al. 2005, Stapf and Han 2006, Elkins and Alley 2007, Llamas, Pérat et al. 2008). Each of these experimental techniques has limitations in the spatial and temporal resolution that can be accomplished, especially when considering reactor size and its operating condition (Kuzeljevic 2010).

Hence, although research literature on liquid distributions within packed bed reactors has been found, most of it has assessed single phase flow or co-current two-phase flow in 2D. Liquid distributions have clearly not been described for two–phase, counter-current flow in 3D. Liquid distributions in a packed bed are essential to its performance; furthermore, for packed bed, post-combustion CO_2 capture technology, it is imperative these distributions are determined while using counter-current, gas-liquid flows.

2.2.4 Liquid Holdup Studies

Liquid hold-up has a strong influence on pressure drop in a packed bed reactor (Pangarkar, Schildhauer et al. 2008). Higher liquid holdup is usually beneficial by giving more efficient mass transfer and higher reaction rates and, therefore, a bed's structure needs to be manipulated to achieve higher liquid holdup (Satterfield 1975). Levec, et al. (Levec, Saez et al. 1986, Levec, Grosser et al. 1988) observed changes in liquid hold up with changes in liquid flow rates in single phase operation. Chu (Chu and Ng 1989) modeled liquid holdup by considering that the upper branch of a hysteresis loop corresponded to film flow under co-current flow. Rode (Rode, Midoux et al. 1994) performed an experimental study using electrochemical shear rate sensors to measure hydrodynamics of packed beds also operating under co-current gas liquid downward.

Some researchers (Raynal and Royon-Lebeaud 2007, Haroun, Legendre et al. 2010, Said, Nemer et al. 2011) have used CFD numerical simulations to study liquid holdup. Lopes (Lopes and Quinta-Ferreira 2009) studied co-current gas–liquid flows through a catalyst bed comprised of mono-sized, spherical, solid particles arranged in a cylindrical container of a pilot Trickle Bed Reactor (TBR) unit that was 50 mm in internal diameter

1.0 m in length. Others studied counter-current flow based on simple geometry (Wen, Shu et al. 2001, Xu, Paschke et al. 2009, Haroun, Raynal et al. 2014). For example, Wen (Wen, Shu et al. 2001) used the Manning formula CFD model to predict liquid holdup with the width of a liquid rivulet on a packing surface modified by the Shi and Mersmann correlation (Shi and Mersmann 1985) but with a simulation geometry that was a small inclined, flat plate which cannot describe wave instabilities for a complex structured packing. Iliuta (Iliuta, Petre et al. 2004) used a one-dimensional (1D) model to predict the irrigated two-phase, total liquid holdup in a gas-liquid, counter-current flow while using structured packing. However, a 3D is significantly different from a 1D model and it is not accurate to use a 1D model to estimate the results for 3D turbulent flow.

Experimental studies also have been reported for the measurement of liquid hold-up in multiphase counter–current, packed reactors but their design is still a major engineering challenge (Maćkowiak 1991, Wu, Khadilkar et al. 1996, Ellenberger and Krishna 1999, Olujić 1999, Wilson 2004, Sidi-Boumedine and Raynal 2005, Toye, Crine et al. 2005, Pangarkar, Schildhauer et al. 2008, Basden, Eldridge et al. 2013, Guo, Sun et al. 2014). Although liquid hold up phenomena are more well studied than liquid distribution and wetted surface area, most of the experimental and simulation research has examined co-current flow or counter-current flow but with a simple geometry. These results, although useful, provide limited information for understanding complex random and structured packing. Hence, it is necessary to study counter-current flow under realistic random or structured packing to help fully understand liquid hold-up.

2.2.5 Wetted Area Studies

Wetting is the ability of a liquid to adhere to and then maintain contact with a solid surface. A larger wetted area can increase the mass transfer area between the gas and liquid phases. If the solid surface is rough or textured, then mass transfer is also increased by having increased turbulence; however, an increase of liquid viscosity will cause a reduction in the mass transfer area and counter-current gas flow will not heavily influence mass transfer area.

De Brito (De Brito, Von Stockar et al. 1994)showed that the interfacial area could be significantly larger than the geometric surface area which was attributed to instabilities in the liquid flow as represented by ripples or waves. A few studies employed more direct methodology to characterize the mass transfer area (Zhao and Cerro 1992, Luo, Li et al. 2009). Green (Green 2006) used x-ray computed tomography to measure the wetted area of a stainless steel structured packing under an irrigated condition and observed it to be well coated on its top and bottom sheet sides but, unfortunately, significant parts on the inside of the sheets were not well covered. Hence, this type of data were not sufficient to discern the wetted area from just the packing surface.

Tsai et al.(Tsai, Seibert et al. 2011) used a dimensionless model to predict the mass-transfer area of structured packing based on experimental studies. His model was based on estimating an efficiency for mass transfer but is considered inaccurate because of the many uncertain parameters which had to be used. Hoffmann (Hoffmann, Ausner et al. 2005) used both experimental studies and numerical simulations to examine gas-liquid flows on an inclined plate. Relatively good agreement was reached between the surface

velocities and wetted area from both the experimental results and numerical simulations. In general, experimental investigations of wetted area for complex packing arrangements are very difficult to accomplish (Hoffmann, Ausner et al. 2005) whereas CFD methods use a meso-scale model which can measure the wetted area of a packing surface directly. This type of information is critical for understanding CO_2 absorption in a packed bed.

2.2.6. Film Thickness Studies

Film thicknesses, distribution and flow mechanisms in a packed bed are also critical to maximize contact between the gas and liquid phases. Hence, a finite volume method-based on a CFD model was developed and used to simulate annular gas-liquid flow through pipes and bends (Tkaczyk and Morvan 2011). Interactions causing film to droplet transitions, i.e. entrainment, and droplets-to-film transitions, i.e. stick, bounce, spread and splash were recreated successfully. However, a structured packing is substantially different than pipes or bends.

Co-current, two-phase flow has been examined extensively. For example, numerical methods have been used to predict film thicknesses (Panday 2003, Groff, Ormiston et al. 2007, Balusu and Mohanty 2011, Min and Park 2011, Schwidder and Schnitzlein 2012, Abdolkarimi 2013), with the results showing detailed changes of film thickness with various input parameters and the effects of the solid surface on the liquid film characteristics (Shetty and Cerro 1995) (Craster and Matar 2009, Luo, Li et al. 2009). Interestingly, these studies found the behavior of the film width was affected greatly by the smoothness of the surface and the degree to which the surfaces were inclined with respect to the co-current flow field. However, film thickness studies for counter-current,

gas-liquid flows over structured packing have not progressed to a point where they can contribute important insight into the design and operation of a CO_2 absorber system.

2.2.7 Pressure Drop Studies

Pressure drop is important in determining energy consumption and in the sizing of system compression equipment. Pressure drop can be affected by liquid and gas flow rates, and the packing type and shape (Petre, Larachi et al. 2003, Pangarkar, Schildhauer et al. 2008). It is possible to manipulate the bed structure, including particle and packing characteristics, to reduce pressure drop and maintain it at acceptable levels.

In a meso-scale model, the pressure drop can be calculated directly. For example, Said et al. (Said, Nemer et al. 2011) elucidated the relationships between pressure drop, channel height dimensions, channel opening angles and corrugation angle changes using CFD simulations for a structured packing. Experimentally, Olujic (Olujić 1999) predicted the effect of column diameter on pressure drop for a corrugated sheet, structured packing and Chu et al. (Chu and Ng 1989) measured the pressure gradient corresponding to fixed gas flow rates.

2.3 CFD Modeling Approaches

CFD is an advanced tool based on the Navier–Stokes equations for analyzing complex flows through the development of a numerical solution from the controlling equations with proper boundary conditions. With the development of super computer and commercial software, CFD is now extensively applied for product design, and academic and industrial research development (Sachdev, Pareek et al. 2012).

Flows through a packed bed can be modeled using appropriate approaches that depending on the objectives and intended uses. Hydrodynamic characterizations of the gas-liquid flows in packed beds have been extensively studied using CFD at three different scales, including micro-scale, meso-scale and macro-scale (Raynal and Royon-Lebeaud 2007). Micro-scale and meso-scale meteorology are sometimes grouped together ("AMS Glossary of Meteorology" 2008-04-12); hence, the wording of meso-scale that is used in the following content represents both micro-scale and meso-scale.

Meso-scale modelling uses parts of a packed bed structure as a simulation object. In this model, the exact geometry of the packing bed is developed for the benefit of developing a detailed understanding of flow pattern, including trickle flow, spray flow, film flow or bubble flow, liquid hold up, pressure drop and wetted areas (Gunjal, Kashid et al. 2005). It has also been used to provide insight into hydrodynamic phenomena inside of the packed bed (Calis, Nijenhuis et al. 2001, Raynal, Boyer et al. 2004, Raynal and Royon-Lebeaud 2007, Haroun, Legendre et al. 2010, Gao, Zhang et al. 2011, Mousazadeh, van Den Akker et al. 2013, Sebastia-Saez, Gu et al. 2013). In general, single-phase flow has been extensively studied (Van Baten, Ellenberger et al. 2001, Petre, Larachi et al. 2003, Gao, Zhang et al. 2011, Said, Nemer et al. 2011, Li, Zhang et al. 2012, Yu 2013, Haroun, Raynal et al. 2014).

Macro-scale modelling is actually a porous media concept approach (Raynal and Royon-Lebeaud 2007). In this approach, an entire packed bed is considered as a porous media zone in which the media is usually represented by spherical particles arranged either in a regular or random fashion (Ranade, Chaudhari et al. 2011). It treats the phases as inter-penetrating continua and entails the use of a very attractive form which does not require

detailed geometry of the system as input (Kuzeljevic 2010). This approach is a main method that has been used to incorporate complexities like chemical reactions into the modelling (Niegodajew, Asendrych et al. 2013) and when scaling up the packed beds. By using the Eulerian k-fluid CFD model (Jiang, Khadilkar et al. 2002) it is possible to include closure equations to describe flow pressure drops. One attribute of the k-fluid CFD model is its computational efficiency, particularly for large-scale systems including packed beds. In the model, a statistical description of the bed structure is introduced into the multiphase k-fluid model framework. It can be applied to gas, liquid and solid phases, but to consider the effects of a solid phase on gas and liquid flows the model has to have the solid as a stationary phase with its porosity and porosity distribution well defined.

In all CFD models, the continuum approximation is applied for all phases. Volume-averaged mass and momentum balance equations for the k-th fluid can be written as:

Mass balance equation:

$$\frac{\partial \varepsilon_k \rho_k}{\partial t} + \nabla \cdot \varepsilon_k \rho_k U_k = 0 \qquad (2.1)$$

Momentum balance equation:

$$\frac{\partial (\varepsilon_k \rho_k U_k}{\partial t} + \nabla \cdot (\varepsilon_k \rho_k U_k U_k) = -\varepsilon_k \nabla P_k + \nabla \cdot (\varepsilon_k \mu \nabla U) + \varepsilon_k \rho_k g + F_{K,R}(U_k - U_R) \qquad (2.2)$$

where ε_k represents the volume fraction of each phase, ρ_k is the density of k-th phase, U_k is the cell velocity of k-th phase, and P is a mean pressure shared by all the phases present in the system. $F_{K,R}$ is an interphase(between k and R phases) momentum exchange term. The left-hand side of Equation 2.2 represents the rate of change of momentum for the k-th phase. The right-hand side represents pressure forces, average shear stresses, gravitational acceleration and interphase momentum exchange.

2.4 Closure Model

The pressure drop is called a closure model in CFD. The first closure model was developed by Darcy (Darcy 1856) who in 1856 proposed a linear relationship between the pressure gradient and superficial velocity in used one phase flow through a porous media, as is shown in equation 2.3. Later, Forchheimer (ANSYS Help) modified this model to a power relationship to also include and quantify viscous and inertial force contributions to the pressure loss, as is seen in equation 2.4.

$$\nabla p = -\frac{\mu}{a}\vec{v} \tag{2.3}$$

,

Where $a = \frac{D_p^2}{150}\frac{\varepsilon^3}{(1-\varepsilon)^2}$

$$-\frac{dP}{dz} = \frac{\mu U}{\varepsilon K} + \frac{\rho U^2}{(1-\varepsilon)g} \tag{2.4}$$

An important and famous empirical relationship is the Ergun equation (Ergun 1952). For turbulent flow in a packed bed reactor, the friction factor of a single particle can be expressed as a fuction of the Reynolds number based on the particle diameter,

$$f_p = \frac{150}{Re_p} + 1.75 \tag{2.5}$$

where the f_p and $\mathrm{Re_p}$ are defined as

$$f_p = \frac{\Delta p}{l}\frac{D_p}{\rho V_\infty^2}\left(\frac{\varepsilon^3}{1-\varepsilon}\right) \tag{2.6}$$

and

$$Re_p = \frac{D_p \rho V_\infty}{(1-\varepsilon)\mu} \tag{2.7}$$

where Δp is the pressure drop across the length of the bed, L the length of the bed, D_p the equivalent diameter of the packing spheres, ρ the density of fluid, V_∞ the superficial

velocity measured upstream of the bed entrance, μ the dynamic viscosity of the fluid, and ε the void fraction of the bed. Substituting Eqs. 2.6 and 2.7 into Eq. 2.5 yields the pressure drop per unit length of the bed,

$$\frac{|\Delta p|}{l} = \frac{150\mu}{D_p^2}\frac{(1-\varepsilon)^2}{\varepsilon^3}v_\infty + \frac{1.75\rho}{D_p}\frac{(1-\varepsilon)}{\varepsilon^3}v_\infty^2 \tag{2.8}$$

Therefore a permeability α and an inertial loss coefficient C_2, and are defined as

$$\alpha = \frac{150}{D_p^2}\frac{(1-\varepsilon)^2}{\varepsilon^3} \tag{2.9}$$

$$C_2 = \frac{3.5}{D_p}\frac{(1-\varepsilon)}{\varepsilon^3} \tag{2.10}$$

The parameters used to describe the characteristics of a porous media are the viscous resistance coefficient and intertial resistance coefficient. The Ergun equation can then be used to predict the pressure drop along the length of a packed bed if fluid velocity, packing size, viscosity and the density of the fluid are known.

Niegodajew (Niegodajew, Asendrych et al. 2013) studied phase transformations and heat transfer based on the Ergun equation for single-phase flow. However, a large number of empirical correlations are available for predicting pressure drop in trickle beds; furthermore, by using a permeability model (Atta, Roy et al. 2007), as shown in equation 2.11, and the pressure drop equation shown in equation 2.12, it is possible to compute pressure drops using a macro-scale model (Gunjal, Kashid et al. 2005), Hosseini et al. (Hosseini, Shojaee et al. 2012) studied the pressure drop in dry and wetted structured packing for a structured 2D packing geometry. In general, no 3D counter-current CFD studies have been found.

Ellenberger et al. (Ellenberger and Krishna 1999) used experimental methods to develop a ‘wet’, empirical pressure drop equation for counter-current flow (see equation 2.13).

Stichlmair et al. (Stikkelman and Wesselingh 1987) developed a generalized model (see equation 2.14 and 2.15) for predicting pressure drop and liquid holdup under counter-current flow; it has been validated for a wide variety of packing, both random and structured on low flow rate. However, this model does not provide information about local flow and transport occurring within the bed.

$$\left(\frac{\Delta p}{l}\right) = \frac{F_g}{\varepsilon_g} = \frac{1}{k_g}\left[A\,\frac{Re_g}{Ga_g} + B\,\frac{Re_g^2}{Ga_g}\right]\rho_g g \tag{2.11}$$

$k_g = s_g^{4.8}$, $s_g = 1 - \frac{\varepsilon_l^0}{\varepsilon}$, A and B are values of Ergun's constants.

$$P_G - P_L = 2\sigma\,\frac{5.416}{D_p}\left(\frac{1-\epsilon}{1-\epsilon_G}\right)^{0.333} F\left(\frac{\rho_G}{\rho_L}\right) \tag{2.12}$$

Where $F\left(\frac{\rho_G}{\rho_L}\right) = 1 + 88.1\frac{\rho_G}{\rho_L}$ for $\frac{\rho_G}{\rho_L} < 0.025$

$$\frac{\Delta p}{l} = \frac{\Delta p_{dry}}{l}\,exp\left[1.3\varepsilon_{L,0c}\left(\frac{Re_{L,oc}}{Fr_{L,oc}}\right)^{0.3}\right] \tag{2.13}$$

$$\frac{\Delta P_{irr}}{l} = \frac{3}{4f_0'\left[\frac{1-\varepsilon'}{\varepsilon'^{4.65}}\right]\rho_g U_g^2}/d_p' \tag{2.14}$$

$$h_0 = 0.555\left(U_L^2\,\frac{a_p}{g\varepsilon^{4.65}}\right)^{1/3}\rho_k \tag{2.15}$$

In this dissertation, a closure equation will be developed for counter-current flow in a packed bed. Modifications to it will be introduced based on comparison between simulation and experimental results, in relationship to the empirical equations. These developments will be explored in depth within Chapter 5.

2.4 Summary

The knowledge about the hydrodynamics within a post combustion, CO_2 capture process using counter-current, multiphase flow is yet in its infancy, but a good understanding of the flows are necessary to enhance the relatively slow CO_2 absorption reaction that takes place during this process (Force 2009, Aferka, Viva et al. 2011, Chen, Yates et al. 2012, Basden, Eldridge et al. 2013, Niegodajew, Asendrych et al. 2013). Although a limited number of numerical studies have examined counter-current flows for packed beds, most of these studies have been based on either single-phase or co-current flow, neither of which represent design reality for a counter-current flow, packed bed reactor.

Pressure drops and liquid holdups are well studied and can be obtained directly from experiments. However, the wetted area, film thickness and the interactions between the two phases under counter-current flows have not been studied sufficiently to provide a clear understanding of their dependencies. Rather, at this time, they can only be deduced from experimentation if certain assumptions are included.

In the CO_2 absorber process, the gas and liquid are in turbulent flow, 1D or 2D simulations of the hydrodynamics are not suitable and 2D film flow cannot describe the flow structure of three-dimensional waves caused by instabilities of the flows (Hoffmann, Ausner et al. 2005). Therefore, a complete three-dimensional meso-scale model for counter-current, multiphase flow needs to be developed for characterizing the liquid film, flow distribution, pressure drop, liquid holdup, wetted area and the interactions between phases. If successfully accomplished, this development will assist in understanding how to maximize contact between phases and to improve CO_2 capture efficiency.

Similarly, macro-scale models that have been used for large scale reactors with a closure model were based on single phase, co-current flow or empirical equations, and are not satisfactory for application in the counter-current flow approach. Therefore, this dissertation will develop a comprehensive CFD model for a counter-current, multiphase flow, packed bed reactor to enable a better understanding of the complex phenomena associated with it. A successful model would help in identifying optimized designs and assist in the development of full scale industrial units (Ghosh 2013).

CHAPTER 3. NUMERICAL STUDY OF SPHERICAL BALL PACKED BED REACTOR

This chapter describes the development of 3D CFD model with counter-current gas-liquid flow and of the analyses of the hydrodynamics within a spherical ball packing, fixed bed reactor configuration. First, an experimental set-up was developed using spherical ball packing materials, after which experimentation was performed to measure pressure drops under various test conditions. Then, the 3D CFD model using a Volume of Fluid (VOF) interface was developed and validated by comparison to the experimental data. Also, the liquid distribution, flow regime, liquid holdup, pressure drop, wetted area, and gas-liquid interactions were studied and characterized parametrically. Finally, the effect of the liquid and gas inlet flow rates and surface tensions were examined and discussed as related to liquid hold up, wetted area and pressure drop.

3.1 Experiments Data Collection

Even though numerical simulation is well developed, and has been confirmed and is applied widely, to provide accurate replications of reactor and reaction phenomena it is understood that the CFD model and its results should be validated by comparisons with experimental results under similar test conditions. For this validation, pressure drops from the experiments were compared with the 3D CFD model results because the flow distribution, wetted area and the interaction between the gas-liquid phases were extremely difficult to measure experimentally.

In the experiments, the absorption reaction was not considered, and air and water were used as the flow fluids. A schematic of the experimental setup is shown in Figure 3.1 and the operating parameters are listed in Table 3.1. The packing materials were spherical,

plastic balls with a diameter of 9.5 mm; they were packed uniformly in the bed with a packed height of 580 mm. By knowing the diameter of the balls, the void fraction within the packed volume was calculated to be 0.39. Air was purged into the column from the bottom and contacted the down flow of water in a counter-current flow setup. Air flow rates were measured via an air mass flow controller (MFC) and water flow rates were produced via a peristaltic pump. The pressure drop along the height of the packed bed was measured using an inclined manometer. A Lab-View program was used for controlling the flow rate devices and for recording data. Gas flow rates were 5, 10 or 15 L/min while the liquid flow rates were 100, 200 or 300 mL/min (See Table 3.1); the test conditions and the resulting pressure drops are listed in Table 3.2.

In the first group of tests, the liquid flow rate was constant at 200 mL/min while gas flow rates were varied between 5-15 L/min. In the second group of tests, the gas flow rate was constant at 10 L/min but the liquid flow rates were varied between 100 to 300 mL/min. The final tests were accomplished with 10 L/min air flow and 300 mL/min water flow.

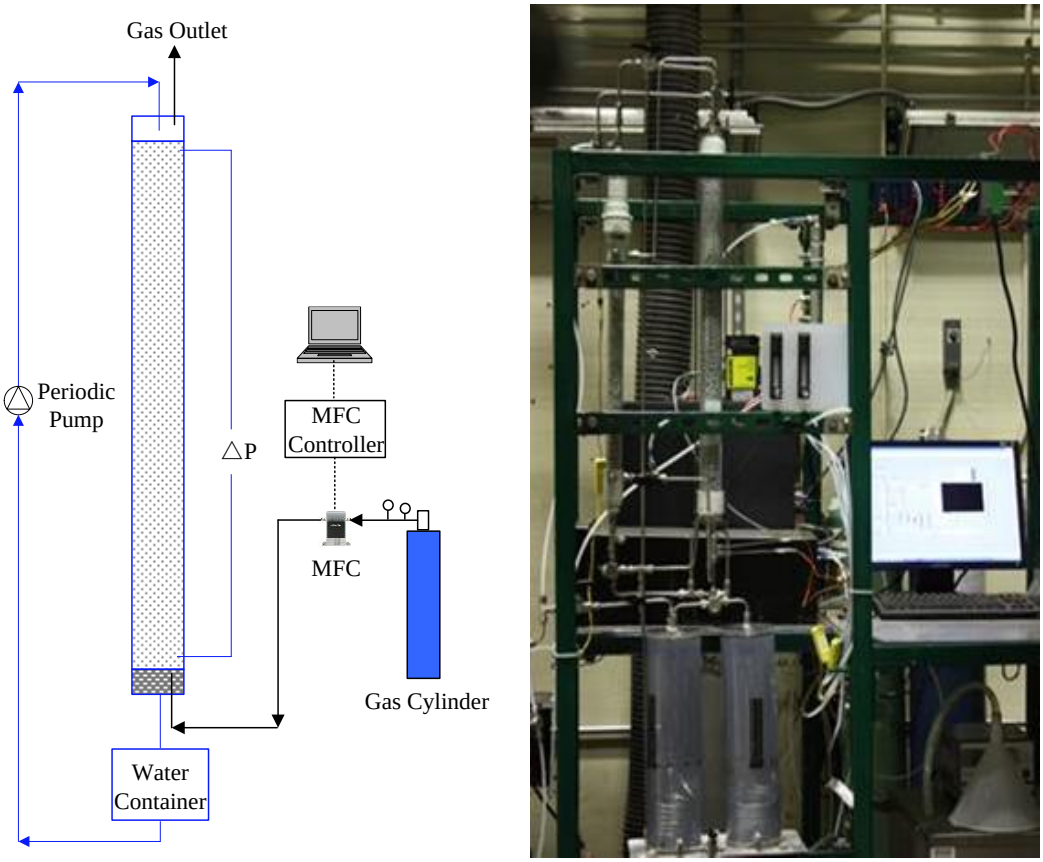

(a) (b)

Figure 3.1 (a) Flow diagram of experiment setup; (b) experimental setup.

Table 3.1 Experimental parameters and operating conditions.

Column diameter (mm)	38.1
Column height (mm)	580
Fluids used	Air-Water
Gas mass flow rate (L/min)	5, 10, 15
Liquid mass flow rate (mL/min)	100, 200, 300
Package materials	Plastic spheres
Diameter of spheres (mm)	9.5
Height of packed area (mm)	550
Void fraction	0.39

Table 3.2 Experimental matrix and gas side pressure drops.

Cases	Gas phase mass flow rate (L/min)	Liquid phase mass flow rate (mL/min)	Gas side pressure drop (Pa/m)
1	5	200	23.64
1	10	200	58.18
1	15	200	105.45
2	10	100	54.55
2	10	200	65.45
2	10	300	72.73

3.2 Development of the Numerical Model

3.2.1 Geometry and Mesh Generation

The geometry of the simulation was same as the packing structure used during the experiments, as depicted in Figure 3.2, but the simulation domain was only a portion of the packed bed to save computational time. The simulation geometry was built using ANSYS Workbench software. The size of the cuboid domain was 19.2 × 19.2 × 52 mm and the diameter of the spheres during simulation was 9.5 mm, which was identical with these used in the experiments. During simulation, a 0.1 mm gap was placed between any two nearby spheres to facilitate meshing on the sphere surface.

The first layer at the top of the simulation included four spheres, and the second layer had one sphere at the center with one semi-sphere on each of its sides, and one ¼th - sphere at each corner. The remaining layers proceeding downward were arranged repeatedly using these patterns to produce a total of six layers along the height of the domain. A 1 mm gap was placed between the top, first layer of spheres and the liquid inlet to enable uniformly developed liquid flow; the same separation distance was placed between the bottom row of spheres and the reactor gas inlet. In this arrangement, the calculated void fraction for the whole domain was 0.40, a value very close to the experimental void fraction of 0.39.

One liquid inlet was placed at the top and one liquid outlet was placed at the bottom; each had a diameter of 7.2 mm. Because of counter-flow, gas entered the bottom hole around which liquid flowed outward and then gas exited the top outlet around which liquid entered. Side wall boundaries were set as symmetric boundaries instead of solid wall boundaries because the cuboid domain was only part of the total packed bed used experimentally; the contact angle of the wall is set as 70°. The fluids are assumed to be Newtonian, isothermal, and incompressible, boundary conditions are listed in Table 3.3.

Table 3.3 Boundary conditions of all simulations.

Boundary	Materials	Type	Value	Velocity	Reynolds Number	Web Number
Liquid inlet	Water	Mass flow rate	100mL/min-1200mL/min	0.012-0.147(m/s)	180-1100	0.014-2.2
Gas inlet	Air	Mass flow rate	5L/min-25L/min	0.076m/s-0.382m/s	99-500	
Liquid outlet		Pressure-outlet	0 Pa			
Gas outlet		Pressure-outlet	0 Pa			

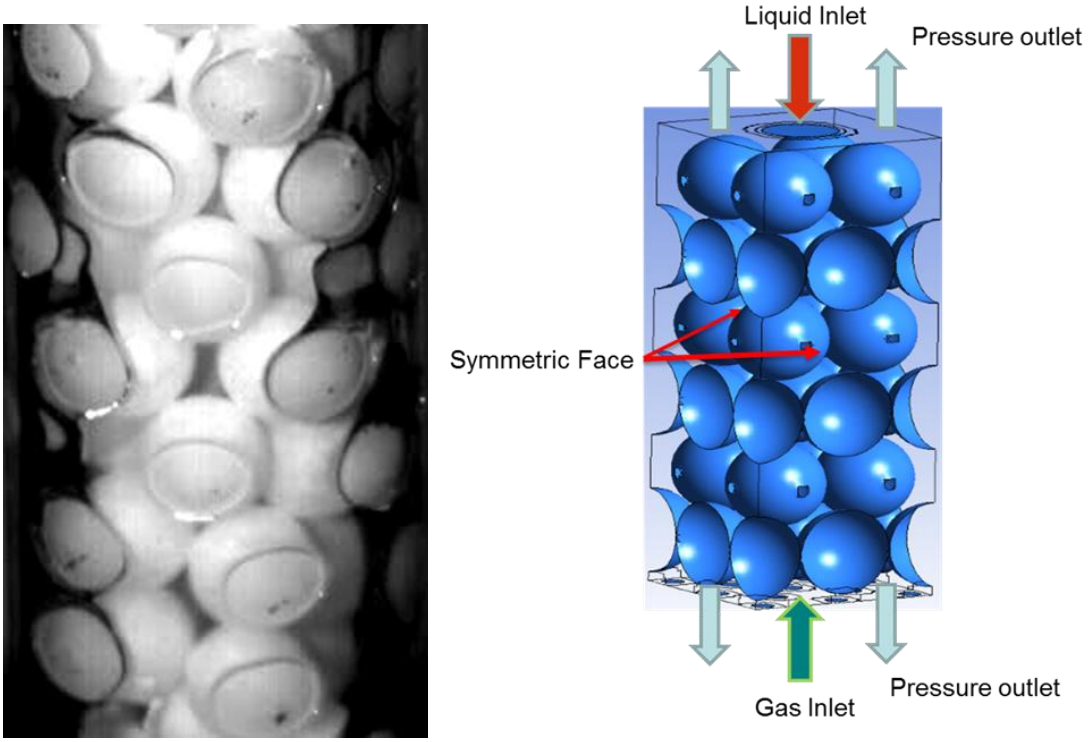

Figure 3.2 Experimental packed column (left) and simulation geometry (right).

The constructed geometry was then exported to a mesh generator using ANSYS software with a fine spacing of between 0.0001 m to 0.0004 m using the CutCell meshing method; details of the mesh structure are provided in Figure 3.3. Overall, the total number of elements was 236,559 within the simulation volume and the grids were denser at the liquid inlet to enable a more accurate determination of liquid film formation and properties. The mesh file was then imported to ANSYS Fluent solver for simulation. After importing, the mesh was first checked by the ANSYS Fluent solver to determine if a warning message was generated; if not, the mesh quality was accepted to be usable for calculations.

Details of "Mesh"

Defaults	
Physics Preference	CFD
Solver Preference	Fluent
Relevance	0
Sizing	
Use Advanced Size Function	On: Curvature
Relevance Center	Coarse
Smoothing	Medium
Curvature Normal Angle	Default (18.0 °)
Min Size	1.e-004 m
Max Size	4.e-004 m
Growth Rate	Default (1.20)
Minimum Edge Length	1.e-003 m
Inflation	
Assembly Meshing	
Method	CutCell
Feature Capture	Program Controlled
Tessellation Refinement	Program Controlled
Statistics	
Nodes	243189
Elements	236559

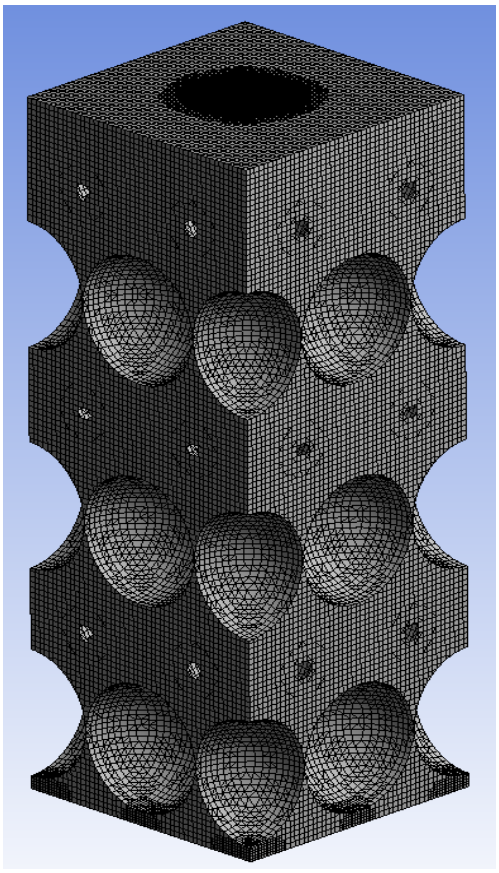

Figure 3.3 Details of the mesh structure.

3.2.2 Governing Equation in the VOF Model

The model was solved using a multi-fluid CFD Volume of Fluid (VOF) model. The VOF model is a surface-tracking technique developed for two or more immiscible fluids where the position of the interface between the fluids is of interest (Zhang, Zhang et al. 2013). In it, a single set of momentum equations is shared by the fluids, and the volume fraction of each fluid in each computational cell is tracked throughout the domain. The phasic volume fraction concept is described as the volume gas and liquid two-phase flow through the packed bed determined by solving the governing equations (Hirt and Nichols 1981). Applications of VOF are quite general and have been quite frequently used for simulating liquid break up and the interaction of two phases (Gueyffier, Li et al. 1999,

Welch and Wilson 2000, Ginzburg and Wittum 2001, Renardy and Renardy 2002, Olsson and Kreiss 2005, Srinivasan 2006). The numerical simulations were carried out using ANSYS Fluent 14.0, which used the finite volume method to solve Navier-Stokes equations for gas-liquid, incompressible and iso-thermal flow (Sebastia-Saez, Gu et al. 2013, Haroun, Raynal et al. 2014). The VOF model is implemented within the software. The governing equations of the two phase flow are given as:

Continuity equation

$$\frac{\partial \rho}{\partial t} + \nabla \cdot (\rho\, \vec{v}) = 0 \tag{3.1}$$

Momentum equation

$$\frac{\partial}{\partial t}(\rho\vec{v}) + \nabla(\rho\vec{v}\vec{v}) = -\nabla p + \nabla\left[\mu\left(\nabla\vec{v} + \nabla\overrightarrow{v^T}\right)\right] + \rho\vec{g} + \vec{F} \tag{3.2}$$

Where $v = \frac{a_1\rho_1 v_1 + a_2\rho_2 v_2}{\rho}$, $\overrightarrow{F}$ is the interface drag force.

Each phase's volume fraction is a_k, where:

$$\sum_{k=1}^{n} a_k = 1 \tag{3.3}$$

For a two phase system:

$$\rho = a_2\rho_L + (1 - a_2)\rho_g \tag{3.4}$$

$$\mu = a_2\mu_L + (1 - a_2)\mu_g \tag{3.5}$$

where a_k ranges from 0-to-1; a zero corresponds to a cell filled with gas phase and a value of one corresponds to a celled filled with the liquid phase. Intermediate values correspond to interfaces between phases. Also, the drag force term in equation 3.2 considered only surface tension.

The surface tension model was developed by (Brackbill, Kothe et al. 1992), and is governed by:

$$\vec{F} = \sigma \frac{\rho k \nabla a_k}{0.5(\rho_l + \rho_g)} \tag{3.6}$$

where k is the free surface curvature, which is defined as

$$k = \nabla \cdot \hat{n} = \frac{1}{|n|}\left[\left(\frac{n}{|n|} \cdot \nabla\right)|n| - (\nabla \cdot n)\right] \tag{3.7}$$

The symbol $\hat{n}$ is a unit normal vector. And $n=\nabla a_k$.

In this study, mass transfer terms between the two immiscible phases were neglected. The VOF model can account for the effect of surface tension along interfaces between the two phases (Chung, Patiño-Echeverri et al. 2011, Srinivasan, Salazar et al. 2011).

3.2.3 Turbulence Model

In fluid dynamics, turbulent flow is characterized by chaotic property changes. These changes include low momentum diffusion, high momentum convection, and rapid variation of pressure and flow velocity in space and time. Multiphase flows in packed beds are often characterized as laminar flow but several studies have reported them to be turbulent (Lopes and Quinta-Ferreira 2009). Dybbs et al. (A. Dybbs, 1984) used laser anemometry and flow visualization technology to investigate liquid flow regimes in hexagonal packing of spheres and rods, and classified four flow regimes for different ranges of Reynolds number. For 1 < Re, the flow was dominated by viscous force; for 1<Re<150, the flow was a steady laminar inertial flow; for 150≤Re≤300, the laminar inertial flow was unsteady; and, for *Re* > 300, the flow was highly unsteady, chaotic and qualitatively resembled turbulent flow.

The Reynolds number has been calculated as:

$$Re = \frac{\rho v d}{\mu} \tag{3.8}$$

Where the characteristic length d is the thickness of the phase inlet, ρ is the density of the fluid (kg/m^3), v is its velocity (m/s) and μ is the viscosity (kg/m/s).

Therefore, since the Reynolds numbers for both liquid and gas phases are within the range of turbulent flow (min: 180, max: 1100), a turbulence model was applied. For turbulent flow, several different models have been developed, such as large eddy simulation (LES), k-ε model and k-omega (CABLE 2009). The k- ε model is only valid for fully turbulent and non-separated flows. The k-omega model is a two-transport-equation model solving for kinetic energy, k, and turbulent frequency, ω; it allows for more accuracy near walls and for a low Reynolds numbers (ANSYS help). The LES model is also popular for turbulent flow simulation, and it emphasizes the interactions between phases. Labourasse (Labourasse, Lacanette et al. 2007) successfully applied LES model to resolve two-phase flow problems and accounted for the complex interactions between turbulence and interfaces. Vincent (Vincent, Larocque et al. 2008) also applied the LES model for phase separation, and Christensen (Christensen and Deigaard 2001) adopted a standard LES model coupled with a VOF free surface approach in a wave break simulation study. Therefore, the LES turbulent model will be used in the simulation of the plastic sphere, packed bed; its solution method setup is described in the following.

The Geo-Reconstruct algorithm method (Sebastia-Saez, Gu et al. 2013) was used for interface reconstruction of the volume fraction, a simple scheme for which was the pressure-velocity coupling. For spatial discretization, the Least Squares Cell Based was

used for the gradient in the spatial discretization set up, the Presto method was used for pressure, the Second Order Upwind method was used for the momentum equation, and the First Order Implicit method was used for the transient formulation.

The simulation used a transient state to observe the growth of the liquid film and the development of gas-liquid interactions. The time step size for this model was 0.00005 second while solving a maximum 30 iterations per time step. The total computation time was close to 96 hrs for one case.

3.3. Results and Discussion

3.3.1 Stationary State Determination

The criteria used to determine attainment of a pseudo-stationary state was the variation in wetted area with time. For example, Figure 3.4 shows the evolution of wetted area with time at various liquid loads (represented by liquid Reynolds number) when the gas flow rate was fixed at $Re_g = 199$; the wetted areas no longer changed at times between 0.30-0.50 s, depending on the liquid load. For example, at a liquid load of $Re_L = 180$, the wetted areas no longer changed at 0.48s, and at a liquid load of $Re_L = 1056$, wetted areas no longer changed at 0.35s. In other words, increased liquid loads at constant gas flow rate caused a decrease in total time for wetted area constancy. By comparing the data in Figure 3.4 with data in Figure 3.5, an increase in the gas load, i.e. gas-side Reynolds number, to $Re_g = 298$ (Figure 3.5) caused an increase in the time for establishing steady state wetted areas relative to those times found when the gas load was $Re_g = 199$ (Figure 3.4).

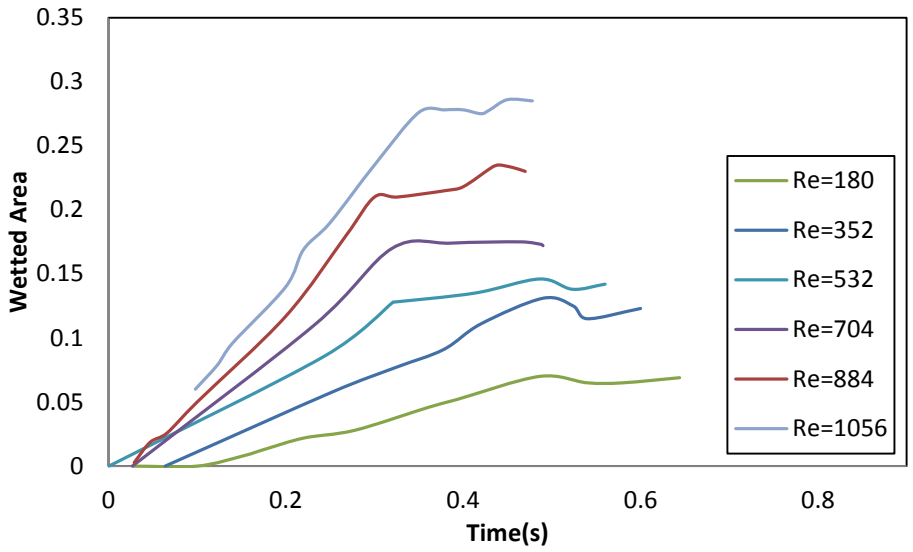

Figure 3.4 The evolution of wetted area as a function of time at various liquid flow rates under fixed gas flow rate of $Re_g = 199$.

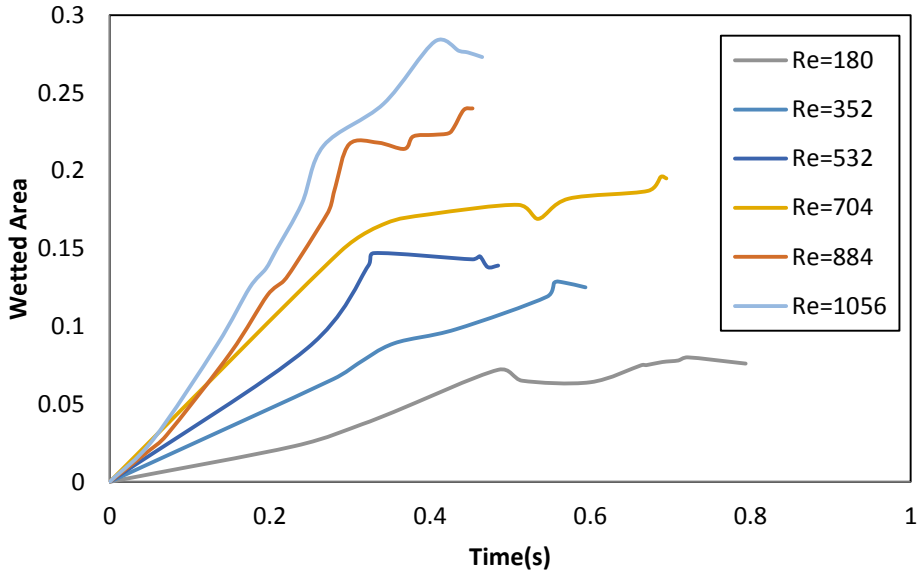

Figure 3.5 The evolution of wetted area as a function of time at various liquid flow rates under a fixed gas flow rate of $Re_g = 298$.

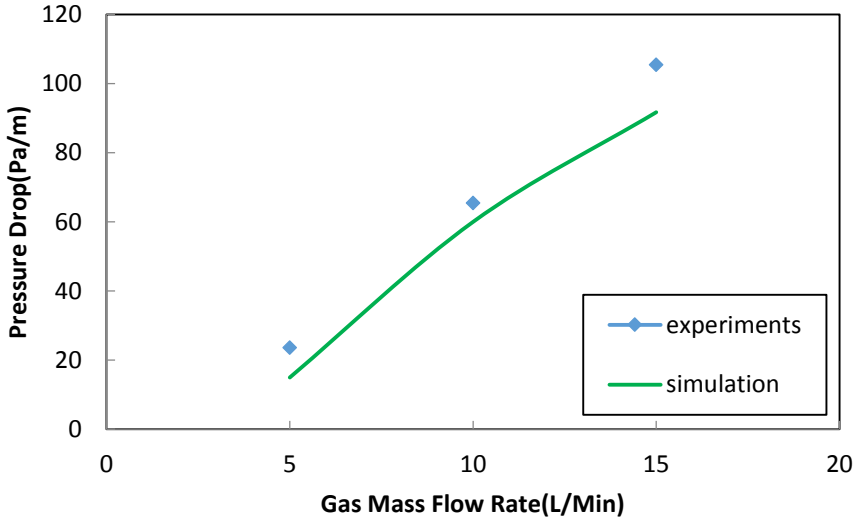

(a)

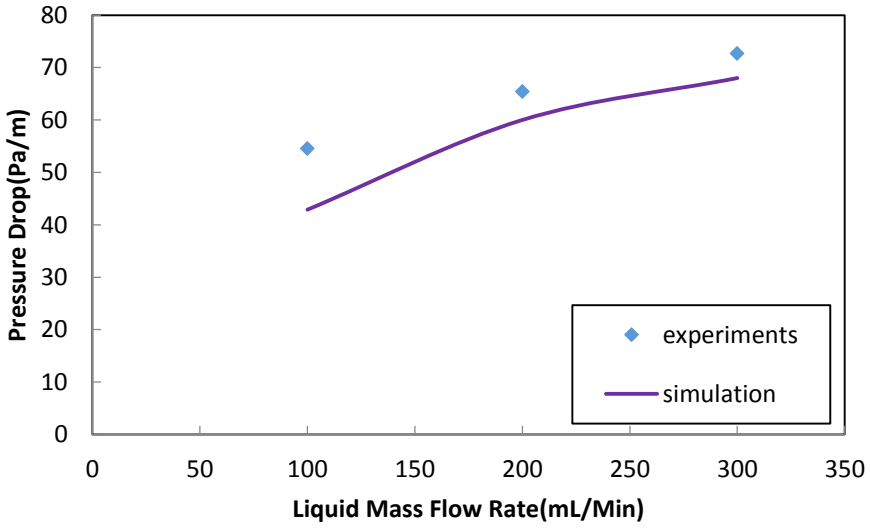

(b)

Figure 3.6 Pressure drops obtained from experiments and simulation using six different conditions. (a) Pressure drop as a function of gas flow rate at a fixed liquid flow rate of V_{water}= 200 (mL/min); (b) Pressure drop as a function of liquid flow rate at a fixed gas flow rate of V_{gas} = 10 (L/min).

3.3.2 CFD Model Validation

The results of CFD assessments of gas-liquid flows are generally validated by comparing pressure drops from the modeling and experimentation (Stikkelman, de Graauw et al. 1989).

Hence, the CFD model for the plastic sphere, packed bed reactor displayed in Figure 3.6 was first applied to obtain six pressure drops using the experimental conditions listed in Table 3.2. A comparison of these CFD pressure drops with experimental pressure drops is shown in Figure 3.6 (a) with a constant liquid flow rate of 200 mL/min and gas flow rates between 5-15 L/min, and in Figure 3.6 (b) at a constant gas flow rate of 10 L/min and liquid flow rates between 100-300 mL/min. The data in these figures show excellent reproduction of the experimental pressure drops by using the CFD model. Therefore, the established 3D CFD model for gas-liquid counter current flow was considered validated.

3.3.3 Liquid Distribution and Flow Regime Characterization

In this section, the flow distribution and flow regimes are characterized at different liquid flow rates. The liquid flow rate, as a Weber number (*We*) (Sebastia-Saez, Gu et al. 2013) is often used for analyzing fluid flow when an interface exists between two different fluids and especially for multiphase flows with strongly curved surfaces (Frohn and Roth 2000). The value of *We* is a measure of the relative importance of a fluid's inertia compared to its surface tension. The *We* is written as:

$$We = \frac{\rho v^2 l}{\sigma} \tag{3.9}$$

where ρ is the density of the fluid (kg/m^3), v is its velocity (m/s), l is its characteristic length - typically the droplet diameter (m), and σ is the surface tension (N/m) of water (0.07 N/m).

With a fixed gas flow rate having $Re_g = 199$, the effects of liquid different liquid flow rates, as represented by the *We*, on the flow distribution and flow regime on gas side *Re* number are shown in Figure 3.7 and Figure 3.8. Figure 3.7 is a visualization of the flow distribution on an iso-surface with a liquid volume fraction of zero with different liquid *We*: the liquid distribution was affected by the *We*. Because at higher *We* the liquid distribution became more uniform. For example, with *We* = 0.014, only a quarter of the domain was filled with liquid whereas with *We*=2.16 the whole domain was filled with liquid.

The color scale in Figure 3.7 refers to the phasic volume fraction of fluid in which a red color represents 100 vol. % of liquid and blue color is 100 vol.% of gas. Different flow regimes such as droplets and film flow were observed and assessed using *We*. At *We* = 0.014, surface tension dominated the flow and the liquid flow was not continuous leading to the formation of droplets. After *We* increased to a value of 0.547, droplet flow disappeared and film flow began. In this latter regime, although surface tension still dominates but the main effect was to reduce the interfacial wetted area. With further increases of *We* to 1.51, the trickle flow gradually engulfed the whole domain and the wetted area also increased.

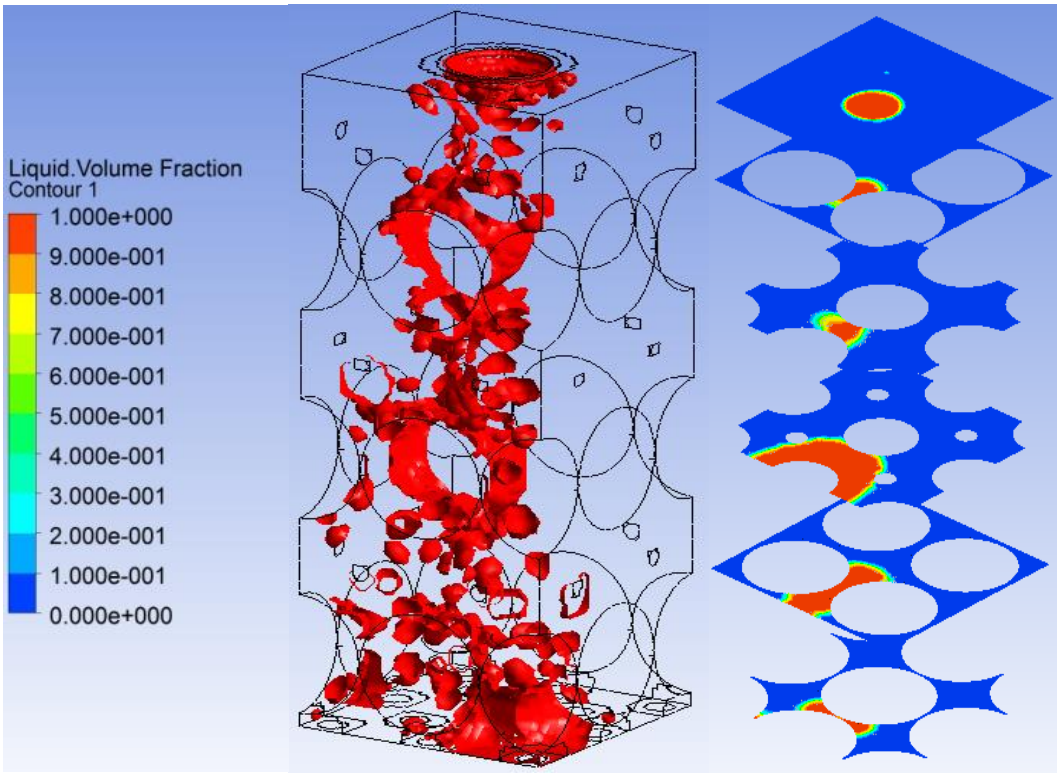

We=0.014

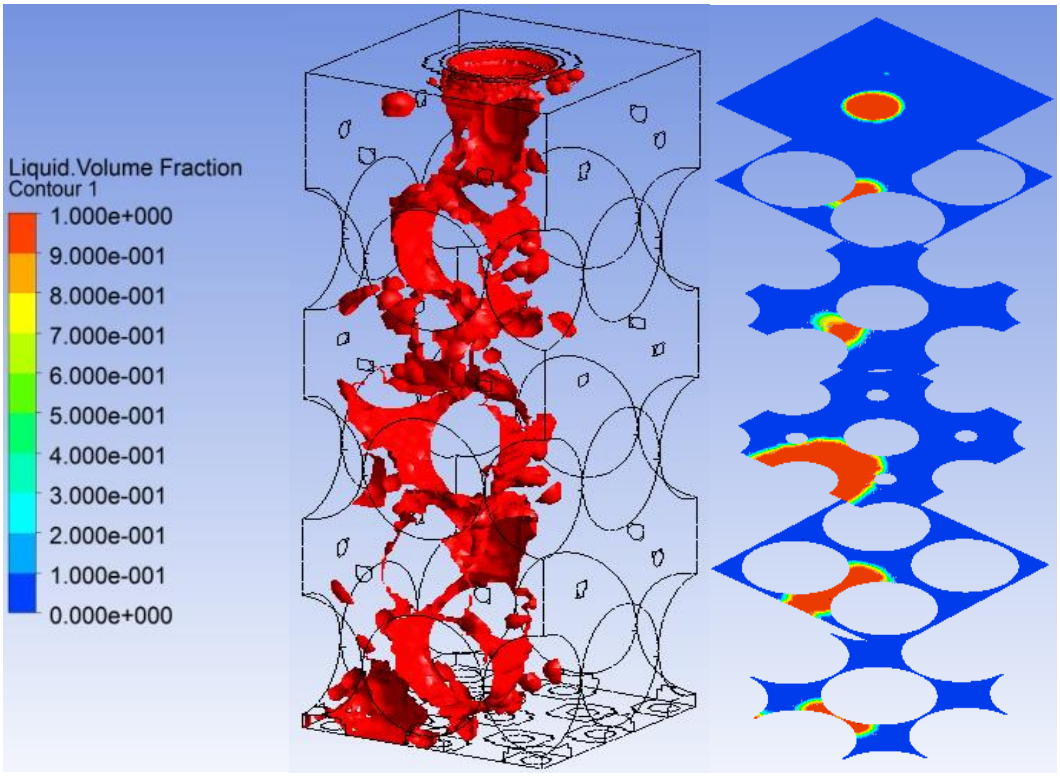

We=0.062

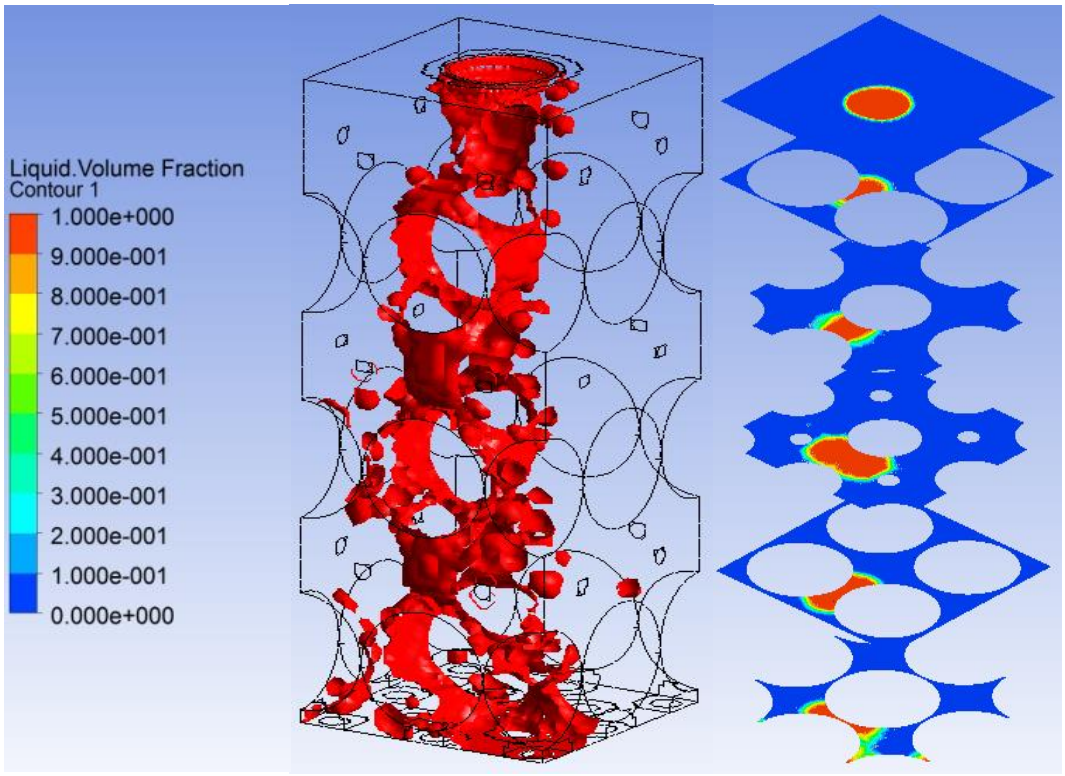

We=0.137

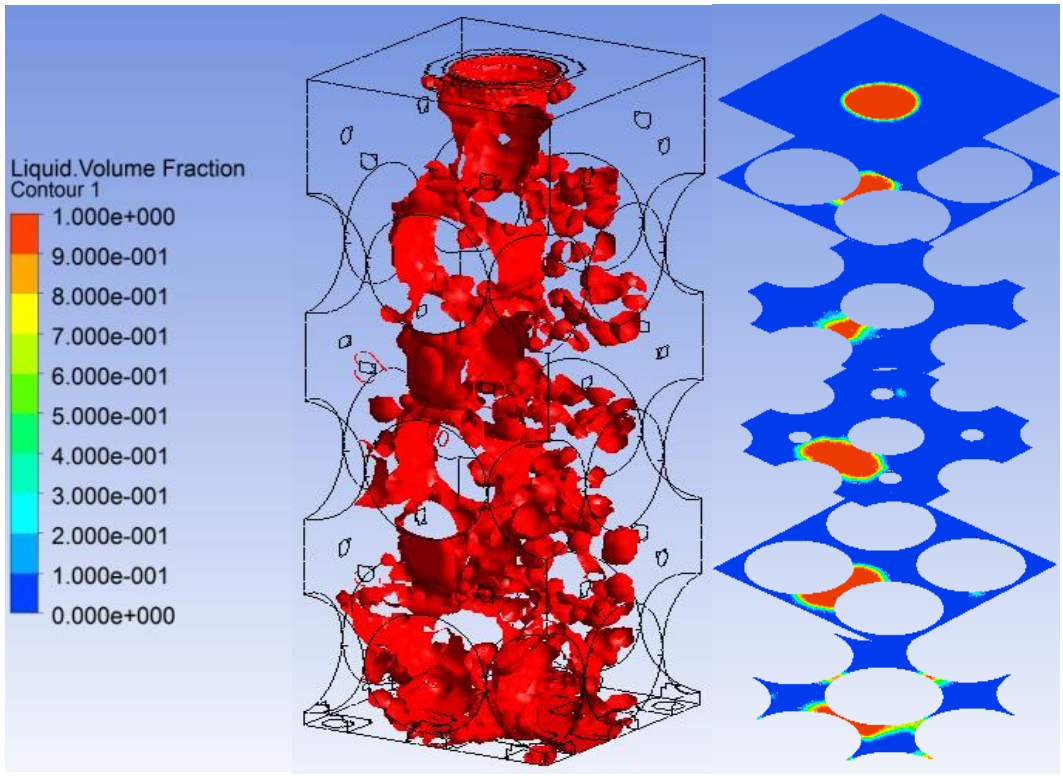

We=0.240

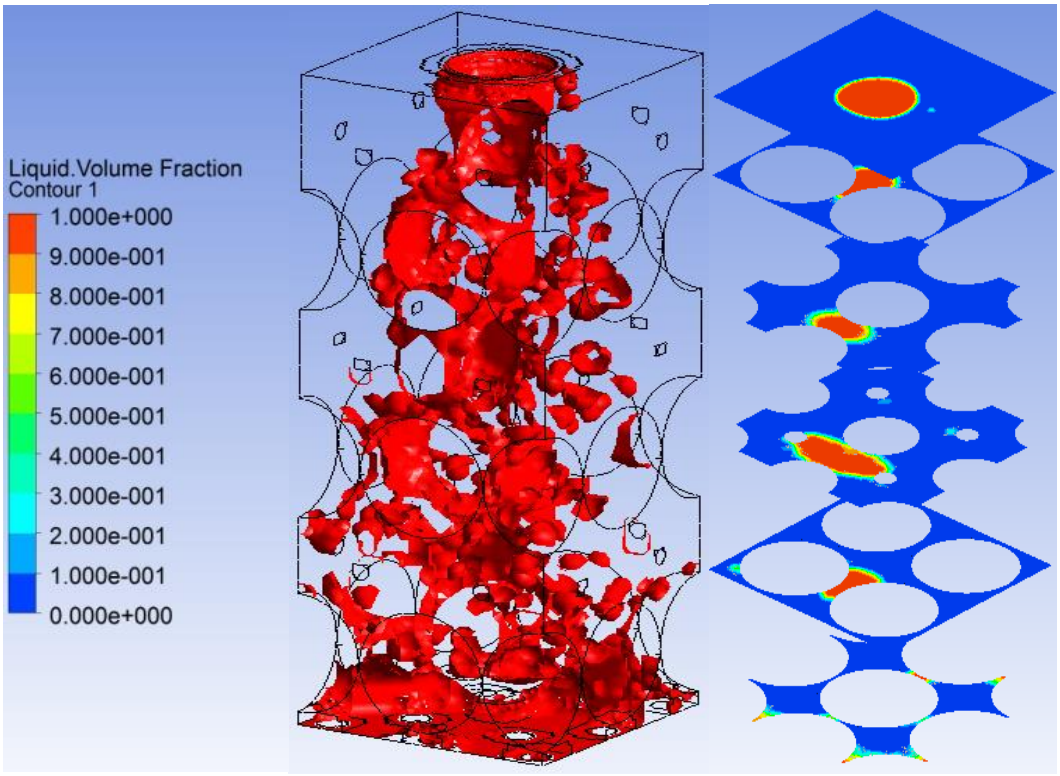

We=0.547

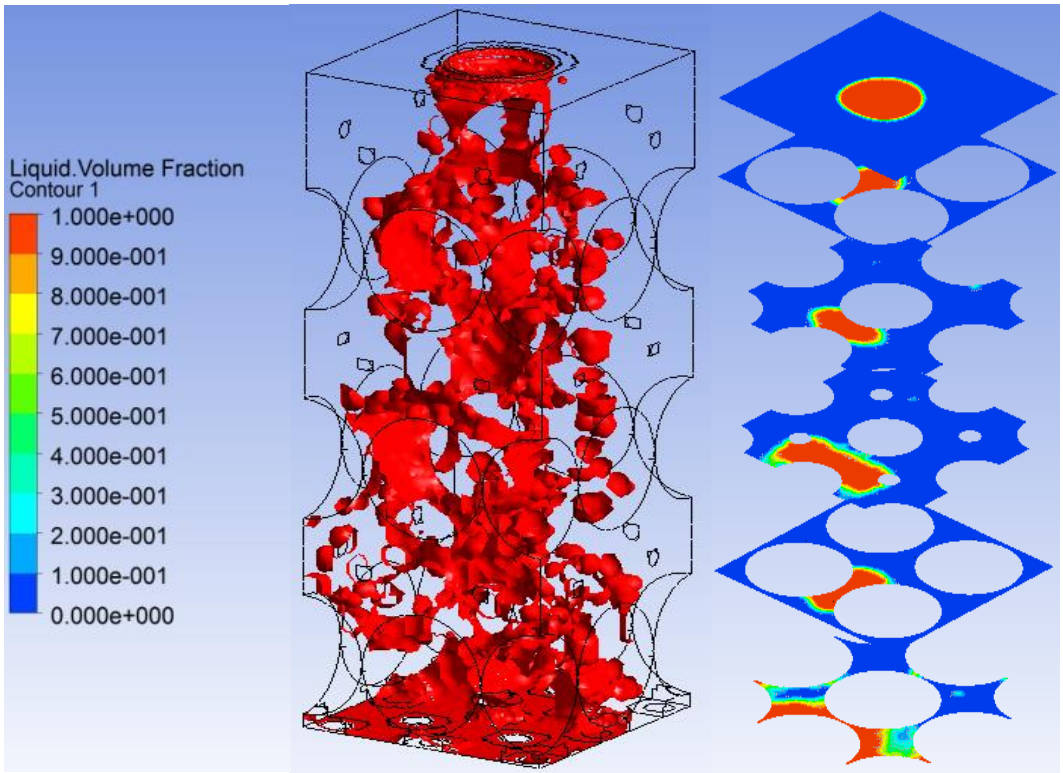

We=0.958

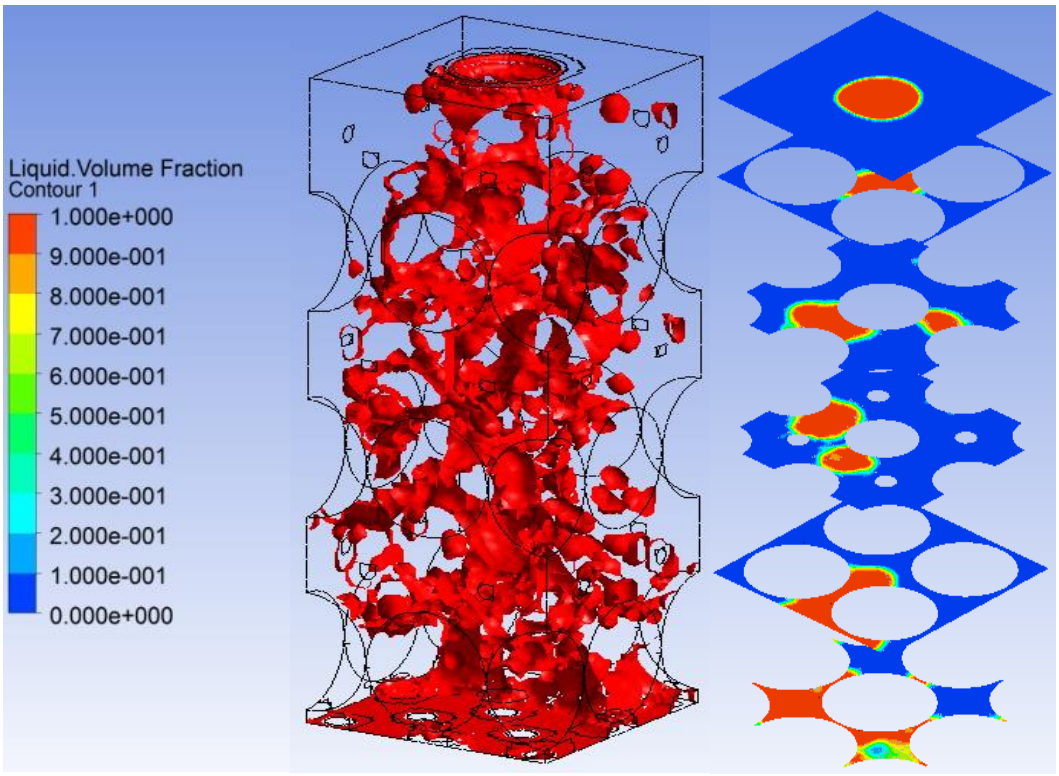

We=1.51

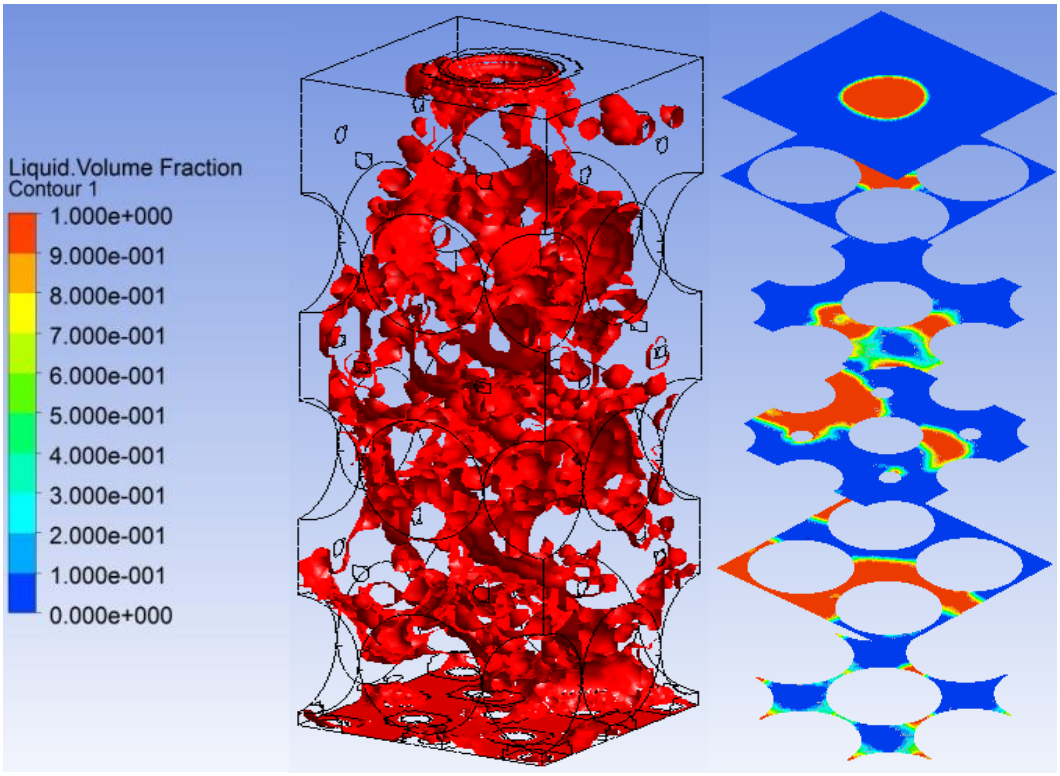

We=2.16

Figure 3.7 Flow distribution of iso-surface 0 at different liquid *We* from 0.014 to 2.16 at fixed $Re_g = 199$.

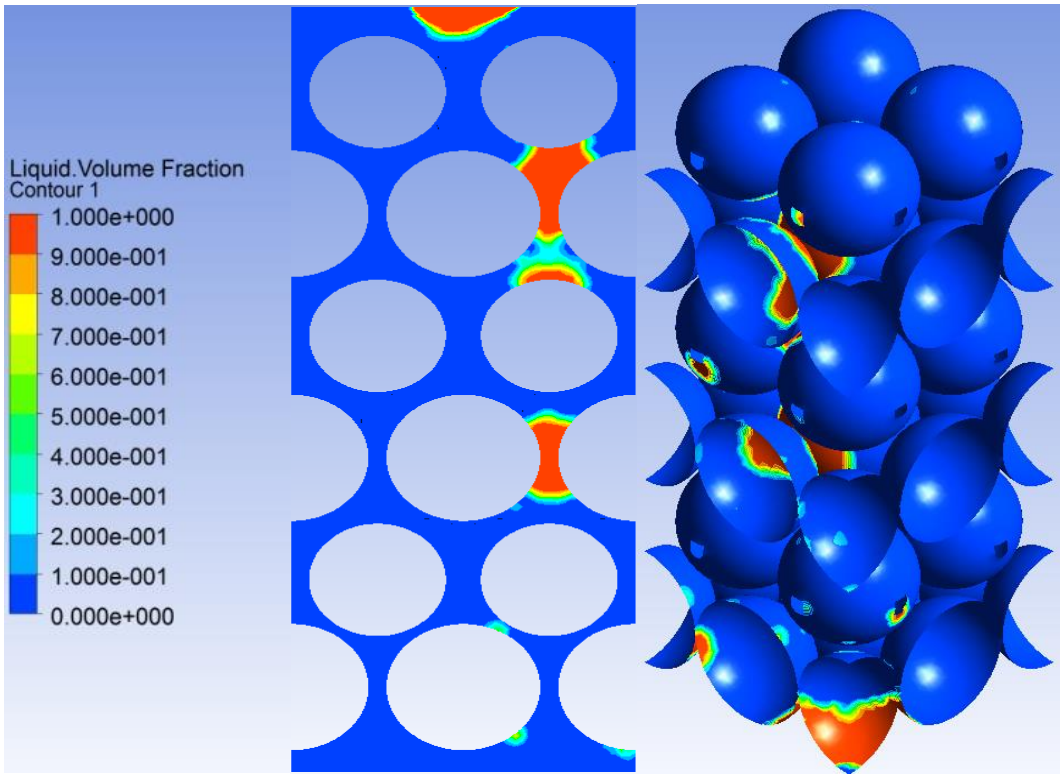

We=0.014

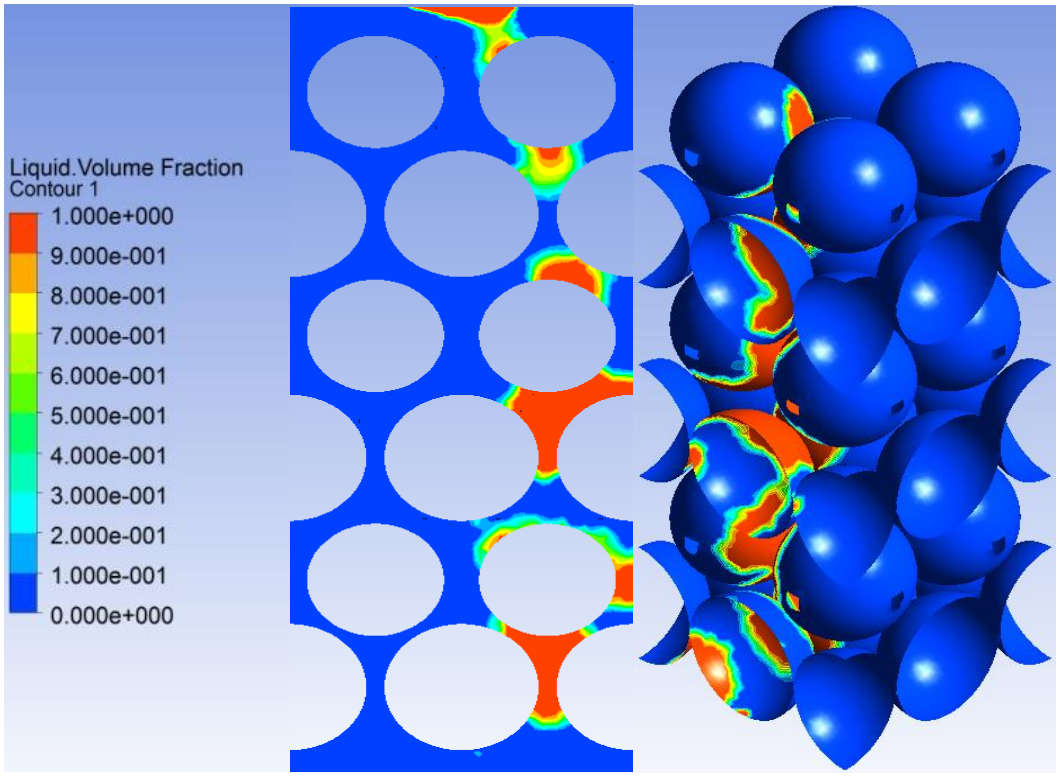

We=0.062

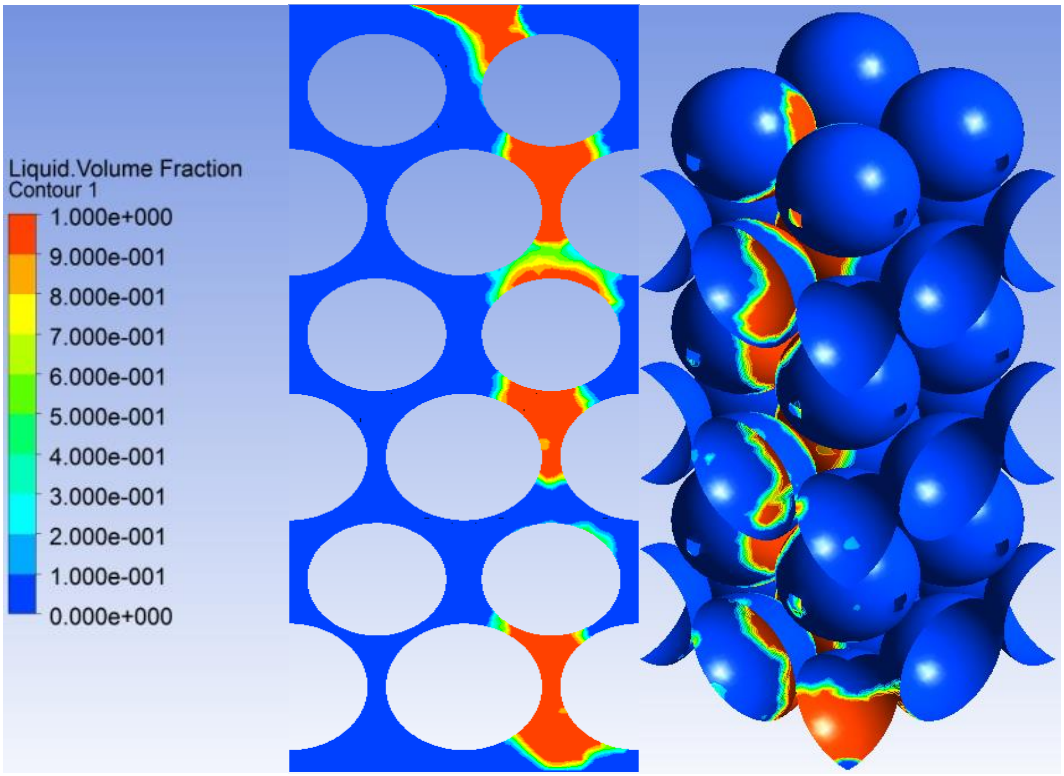

We=0.137

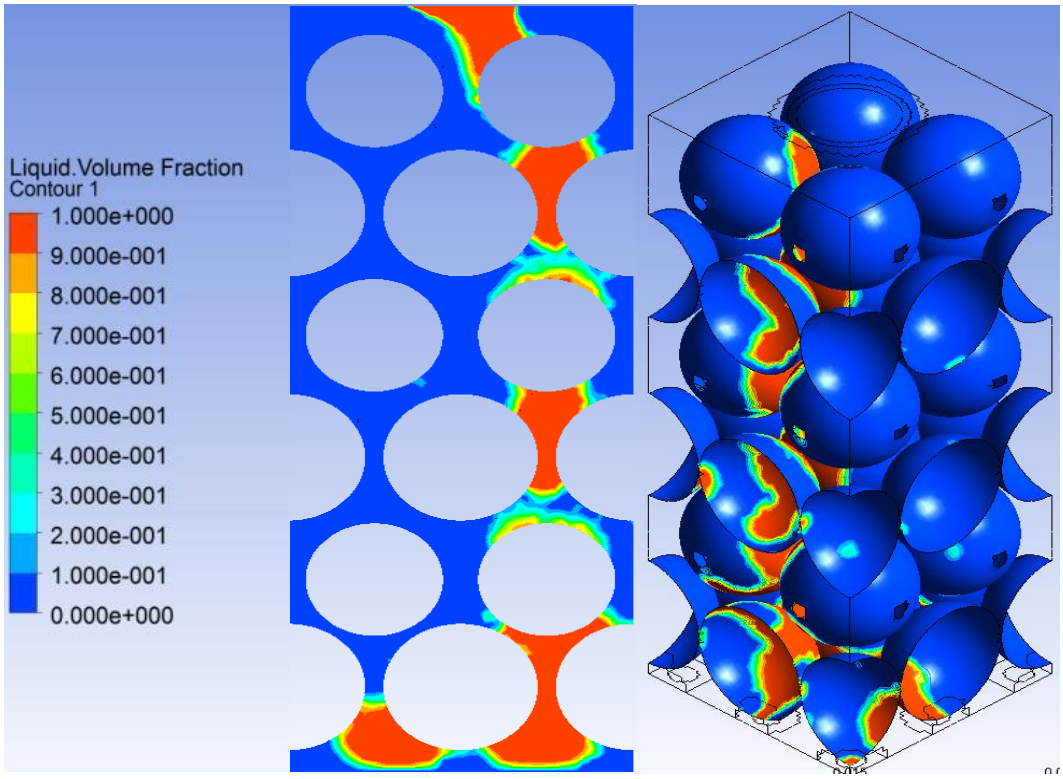

We=0.240

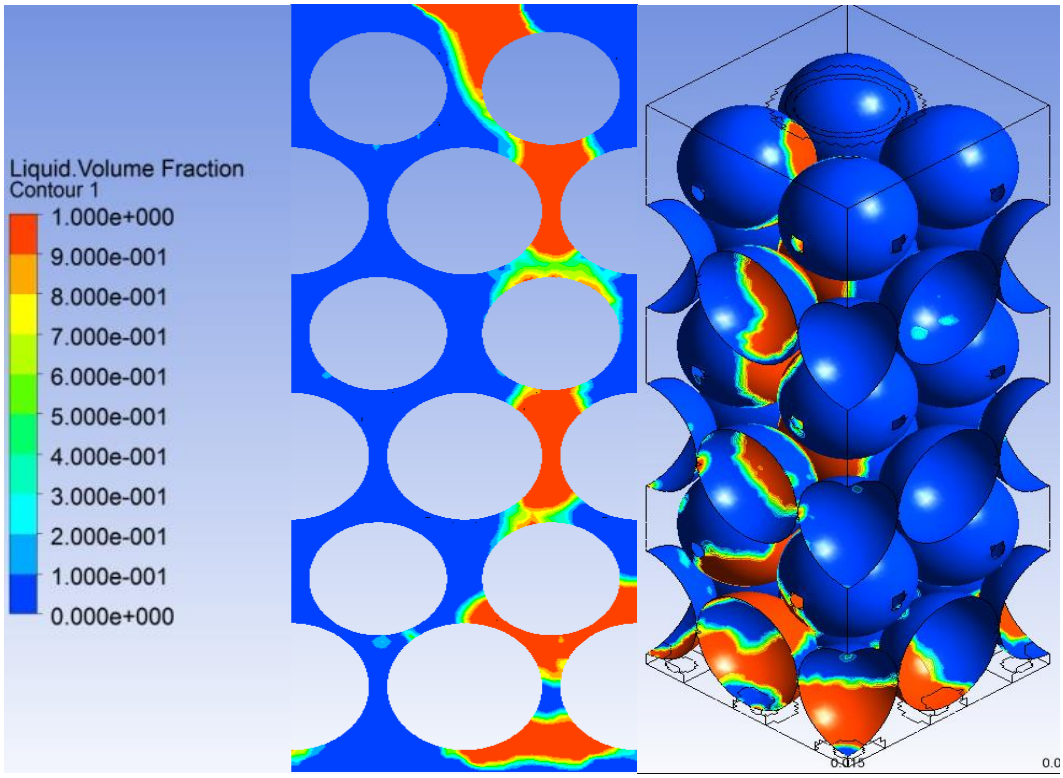

We=0.547

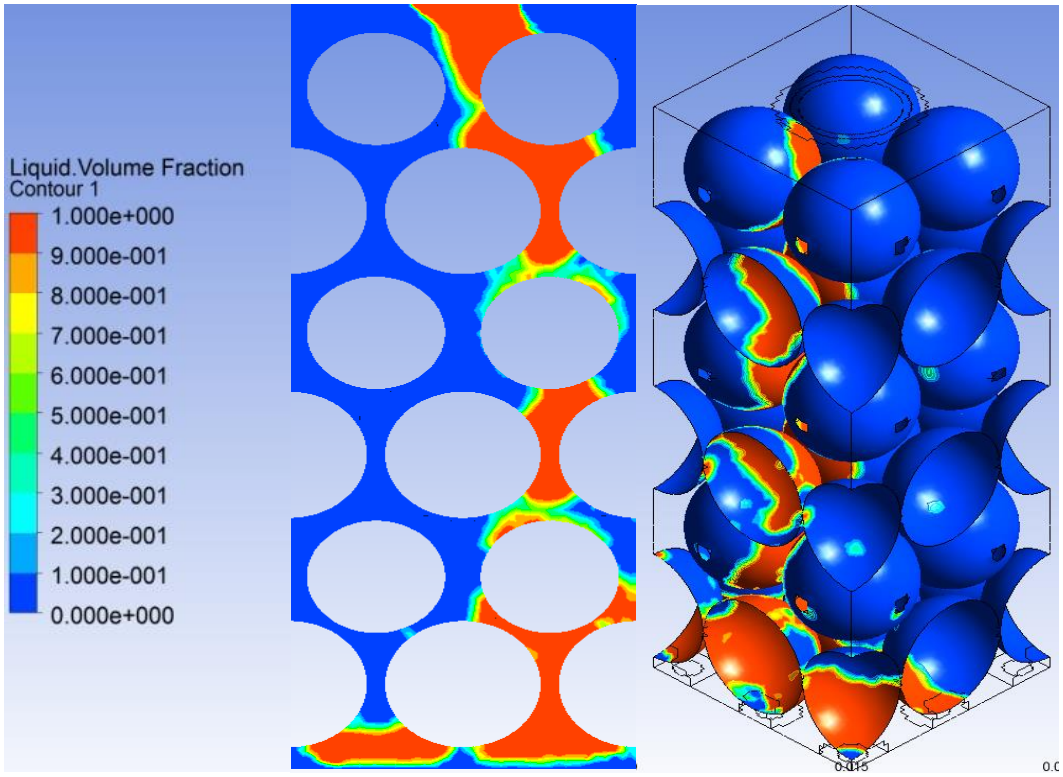

We=0.958

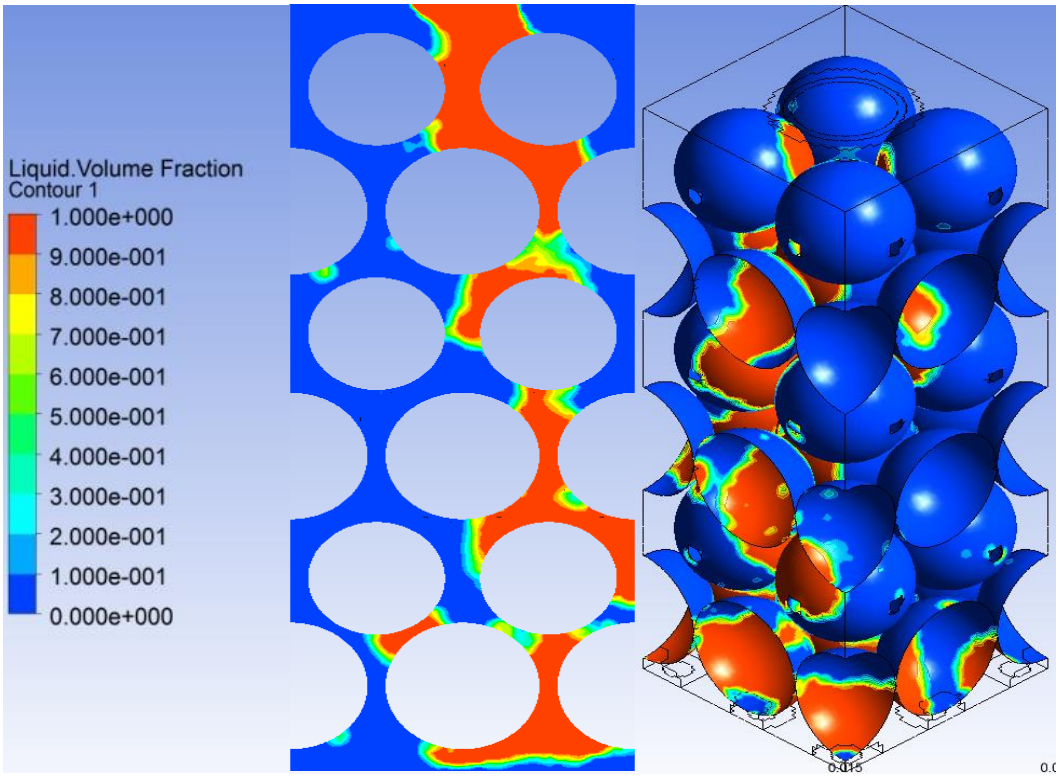

We=1.51

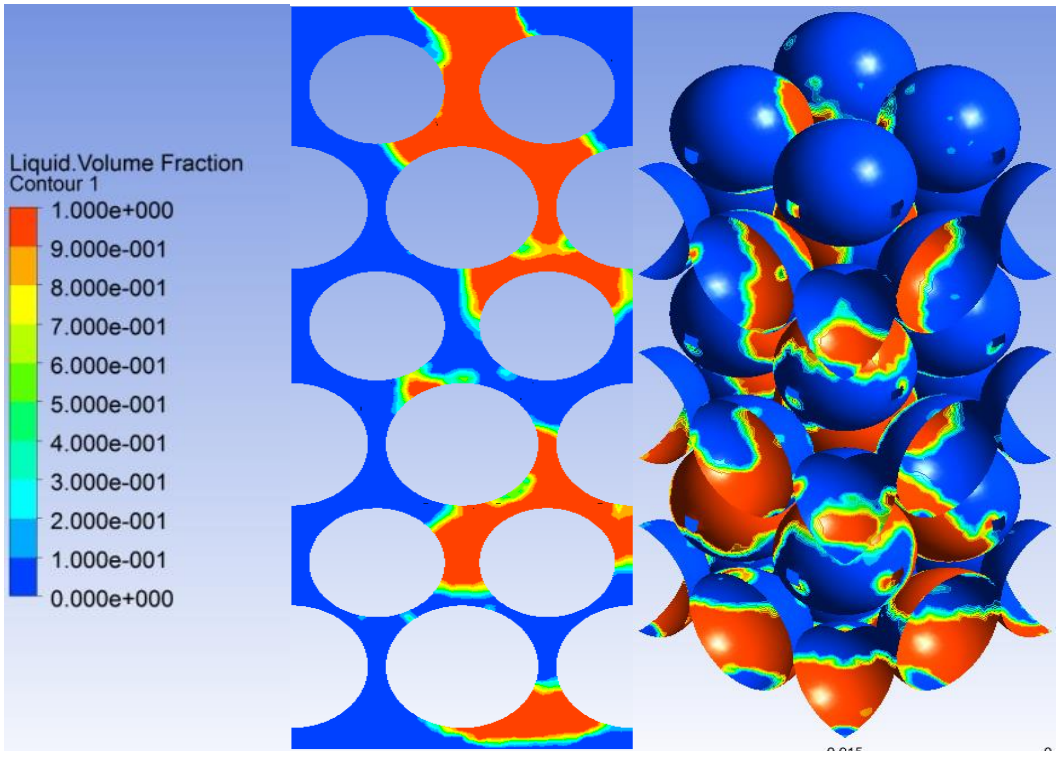

We=2.16

Figure 3.8 Liquid flow regime and wetted area at different liquid *We* numbers from 0.014 to 2.16 at fixed $Re_g = 199$.

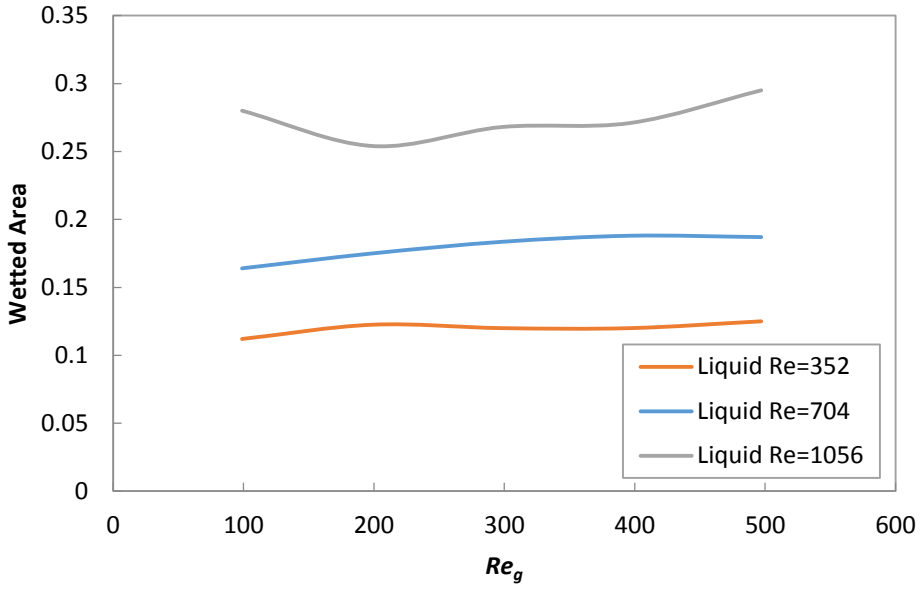

(a)

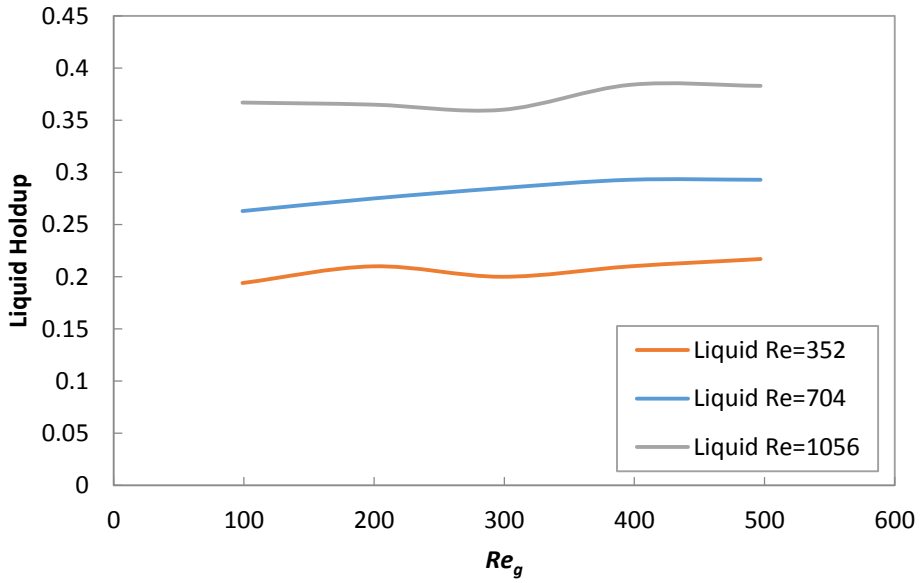

(b)

Figure 3.9 Influence of gas velocity with fixed liquid velocities on (a) wetted area, (b) liquid hold up.

3.3.4 Liquid Holdup, Pressure Drop, Wetted Area, Gas-Liquid Interactions

Figures 3.9 (a) and (b) are plotted to examine dependencies of gas and liquid flow rates on wetted areas and liquid holdups. At a fixed gas flow rate, the wetted area and liquid holdup increased with increased liquid flow rates. However, an increase of gas flow rate had no significant effect on the wetted areas and liquid holdup. These outcomes are distinct from the results of co-current flow modeling analyses (Gunjal, Kashid et al. 2005) in which both wetted areas and liquid holdups decreased with increased gas flow rates.

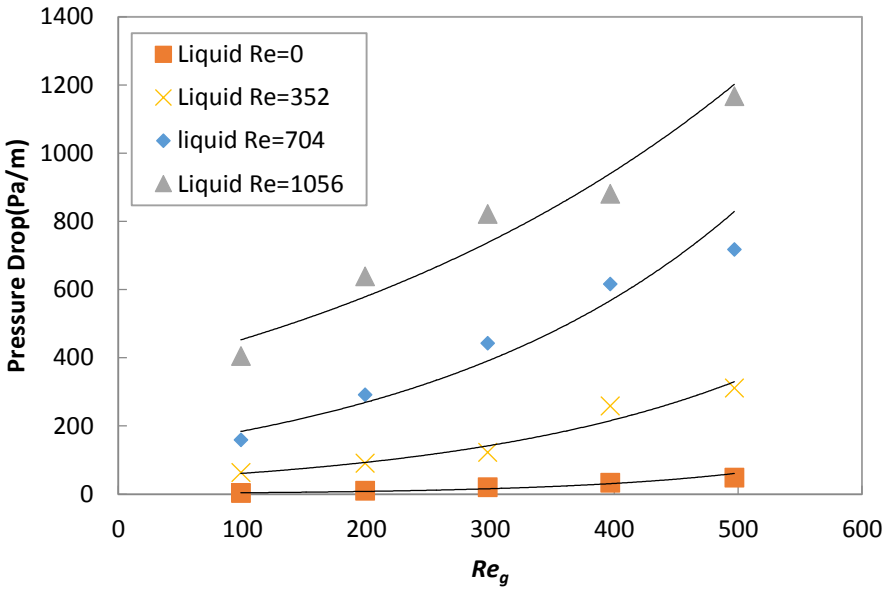

Figure 3.10 Influence of gas flow rate with fixed liquid velocities on pressure drop.

Gas side pressure drops were modeled as a function of liquid flow rates under constant liquid flow rate, as shown in Figure 3.10. The results show that the gas phase pressure drop per unit length of packing increased with both gas and liquid flow rates. At a $Re_L = 0$, the gas side pressure drop was minimal, and then increased rapidly as the liquid flow

rates were increased such that with a $Re_g = 500$ and $Re_L = 1056$ the gas side pressure drop was close to 1200 Pa per meter.

Another representation of use that demonstrates gas-liquid interactions are gas and liquid velocity vectors. Figure 3.11, 3.12 and 3.13 show the gas and liquid velocity vectors when the gas Reynolds number, Re_g, was varied between $Re_g = 199$ to 497 and the liquid Reynolds number, Re_L, was varied between $Re_L = 180$ to 1056. In these three figures the upward vectors depicts gas velocities and the downward vectors depict liquid velocities. At the lowest Reynolds numbers in Figure 3.11, the interaction between the two phases is weak with gas phase flow dominating the middle region of the domain. Increasing the liquid flow rate to $Re_L = 884$, as shown in Figure 3.12, increased interactions between gas and liquids were observed, and these interactions further intensified when increasing flows rate to $Re_g = 497$ and $Re_L = 1056$, as shown in Figure 3.13. In this latter figure, the liquid phase dominates the middle region and the gas phase is entrained into the liquid region. As the liquid fills the domain less space was available for the gas to flow through, hence the velocity of gas phase will be forced to increase and lead to an increase in shear rates at the gas-liquid interfaces.

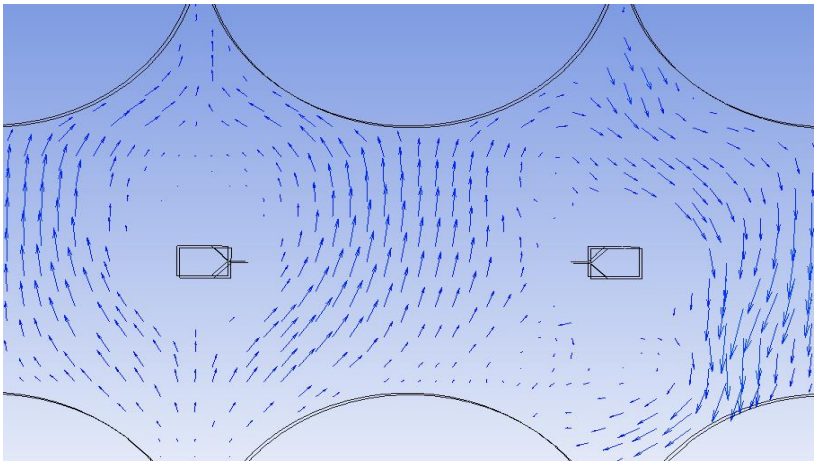

Figure 3.11 Gas and liquid velocity vectors at $Re_g = 199$ and $Re_L = 180$.

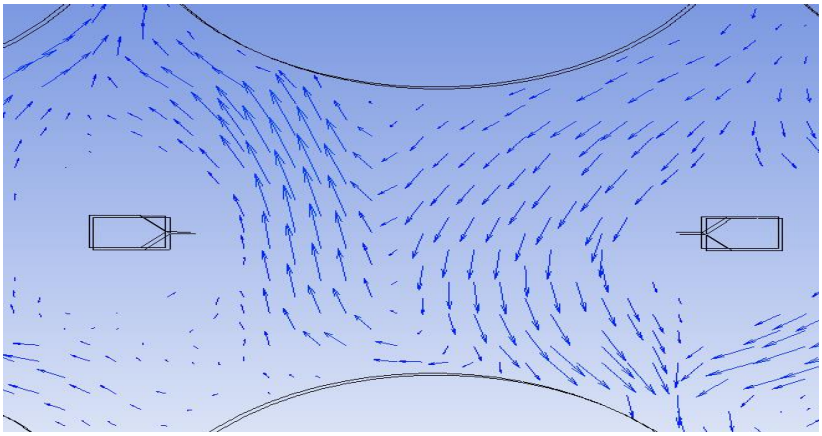

Figure 3.12 Gas and liquid velocity vectors at $Re_g = 199$ and $Re_L = 884$.

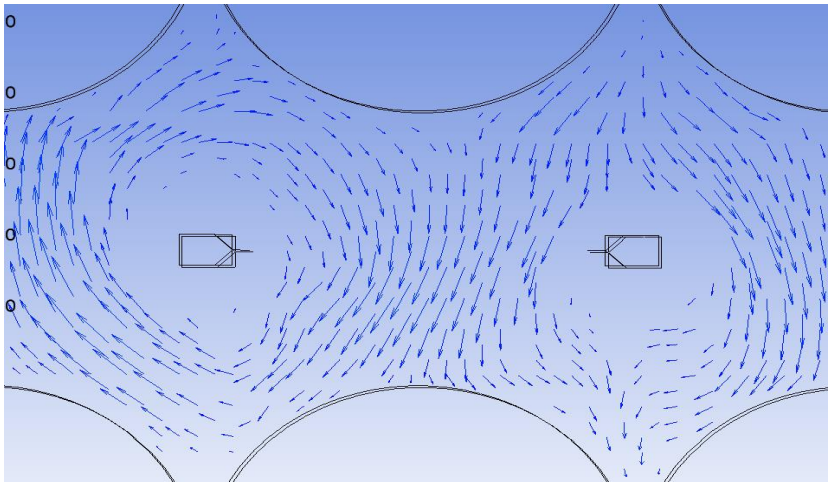

Figure 3.13 Gas and liquid velocity vectors at $Re_g = 497$ and $Re_L = 1056$.

3.3.5 Effect of the Number of Liquid Inlets

The entrance of the reactor is an important region in which flows are initially developed and it can be expected that different flow injection geometry and distribution will affect flow hydrodynamics (Johnston, Zhu et al. 1999) (Maharaj, Pocock et al. 2007). Hence, three different inlet models were constructed to study the effect of the number of inlets. Figure 3.14 shows the three models, with the number of inlets varied between 1-to-4-to13 and their respective diameters varied between 0.0072m, 0.0036m and 0.002m; the diameters were decreased as the number of inlets was increased to maintain a constant liquid inlet area and, hence, a constant inlet velocity. All three models were simulated using identical operation conditions.

Figure 3.15 demonstrates the influence of the number of inlets on wetted area, liquid hold up, pressure drop in which the inlet configurations with four inlets had the highest wetted area and liquid hold up. When the number of inlets was increased from 1-to-13, both the wetted area and liquid hold up was smaller than for four inlets. This result may be a consequence of the ease with which liquid was distributed as small droplets when 13 inlets was used as compared to when four inlets was used. An increased ease of forming small droplets would not be beneficial to liquid film development. The pressure drops were the highest for the case of 13 inlets. Among these three inlet configurations, the best choice from a point of view of mass transfer efficiency because of having the highest liquid hold up and wetted area and lower pressure drop is for four inlets.

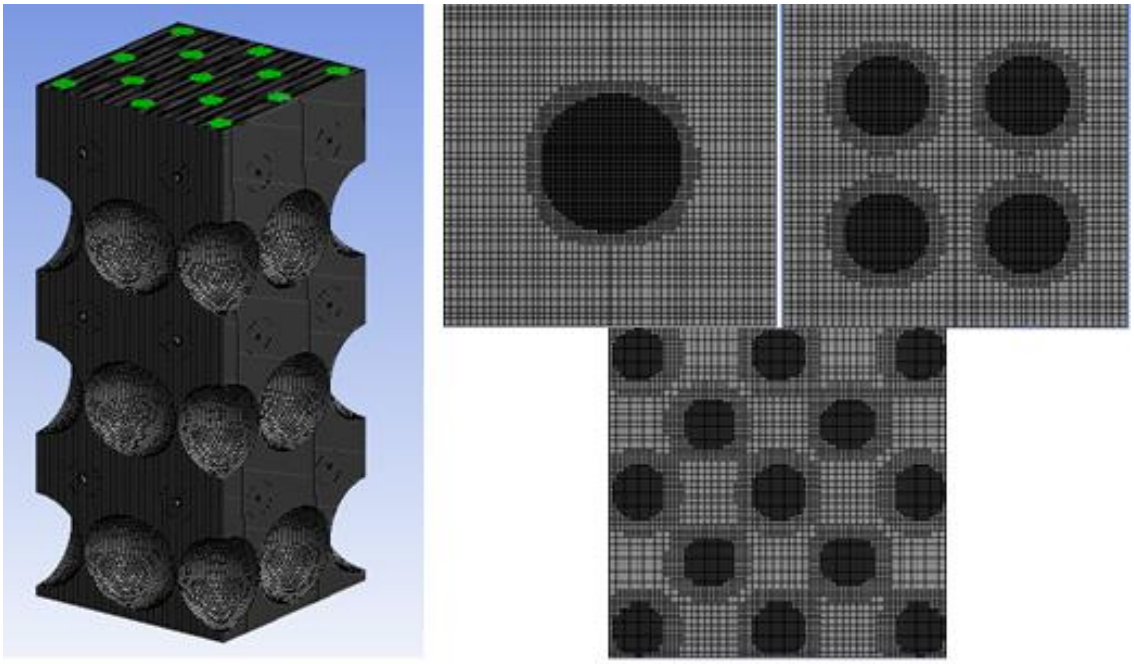

Figure 3.14 CFD model with different numbers of liquid inlet.

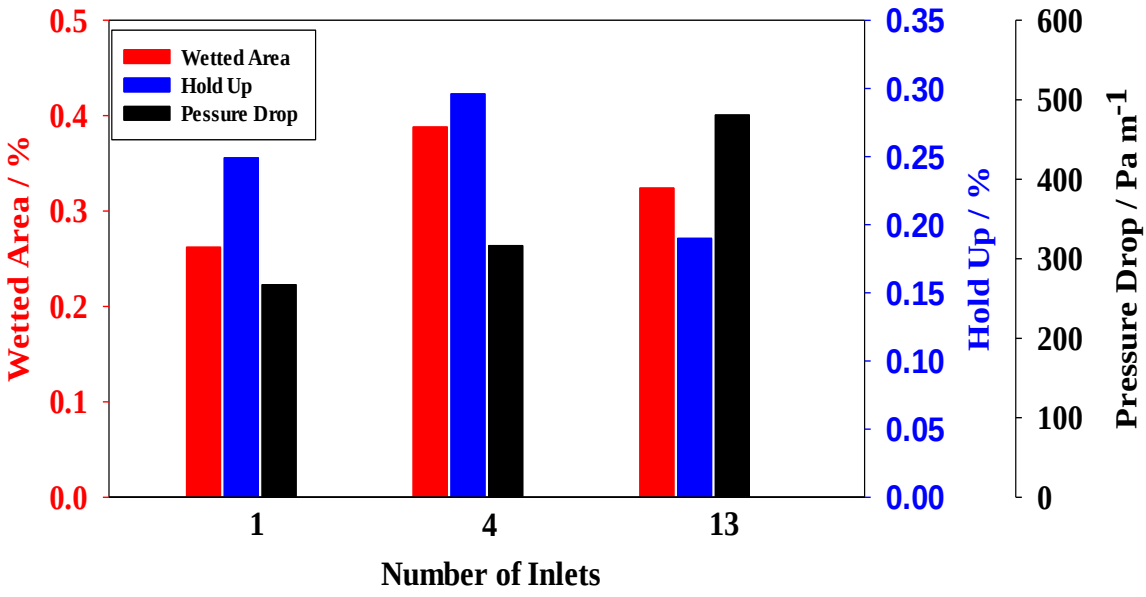

Figure 3.15 Influence of liquid inlet numbers on wetted area, liquid hold up, pressure drop.

3.3.6 Effect of Liquid Surface Tension

During a commercial CO_2 absorption process in a fixed bed, the temperature of the MEA solvent and the carbon loading in the solvent will change with locations in the absorber column which in turn will lead to changes in solvent surface tension. Accordingly, the effects of surface tension on the hydrodynamics in the packed bed were also examined. In this modeling, water was still used as the liquid but its surface tension was changed to mimic expected changes that would occur in a large-scale reactor. Because the surface tension of water is larger than MEA or MDEA solvents used for absorbing CO_2 (Fu, Wei et al. 2013), the surface tension values selected were between 0.005 to 0.07 N/m.

The effects of surface tension on pressure drop, liquid holdup, wetted area and film thickness are shown in Figures 3.16, 3.17, 3.18 and 3.19 in which it can be concluded that the surface tension had an insignificant influence on pressure drop and liquid holdup. However, a lower surface tension did provide a larger wetted area and a thinner film. It is expected that a thick film will not form when the surface tension is small because the liquid would be influenced more by gas flow than if its surface tension was higher. Larger wetted areas and thinner films are preferred in a chemical reaction; hence, a solvent with lower surface tension would be preferred.

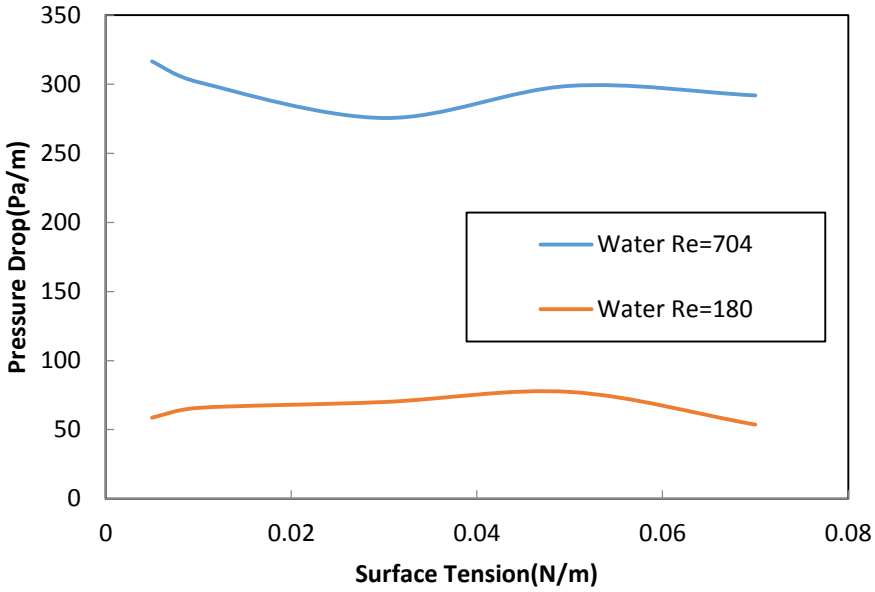

Figure 3.16 Influence of surface tension on pressure drop under liquid flow rate of $Re_L = 180$ and 704.

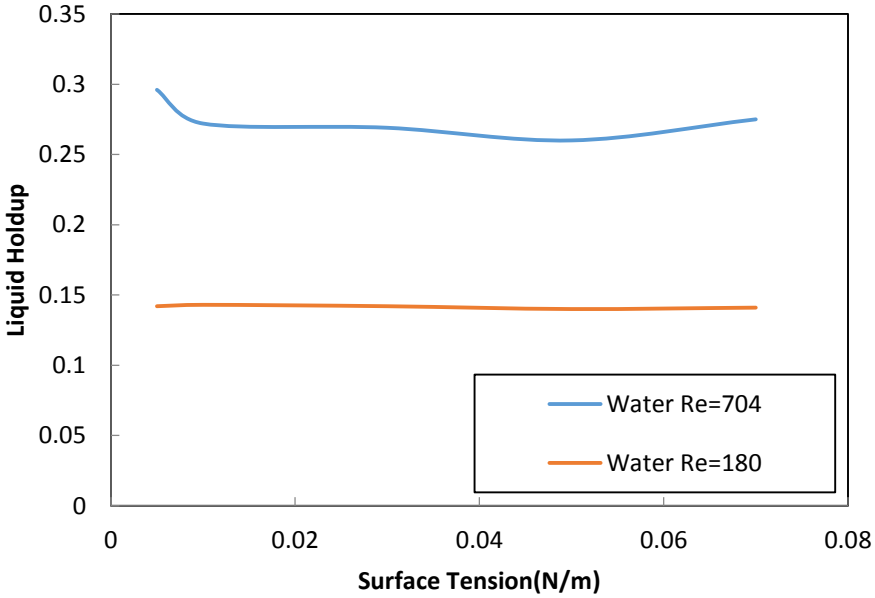

Figure 3.17 Influence of surface tension on liquid holdup under liquid flow rate of $Re_L = 180$ and 704.

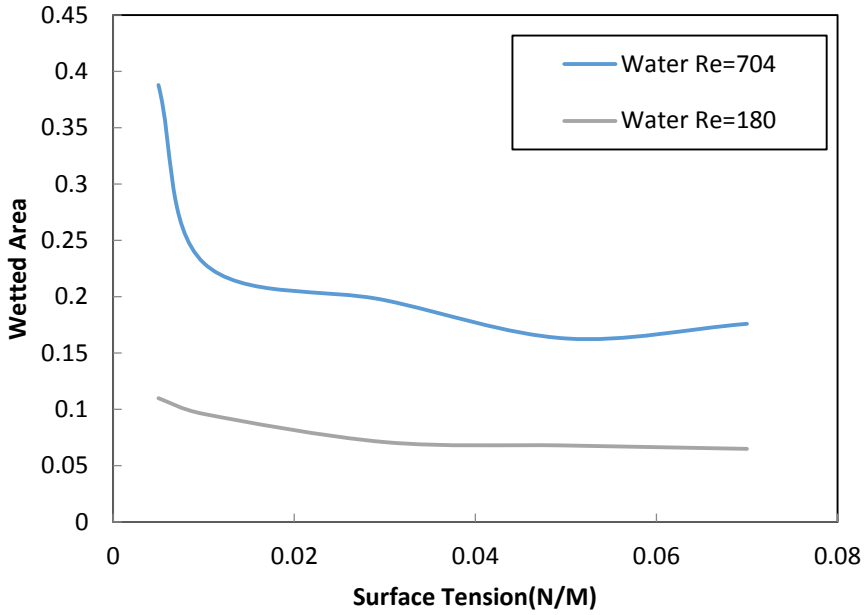

Figure 3.18 Influence of surface tension on wetted area under liquid flow rate of $Re_L = 180$ and 704.

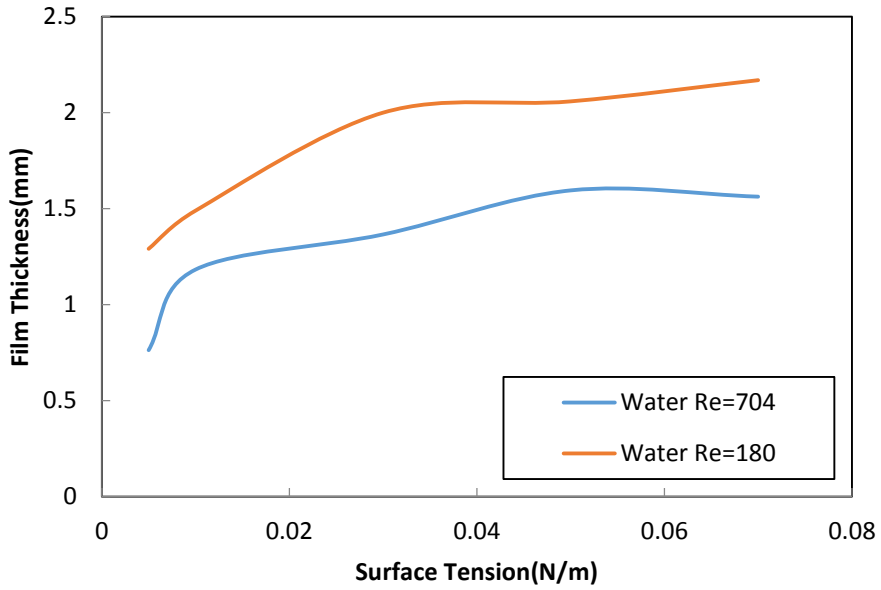

Figure 3.19 Influence of surface tension on film thickness under liquid flow rate of $Re_L = 180$ and 704.

3.4. Conclusions

The hydrodynamics of packed beds with spherical balls was investigated experimentally and computationally. The pressure drops under six different test conditions were obtained during the experimental study. A comprehensive 3D CFD model for counter-current multiphase flow was then developed and validated by comparing its pressure drop results with those from the experiments. Because of model validation, the hydrodynamics of a packed bed reactor with plastic spheres of a specific size and geometry were investigated under various operation conditions. The key findings of this research are as follows:

(1) The 3D CFD model was useful for understanding counter-current flow in a packed bed reactor.

(2) An increase of *We* values led to a more uniform liquid distribution. The flow regime in the bed with spherical ball packing was film flow when *We* was greater than 0.547; the larger the values of *We* to 1.57, the more trickle flow areas were observed.

(3) Liquid holdup and wetted area were increased linearly with increasing liquid flow rates, while gas flow rates had no significant effect on either liquid holdup or wetted area.

(4) Gas side pressure drops increased with increased gas flow rates and liquid flow rates.

(5) Gas-liquid interactions were illustrated using gas and liquid velocity vectors, with these interactions becoming stronger with increasing *Re* values.

(6) The number of liquid inlets affected flow behavior. Increasing the number of inlets did not always enhance wetted areas or liquid holdups. A liquid inlet number of four provided the most wetted area and liquid holdup.

(7) Surface tension had an insignificant influence on pressure drop and liquid holdup; however, lower surface tension provided a larger wetted area and a thinner film.

CHAPTER 4. NUMERICAL SIMULATIONS OF A STRUCTURED PACKED BED

In this chapter the hydrodynamics associated with structured packing in a reactor, based on the CFD model developed in Chapter 3, will be examined. The simulation geometry will be identical to that of the laboratory scale packed bed that was used for CO_2 capture testing. Pressure drop, liquid distribution, liquid hold-up, wetted area and film thickness, as well as liquid-gas interfacial areas, will be analyzed.

4.1 CFD Model Development.

A structured packing in packed beds, as opposed to random packing, is preferred in industrial applications because it can be precisely assembled to control parameters such as packing surface area and void fraction; thereby it is possible to estimate, a priori, the degree to which pressure drops and intimate mixing of phases could be expected. The prevailing structured packing types are listed in Table 4.1. Their primary differences include specific surface areas of the packing,$a_p(m^2m^{-3})$, void fraction, $\epsilon(\%)$, inclined angle, $a(\text{deg})$ and the channel dimensions. Among these, the Sulzer's Mellapak 250 Y is one the most popular packing type that has been quoted within literature on CO_2 absorber processes (Owens, Perkins et al. 2013); the number 250 in its designation indicates a specific surface area of 250 m^2m^{-3} and the symbol of Y means a surface inclined angle of 45^o relative to the flow direction. It may be expected that the hydrodynamics for this packing would be different than that for spherical ball packing discussed in Chapter 3. In this Chapter 4 research, a 3D meso-scale CFD model will be developed to investigate the hydrodynamic characteristics of this complex structured packing with gas-liquid counter-current flows.

Table 4.1 Packing and column characteristics (Petre, Larachi et al. 2003).

Packing type	$a_p(m^2m^{-3})$	$\epsilon(\%)$	$a(\text{deg})$	Channel dimensions(m)		
				Base b	Height h	Sides s
Flexipac 1Y(Koch-Glitsch)	453	91	45	0.0127	0.0064	0.009
Flexipac 2Y(Koch-Glitsch)	223	95	45	0.0255	0.0127	0.018
Flexipac 3Y(Koch-Glitsch)	115	96	45	0.0509	0.0255	0.036
Gempak 1A(Koch-Glitsch)	115	96	45	0.0509	0.0255	0.036
Gempak 2A (Koch-Glitsch)	223	95	45	0.0255	0.0127	0.018
Gempak 3A (Koch-Glitsch)	453	91	45	0.0127	0.0064	0.009
Mellapak 250Y (Sulzer)	250	96	45	0.0267	0.012	0.017
Mellapak 250X (Sulzer)	250	96	60	0.0267	0.0119	0.017

Sulzer's Mellapak 250 Y is made of corrugated metal sheets arranged side-by-side with opposing channel orientations, as illustrated in Figure 4.1 (a) and (b). The structure is mathematically represented by stacked slices; to save on computational time, the modeling of each slice was simplified by assessing only one, averaged channel with a simulation geometry as shown in Fig. 4.1 (c). A single "sandwiches-like" packing was generated and had a 12mm height, 26.7 mm width and 2mm air gap between the slices with an inclined angle of 45^o with respect to the inlet flow direction. The liquid inlet was at the top of the domain with a depth of 1mm between the inlet and the top of the packing; the total height of the packing was 80mm.

Water and air were used as the flow agents, and they flowed in counter-current directions, as shown in Figure 4.3. Because the "sandwich-like" domains were only part of the packed bed from a packed column, the side wall boundaries were set as symmetric boundaries with boundary conditions given in Table 4.2. As described in Chapter 3, the VOF model was used during the simulations.

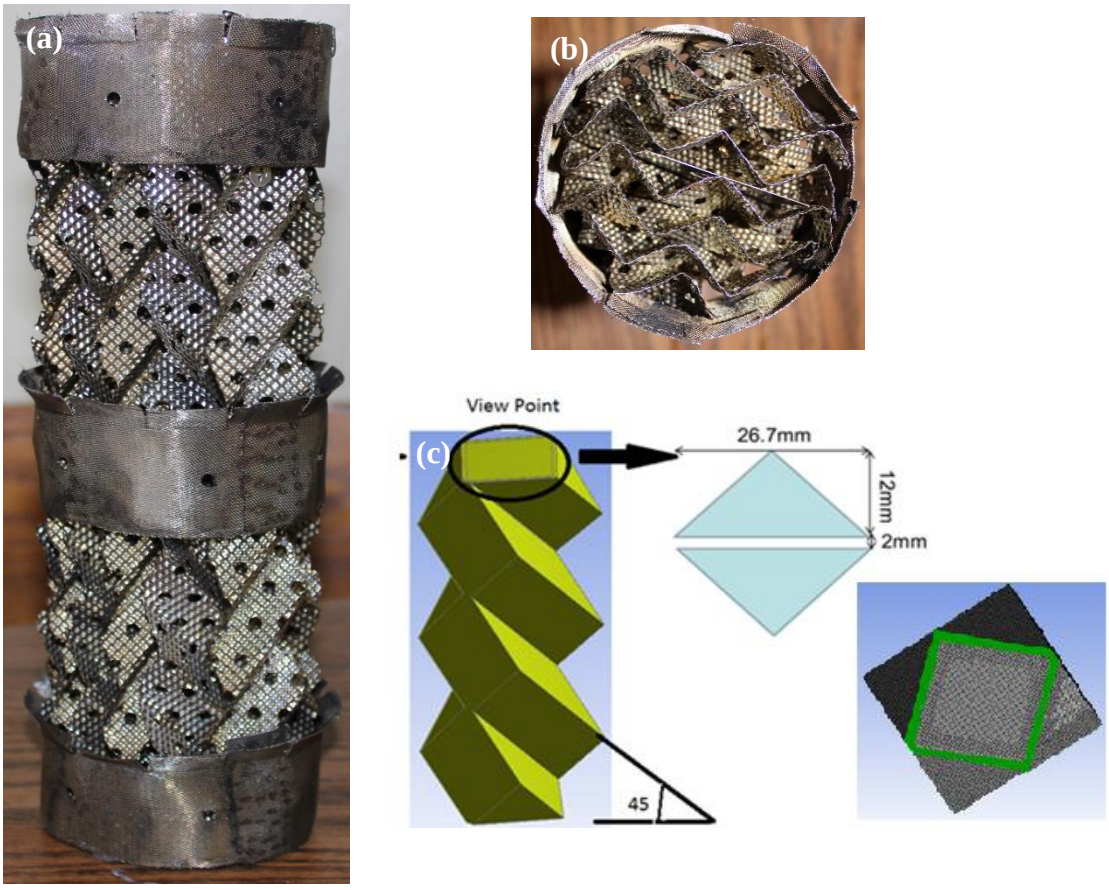

Figure 4.1 Images of the structured packing within a bed: (a) Overview; (b) Top View; and (c) the geometric model used during CFD analyses.

Mesh generation followed the procedures described in Chapter 3. The CutCell meshing method used a mesh spacing from 2×10^{-4} m to 8×10^{-4} m; in total, the mesh included 3.7×10^{5} elements. Close to solid surfaces the mesh was refined for a more accurate

determination of the liquid-film thickness, and it became coarser away from these surfaces. Details of the mesh structure are provided in Figure 4.2.

The meshed file was imported into and checked by the ANSYS Fluent solver which assessed issues that would create warning messages. The simulation also used a transient state model to observe the growth of liquid film and the development of gas-liquid interactions. The time step size for this model was 5.0×10^{-4} s while solving a maximum of 30 iterations per time step. When the time step size was then changed to 5.0×10^{-5} s for a better convergence, the total computation time was close to 120 hours for each case. Table 4.2 show the details of boundary conditions of all simulations.

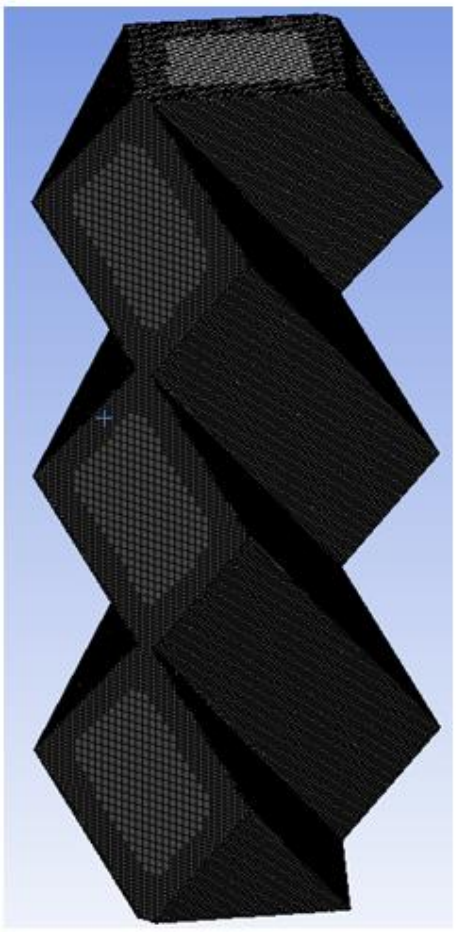

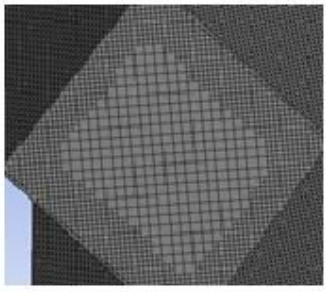

Details of "Mesh"	
Physics Preference	CFD
Solver Preference	Fluent
Relevance	0
Sizing	
Use Advanced Size Function	On: Curvature
Relevance Center	Coarse
Smoothing	Medium
Curvature Normal Angle	Default (18.0 °)
Min Size	2.e-004 m
Max Size	8.e-004 m
Growth Rate	Default (1.20)
Minimum Edge Length	1.3514e-005 m
Inflation	
Assembly Meshing	
Method	CutCell
Feature Capture	Program Controlled
Tessellation Refinement	Program Controlled
Statistics	
Nodes	356092
Elements	370804
Mesh Metric	None

Figure 4.2 Mesh model and the details of the mesh.

Table 4.2 Details of boundary conditions of all simulations.

Boundary	Materials	Type	Value	Velocity	Reynolds Number	Weber Number
Liquid inlet	Water	Mass Flow Rate	12.2-48.8(m^3/m^2/h)	0.015-0.488(m/s)	15-488	0.02-3.4
Gas inlet	Air	Velocity(m/s)	0.5-1.1(m/s)	0.5-1.1(m/s)	325-1226	
Liquid outlet		Pressure-outlet	0 Pa			
Gas outlet		Pressure-outlet	0 Pa			

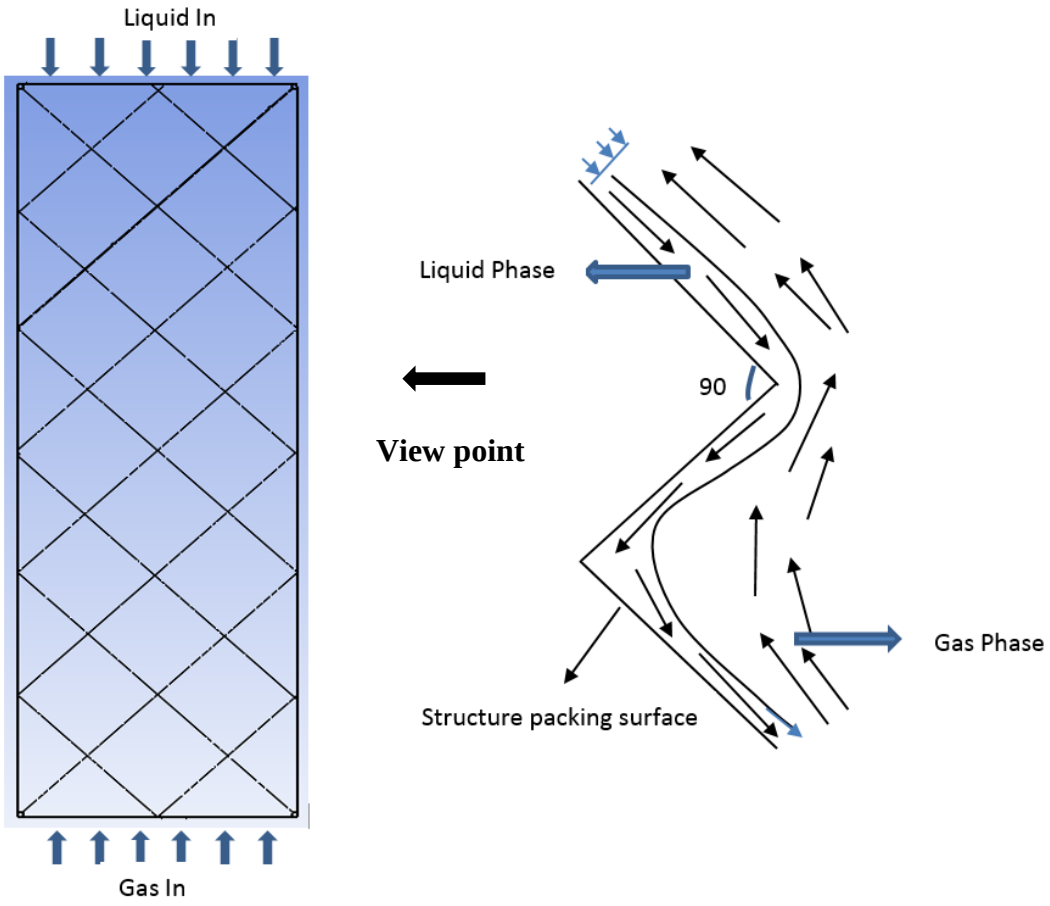

Figure 4.3 Schematic overview of flow directions.

4.2 Results and Discussion

4.2.1 Steady State Determination

Figure 4.4 shows the evolution of wetted area as a function of time at various liquid flow rates (represented by the liquid Reynolds numbers) with the gas flow rate fixed at $Re_g = 911$. The time to achieve a steady state flow area was near 0.35 s when the liquid flow rate was $Re_L = 15$ and this time dropped to 0.23 s for liquid flow rate of $Re_L = 488$. Increasing the gas flow rate (as represented by the gas side Reynolds number) increased the time needed to attain steady state wetted area; this trend was more obvious at the lower liquid flow rates.

The data in Figure 4.5 show that when the gas flow rate was $Re_g = 1106$ and the liquid flow rate was $Re_L = 15$ the time to attain steady state in wetted area was 0.45s; steady state was attained within 0.25 s at $Re_L = 488$ and $Re_g = 1106$. Hence, increased liquid flow rates at constant gas flow rates decreased the time to achieve steady state, as was also observed in Figure 4.4. However, a higher gas flow rate increased the time to achieve steady state for each liquid flow rate. The flow in the packed bed was considered steady or pseudo-steady at times beyond that needed to achieve steady state wetted area.

4.2.2 Liquid Holdup and Pressure Drop

Empirical models to predict the liquid holdup and pressure drop have been developed for a structured packing (Billet R., 1984) using for eight different packing types; empirical relationship for liquid holdup prediction was:

$$h_0 = 0.555\left(U_L^2 \frac{a}{g\varepsilon^{4.65}}\right)^{1/3} \quad (4.1)$$

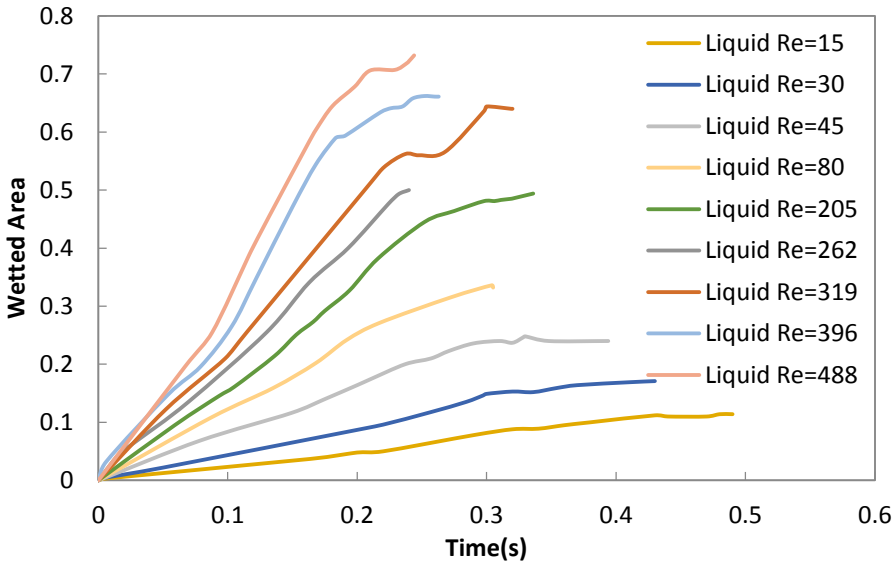

Figure 4.4 The evolution of wetted area with time while varying liquid flow rates at a fixed the gas flow rate of $Re_g = 911$.

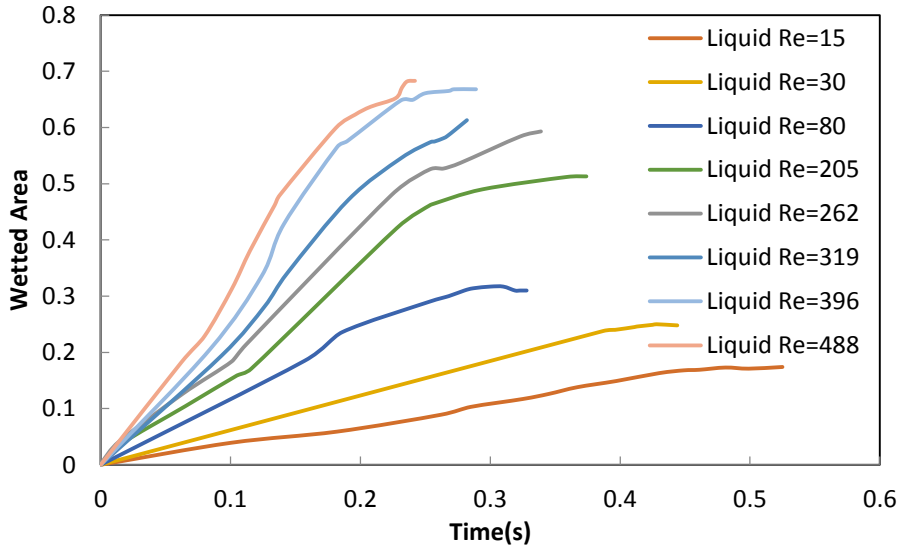

Figure 4.5 The evolution of wetted area with time with varying liquid flow rates and a fixed gas rate of $Re_g = 1106$.

where U_L is the liquid velocity in m/s, a is the specific surface area in m^2 m^{-3}, g is the gravity in m/s^{-2}, and ε is the void fraction. This result predicted that liquid hold-up was

affected by the liquid velocity, specific area of the packing and the void fraction, and then was validated for an air/water system at low flow rates. Hence, the simulation of liquid holdup using the CFD model developed firstly, also at low liquid flow rates and three different gas flow rates, were compared to this empirical equation to assess whether agreement between the two results of the two approaches; this comparison is presented in Figure 4.6 for liquid holdup. Good agreement for the liquid holdup is found for the results of this comparison. The simulation results indicated that different gas flow rate had only a very weak effect on liquid holdup which is consistent with data from the empirical model study. Such weak dependency to the gas flow rates may be a result of the liquid film becoming thinner with increasing gas flow rates (Iliuta and Larachi 2001).

Figure 4.7 (a)-to-(c) show a comparison of gas phase pressure drops as calculated from an empirical model (Stikkelman, de Graauw et al. 1989) displayed in Equation 4.2 and from CFD calculations during this dissertation research. The foundation of this empirical relationship was the Ergun equation (Ergun, S. 1952) after modification to account for the presence of a liquid; it predicts that changes in the pressure drop are caused by the liquid and independent of liquid drag on the gas flow. From Figure 4.7 (a), (b) and (c), pressure drops from both the empirical model and the CFD simulation increased monotonically with increased liquid flow rates and gas flow rates, and simulation results agreed quite very well with Stichlmair model, except that for the case when $Re_g = 1431$. Because, perhaps, the Stichlmair model was validated for gas side Re_g is only between 1 and 1000. Because the pressure drops and liquid holdups obtained from the current simulation were consistent with two different empirical models, the CFD model was considered validated for structured packing.

$$\frac{\Delta P}{l} = \frac{3}{4f_0'\left[\frac{1-\varepsilon'}{\varepsilon'^{4.65}}\right]\rho_g U_g^2} / d_p' \tag{4.2}$$

Where $f_0' = f_0\left\{\left[1-\varepsilon\left(1-\frac{h_o}{\varepsilon}\right)\right]/(1-\varepsilon)\right\}^{c/3}$, ρ_g is gas density, Ug is gas velocity.

$f_0 = \frac{C_1}{Re_g} + \frac{C_2}{Re_g^{1/2}} + C_3$, in this type packing, $C_1 = 5$, $C_2 = 3$, $C_3 = 0.45$

$$\varepsilon' = \varepsilon(1-\frac{h}{\varepsilon})$$

$$c = \frac{[-\frac{C_1}{Re_g} - \frac{C_2}{2Re_g^{\frac{1}{2}}}]}{f_0}$$

$$d_p' = d_p\left\{\left[1-\varepsilon\left(1-\frac{h}{\varepsilon}\right)\right]/(1-\varepsilon)\right\}^{1/3}$$

$$d_p = 6(1-\varepsilon)/a$$

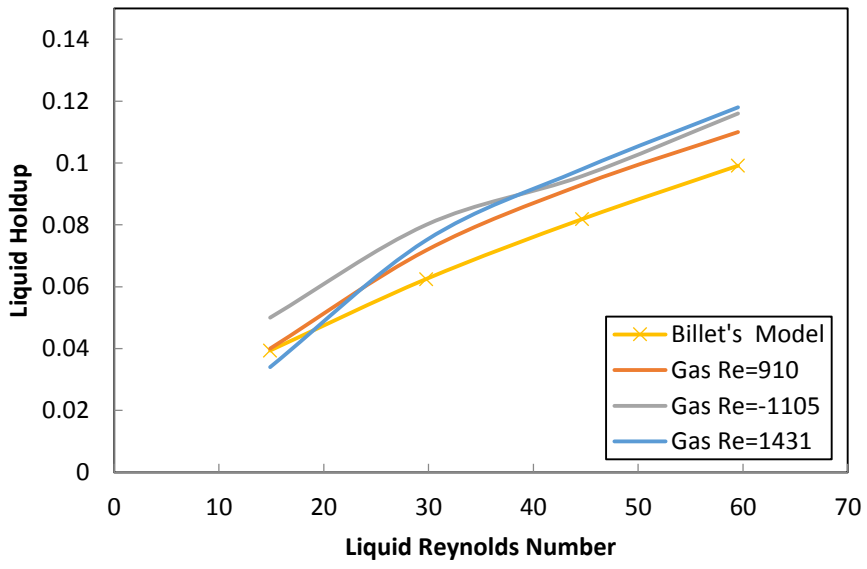

Figure 4.6 Comparison of liquid hold up when using Billet's (Billet, R. and Mackowiak, 1984) empirical model and CFD simulation results at different gas flow rates.

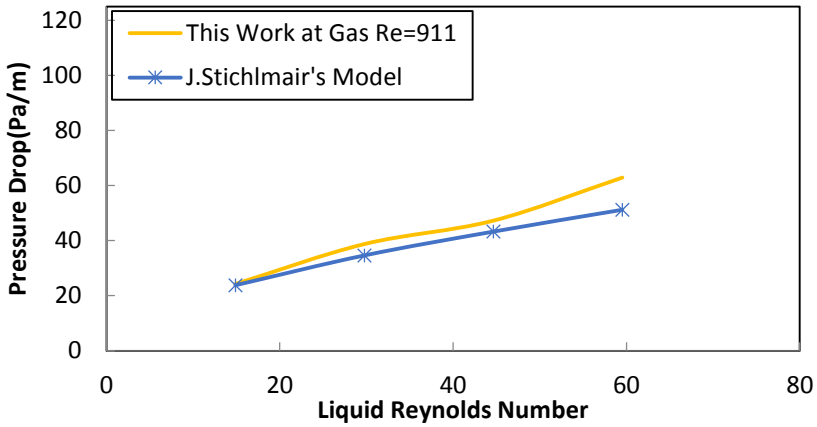

(a)

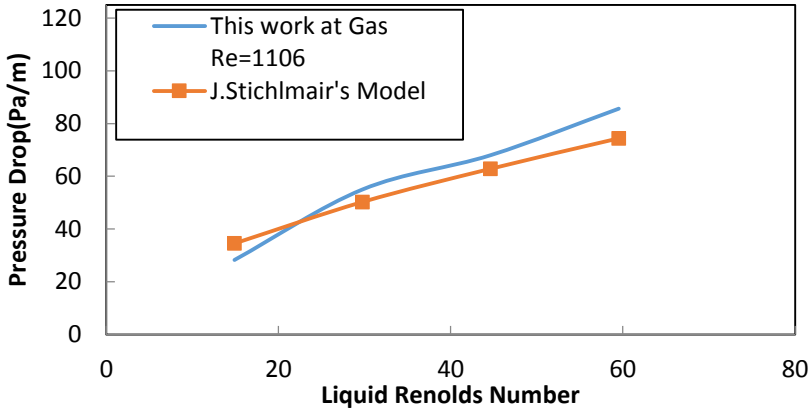

(b)

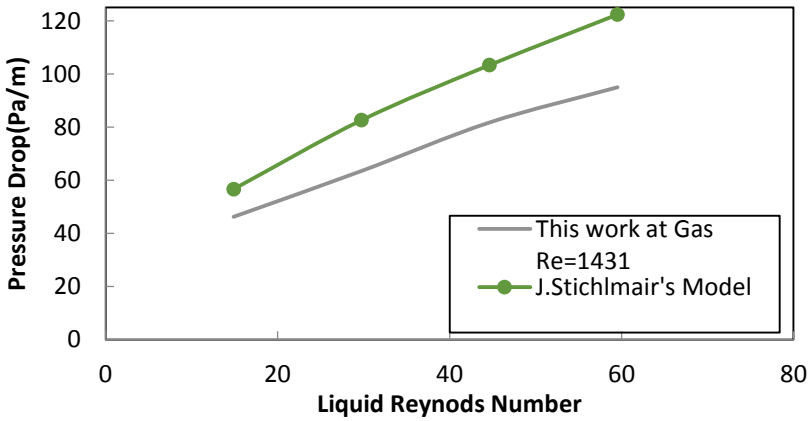

(c)

Figure 4.7 A comparison of pressure drops from J.Stichlmair's (Stikkelman, de Graauw et al. 1989) empirical model and the CFD simulation results for three different gas flow rates: (a) $Re_g = 911$, (b) $Re_g = 1106$, (c) $Re_g = 1431$.

Since the validity of the empirical models was limited to low liquid flow rate, it was considered of possible interest to study pressure drop and liquid hold up at high liquid and gas flow rates. Figure 4.8 shows liquid holdups and Figure 4.9 shows pressure drops when using high liquid flow rates, withe Re_L between 205-to-488, and varying gas flow rates. In agreement with the previous results when using low liquid flow rates, the gas flow rate had no significant effect on liquid holdup although liquid holdup did increase as the liquid flow rate was increased. Pressure drops, in general, showed monotonic increases with both increased gas and liquid flow rates, with the dependency on gas flow rates more pronounced when the gas flow rate $Re_g$was greater than 911 and when higher liquid flow rates were used. For example, at a high liquid flow rate of $Re_L = 488$ and increasing of the gas flow rates resulted in sharp increases of the pressure drop, whereas at liquid flow rate of $Re_L = 205$ the increases in gas flow rates did not appreciably affect pressure drop. These differences may be explained by enhanced gas-liquid interactions at the higher gas and liquid flow rates. For example, by viewing the results in Figure 4.10 it is evident that the extent to which the liquid was in contact with the solid surface was less for $Re_g = 650$ than for $Re_g = 911$. In other words, more of the liquid is blown away from the surface at the higher gas flow rates and, when this occurs, some of the liquid film would have transitioned into droplets. If so, the flow regime would have changed from film flow to trickle flow and more energy, as evidenced by a rapid increase in pressure, is consumed to support droplets formation.

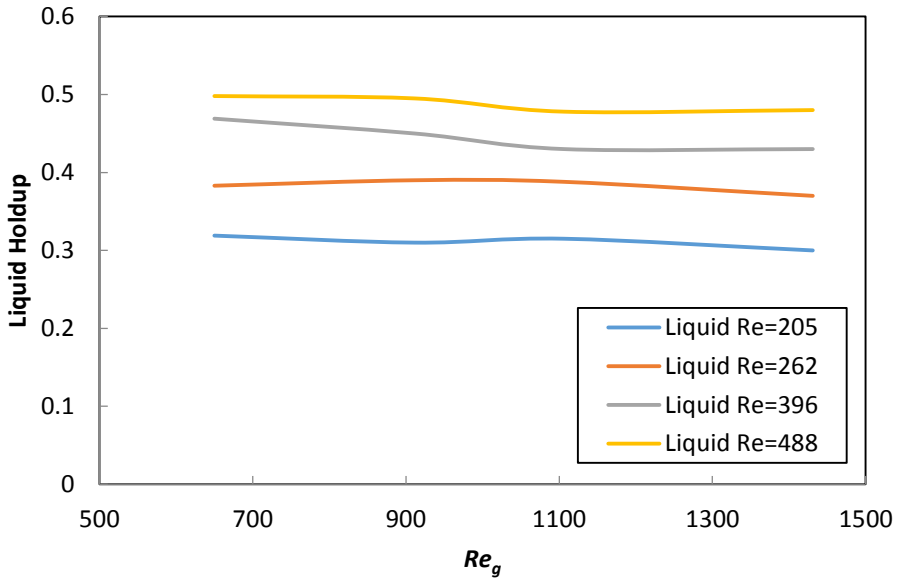

Figure 4.8 Influence of gas flow rate with fixed liquid flow rate on liquid holdup.

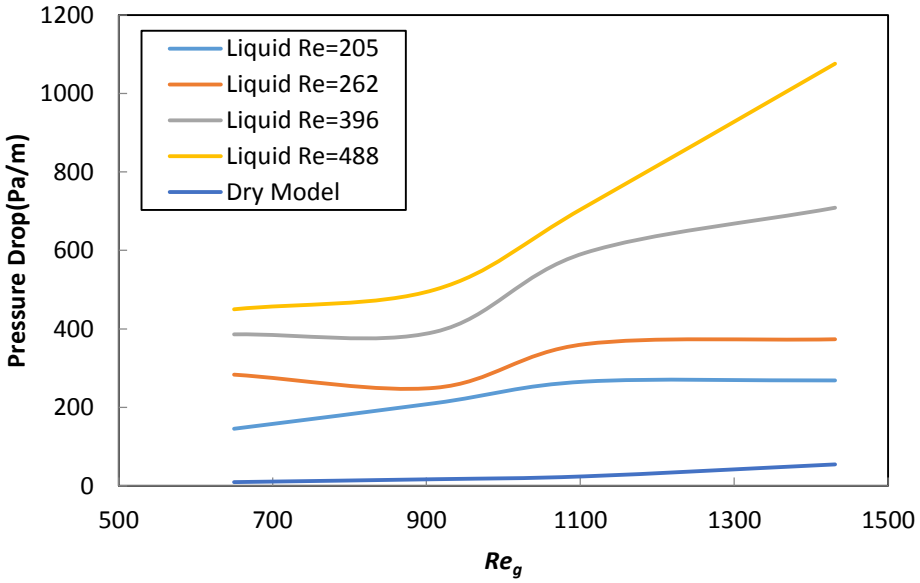

Figure 4.9 Influence of gas flow rates with fixed liquid velocities on pressure drop.

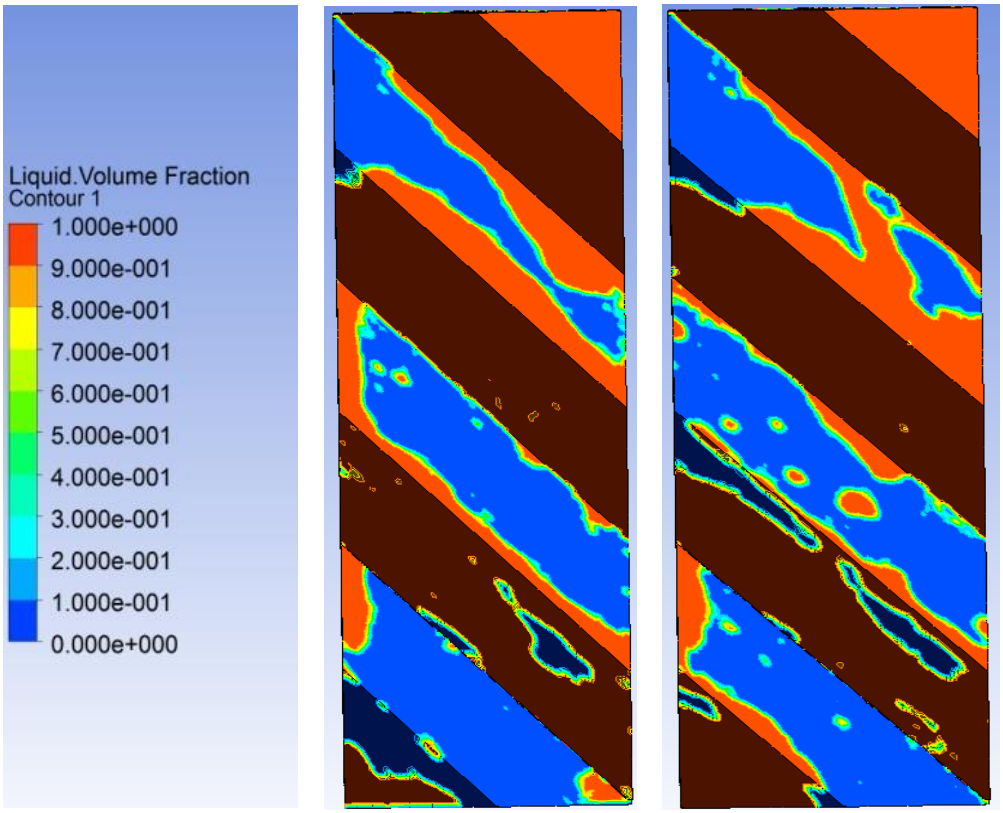

(a) Gas Re=650, (b) Gas Re=911

Figure 4.10 Liquid distribution at (a)$Re_g = 650$; (b) $Re_g = 911$ under $Re_L = 488$.

4.2.3 Liquid Distribution, Flow Regime, Film Thickness and Gas-Liquid Interactions

The development of various flow regimes and liquid distributions as We was increased from 0.57 to 5.13 are depicted in Figure 4.11 as iso-surfaces for a liquid volume fraction of 0.005; the gas flow was fixed with $Re_g = 1431$. Because the side walls were set as symmetrized segments, the flow is shown in a rotated orientation and the liquid is shown to continuously flow down the packing surface following a "Z" shape. When *We* = 0.57, the flow regime was film flow and the surface of the packing was partially wetted. When *We* = 2.21, the flow regime was close to trickle flow and some of the liquid was broken into droplets which are supported by the gas phase flow; at this condition, the surface of

the packing was almost fully wetted with some areas not fully wetted which we called is dead zone. In general, as *We* was increased, the dead zone of the packing surface were decreased but not fully eliminated.

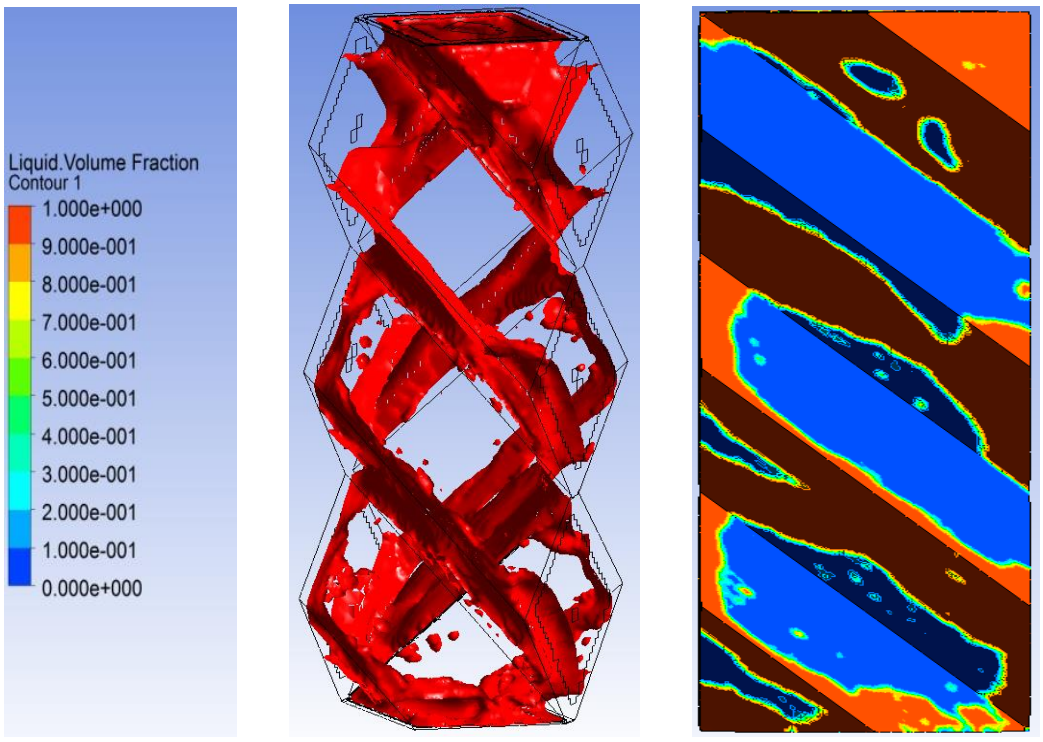

We=0.57

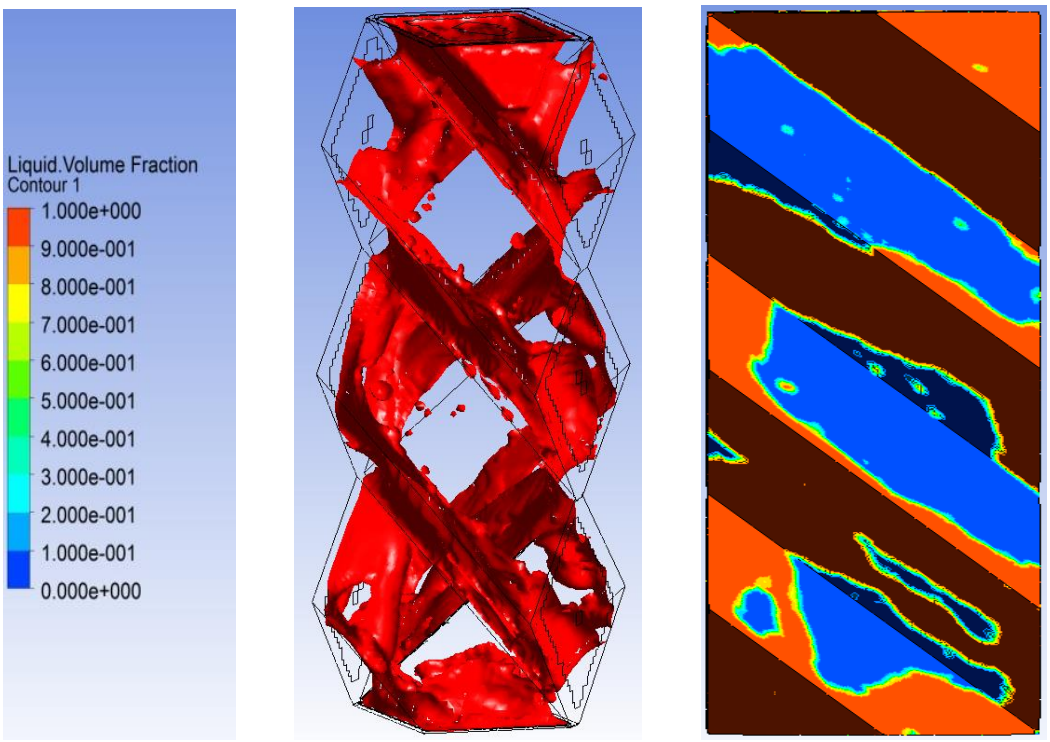
Liquid.Volume Fraction
Contour 1
1.000e+000
9.000e-001
8.000e-001
7.000e-001
6.000e-001
5.000e-001
4.000e-001
3.000e-001
2.000e-001
1.000e-001
0.000e+000

We=0.96

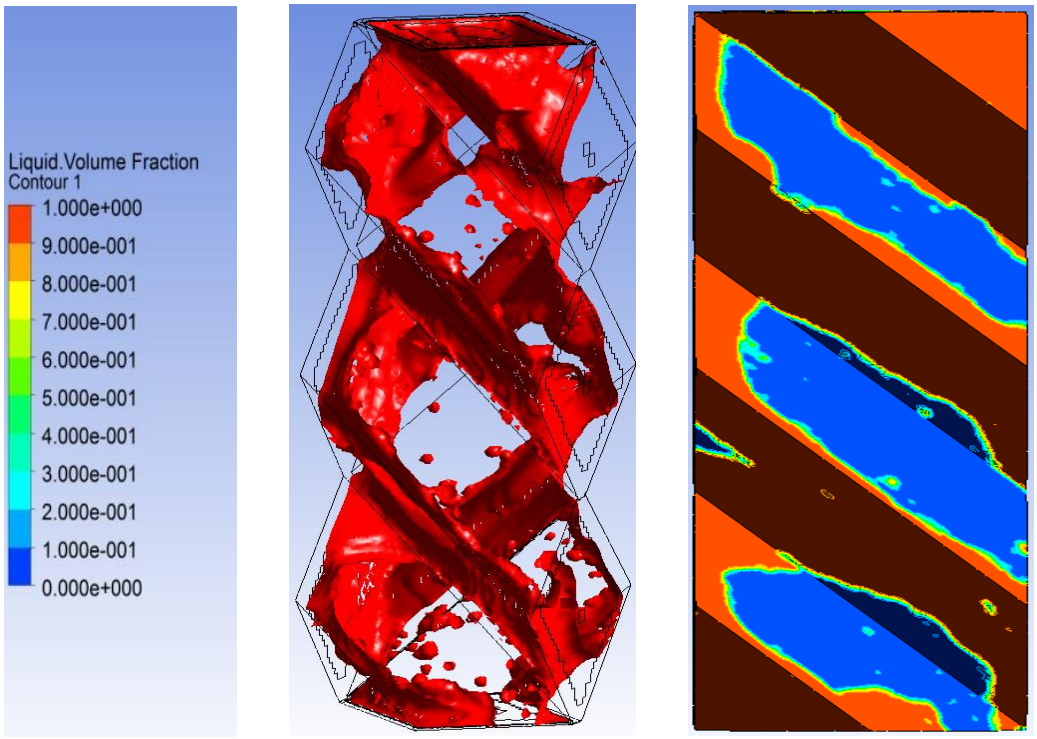
Liquid.Volume Fraction
Contour 1
1.000e+000
9.000e-001
8.000e-001
7.000e-001
6.000e-001
5.000e-001
4.000e-001
3.000e-001
2.000e-001
1.000e-001
0.000e+000

We=1.46

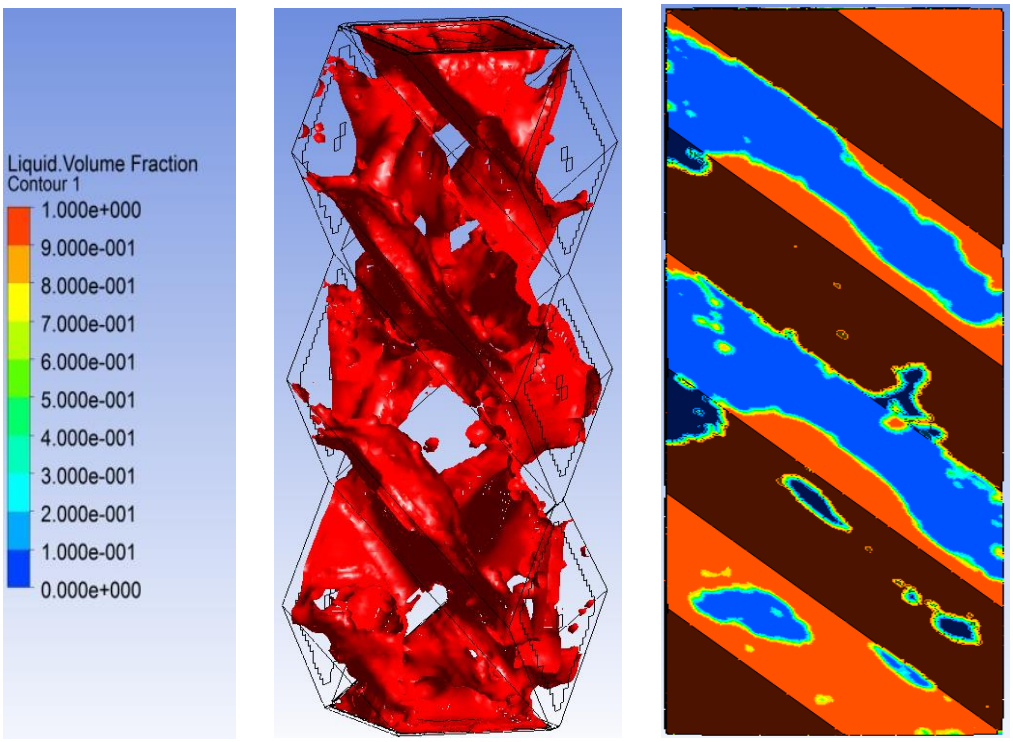
Liquid.Volume Fraction
Contour 1
1.000e+000
9.000e-001
8.000e-001
7.000e-001
6.000e-001
5.000e-001
4.000e-001
3.000e-001
2.000e-001
1.000e-001
0.000e+000

We=2.21

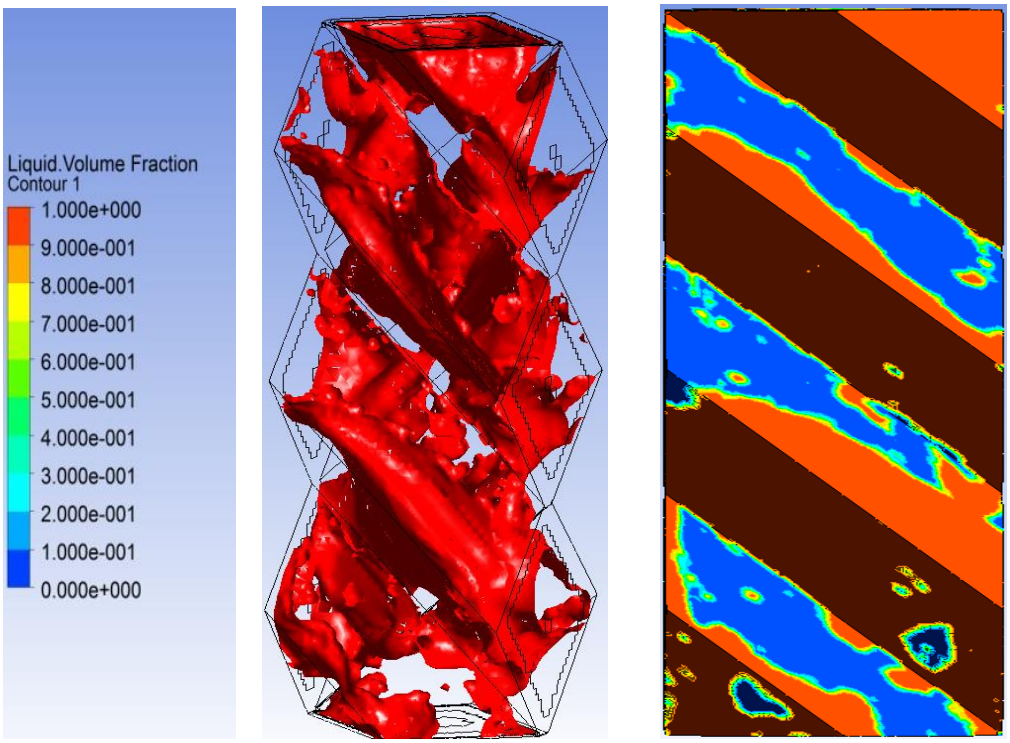
Liquid.Volume Fraction
Contour 1
1.000e+000
9.000e-001
8.000e-001
7.000e-001
6.000e-001
5.000e-001
4.000e-001
3.000e-001
2.000e-001
1.000e-001
0.000e+000

We=3.28

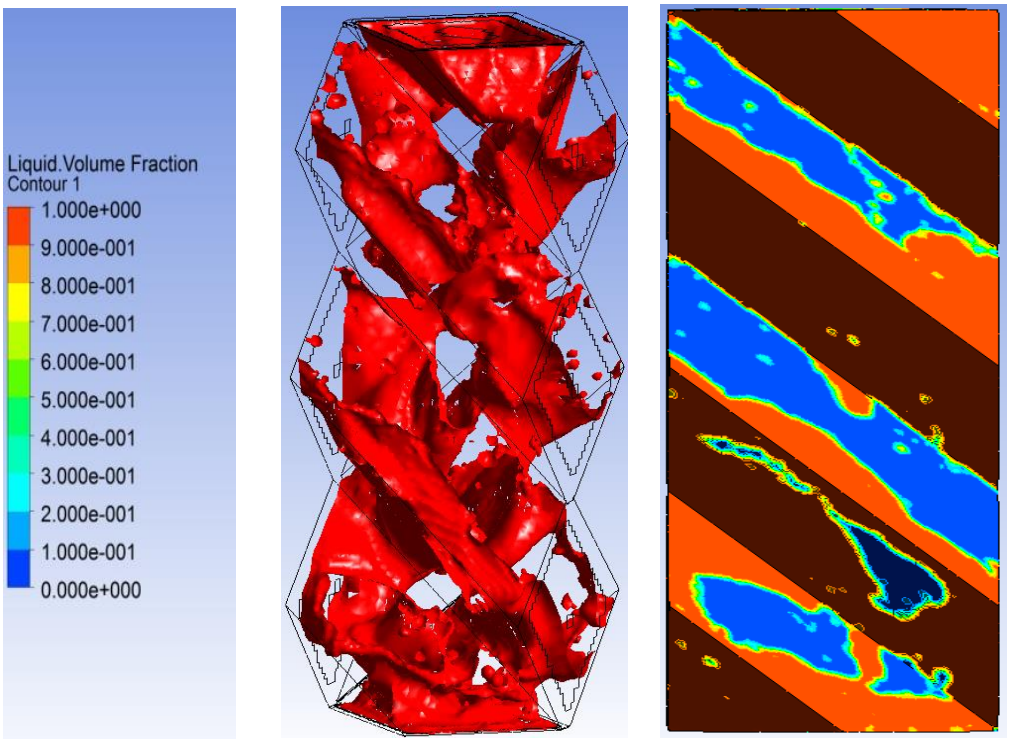

We=5.13

Figure 4.11 Flow regime and liquid distribution at different liquid Weber numbers from 0.57 to 5.13 at fixed $Re_g = 1431$.

Figure 4.12 shows a time series of liquid distribution for the dynamic flow field with $Re_g = 1431$ and $Re_L = 488$. At t = 0.011 s, the liquid begins to contact and wet the packing surface as it followed the packing surface along its 45 degree trajectory. At t = 0.058 s, the liquid fully wetted the first element, and begins to flow into the second elements. At t = 0.134 s, the second element was fully wetted and at t = 0.232 s, liquid flow was completed throughout the whole domain. Under these gas and liquid flow rates, the liquid flow not only followed the 45 degree trajectories of the packing surfaces but also flowed vertically to wet more area than otherwise would have occurred.

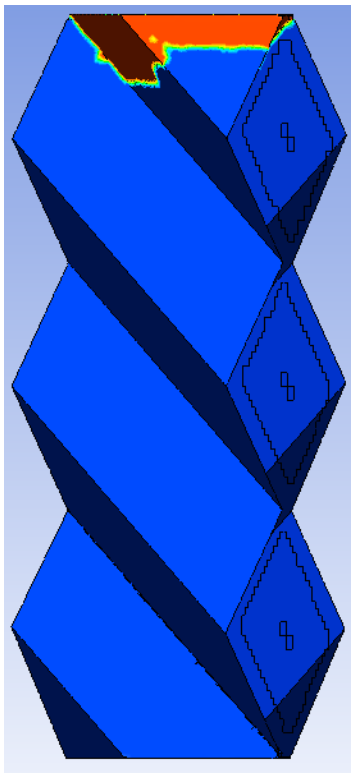

0.011s

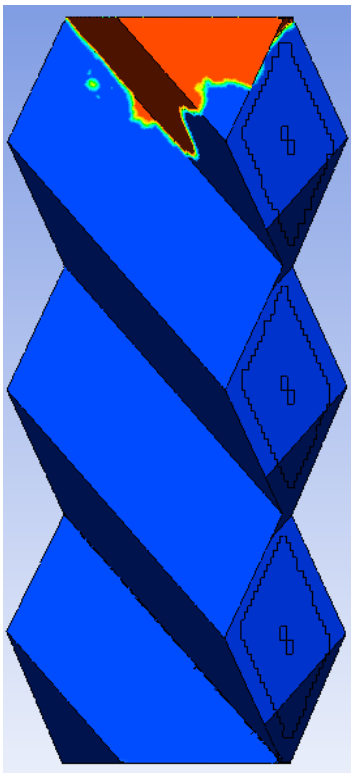

0.025s

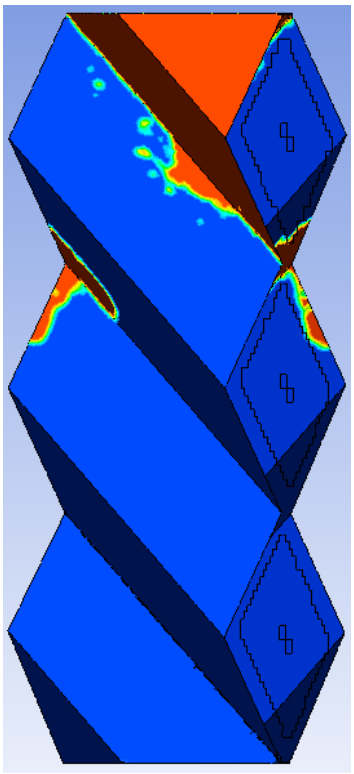

0.058s

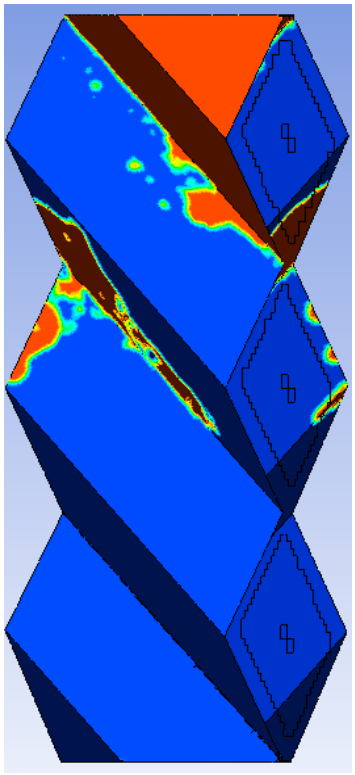

0.07s

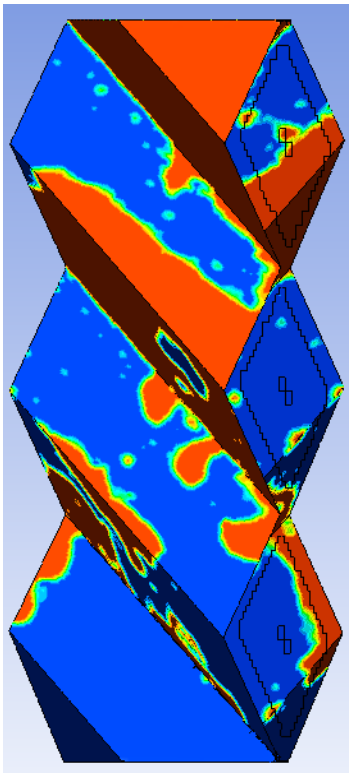

0.134s

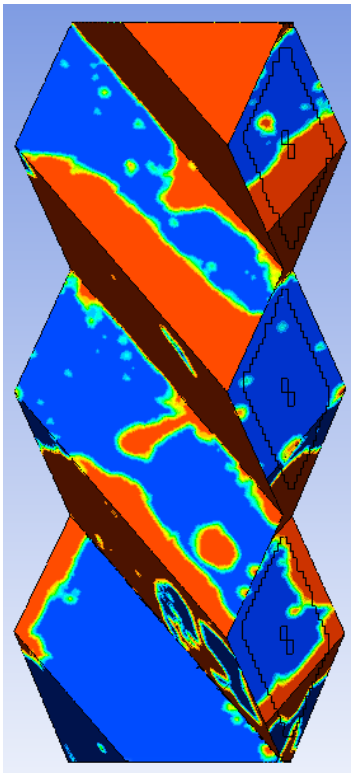

0.157s

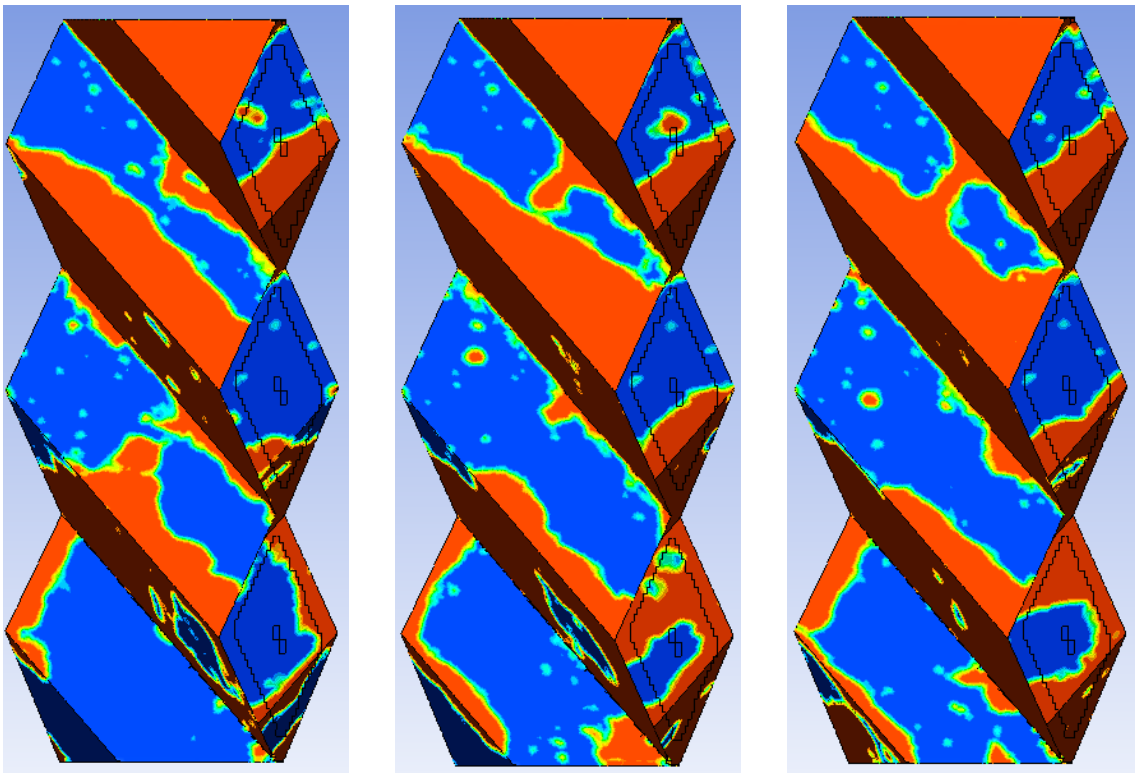

0.17s 0.204s 0.232s

Figure 4.12 Flow development with time at $Re_g = 1431$ and $Re_L = 488$ (in which a red color represents 100 vol. % of liquid and blue color is 100 vol.% of gas.).

Figure 4.13 shows the film thickness with different liquid flow rate with $Re_g = 1431$ and varying liquid flow rates as expressed in *We* values. For *We* below 2.21, surface tension was assumed to dominate the flow because not all of the packing surface was fully wetted and the film thickness was not uniform. When *We* = 2.21, the film thickness became more uniform. And it continued to increase in thickness when *We* = 5.13. However, at *We*=5.13, a strong interaction between the gas and liquid phases could also be observed because the liquid film was not stable. Such instabilities will increase the mass transfer area between the two phases.

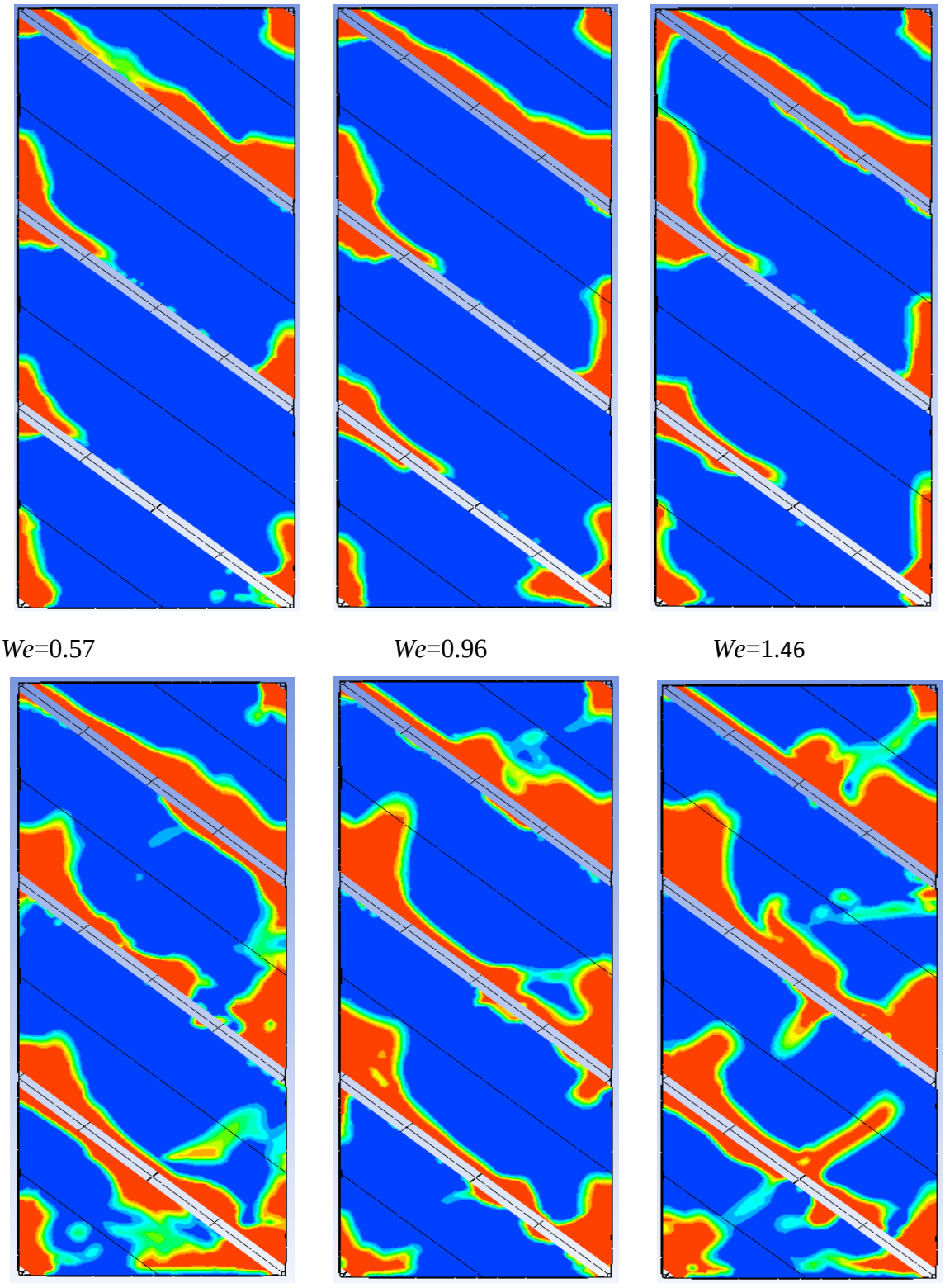

Figure 4.13 The film thickness as a function of liquid flow rate at constant $Re_g = 1431$ (in which a red color represents 100 vol. % of liquid and blue color is 100 vol.% of gas.).

Figure 4.14 depicts gas and liquid velocity vectors when $Re_g = 1431$ and $Re_L = 488$; downward pointing arrows in (b) represent liquid flow directions and upward pointing arrows represent gas flow directions. The gas phase has higher velocity than liquid phase. In general, liquid flowed along the surface of the packing. Within the interfaces between liquid and gas the gas and liquid velocity vectors were not parallel to the packing channels. The gas velocities were shifted more away from being parallel to the channels than the liquid velocities, indicating gas-liquid interactions which would enhance mass transfer area between the two phases.

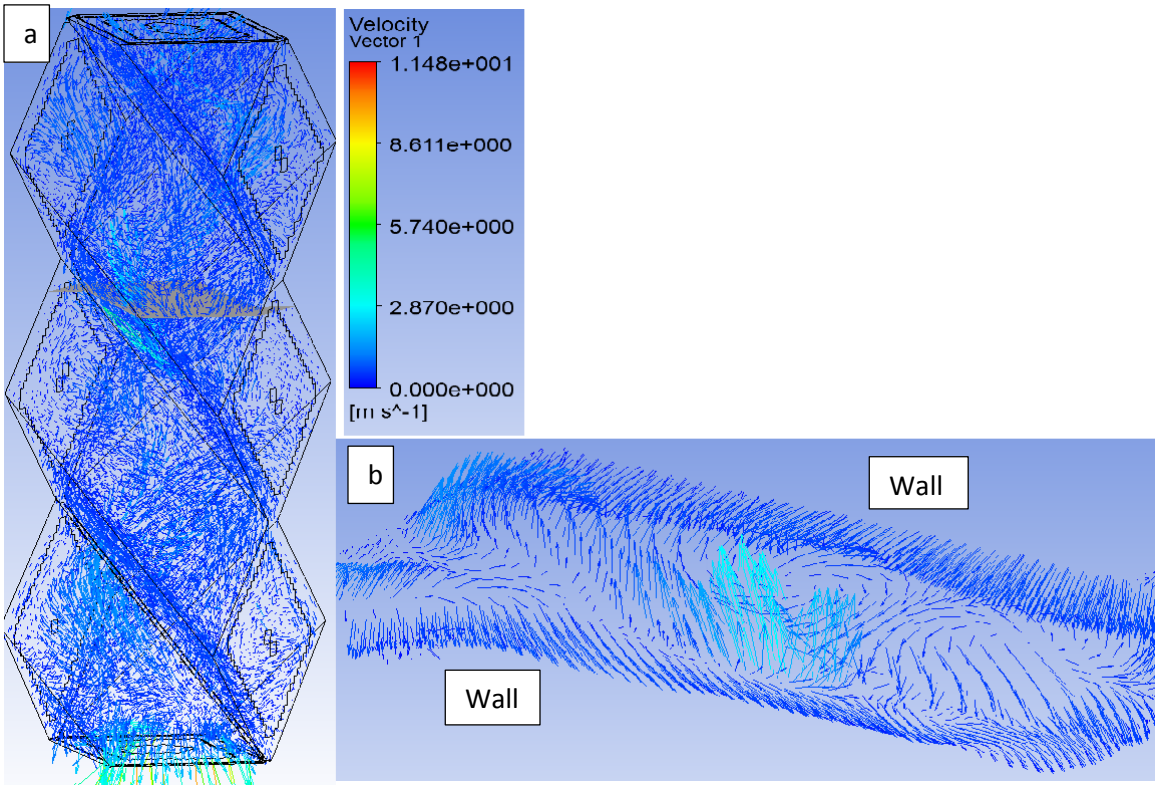

Figure 4.14 Gas and liquid flow vectors at $Re_g = 1431$ and $Re_L = 488$. (a) The velocity vector in the whole domain. (b) Velocity vector in an element channel.

4.2.4 Wetted Area and Film Thickness

The influence of gas flow rate with different liquid flow rates on the wetted area and film thickness are shown in Figure 4.15 and Figure 4.16, respectively. Whenever the liquid flow rate was increased the amount of wetted area increased incrementally and, although increasing gas flow rates caused small declines in wetted area at any particular liquid flow rate, the effects of changing gas flow rates were much smaller in magnitude than were the effects of liquid flow rates. These results are distinct from those with the spherical ball packing that were discussed in the Chapter 3. It can be anticipated that stronger gas-liquid interactions occur in this structured packing because the curved edges and flow channels would create conditions more conducive for gas-liquid interactions, which also generates more liquid droplets However, the formation of droplets will also slightly decrease the wetted area.

Figure 4.16 shows the influence of gas flow rates on average film thickness under different liquid flow rates. Larger liquid flow rated created thicker liquid films; for example, the film thickness was 0.62 mm at $Re_L = 205$ and 0.7mm when $Re_L = 488$. However, changing the gas flow rates had no apparent effect on film thickness.

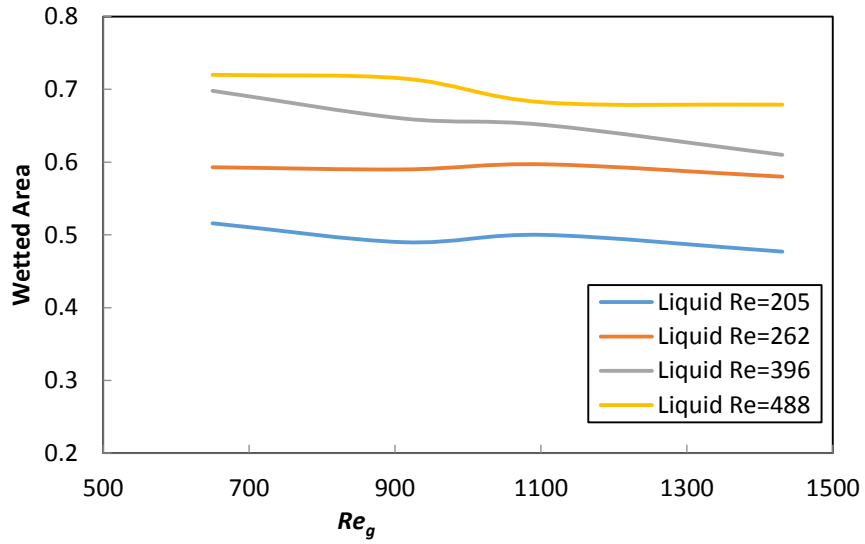

Figure 4.15 Influence of gas flow rate with fixed liquid flow rate on wetted area.

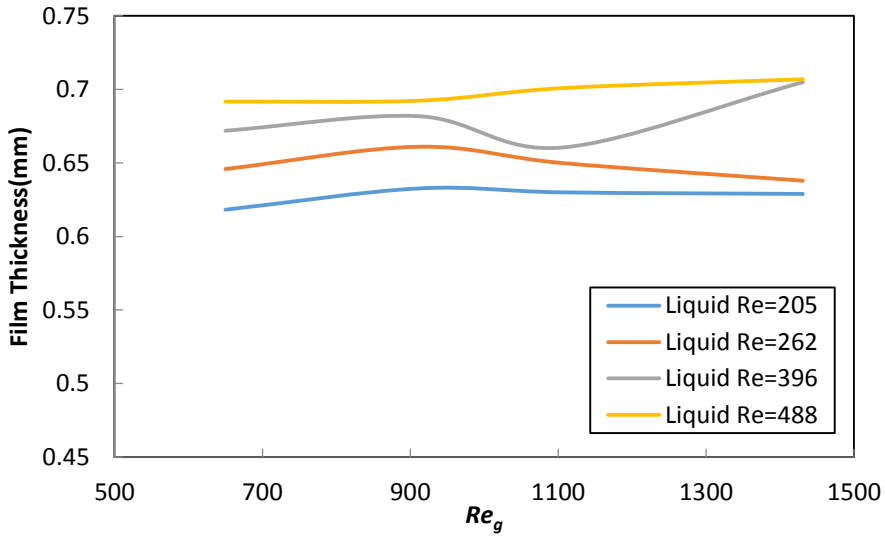

Figure 4.16 Influence of gas flow rate on film thickness under fixed liquid flow rate.

4.3 Conclusions

The hydrodynamics of structured packing in a packed bed reactor was investigated computationally using a three dimensional, comprehensive CFD model with counter-

current gas-liquid flows. The CFD model was validated, first, by comparing its results to those of published results based on empirical models. Then, the hydrodynamics in a structured packing was investigated under various conditions of liquid and gas flow rates. The key findings of this research were:

(1) The three dimensional CFD model was useful to study and understand flow hydrodynamics in a structured packing that had been previously described for application to a CO_2 absorption system.

(2) Liquid holdup was more affected by liquid flow rates than gas flow rates.

(3) Pressure drop was dependent on both liquid and gas flow rates, but more dependent on liquid flow rates than gas flow rates.

(4) The wetted area increased with increased liquid flow rates, and decreased slowly with increasing gas flow rates due to the formation of droplets.

(5) The film thickness increased with increased liquid flow rates, the gas flow rates had no significant effect on film thickness, but it makes the liquid film not stable. Such instabilities will increase the mass transfer area between the two phases.

(6) An increase of *We* values led to a more uniform liquid distribution within the packing channels.

(7) The flow regime changed from film flow to trickle flow when *We* was greater than 2.21.

(8) With increasing *We* values the wetted areas increased, but at all *We* values studied a small dead zone was always found.

CHAPTER 5. DEVELOPMENT OF MACRO-SCALE MODEL

In this chapter, a CFD model based on the porous media concept is developed and discussed for modelling the hydrodynamics of two-phase flow in spherical ball packed bed. The aim of this research is to assess a closure model using the porous model in multi-phase, counter-counter flow system and to determine what type of alterations may be required to success the multiphase counter-current flows.

5.1 Macro-scale Model Description

As described in Chapter 2, the macro-scale modelling using the porous media concept entails the entire packed bed considered as a porous medium. The phases are treated as inter-penetrating continua and the modelling has a very attractive form which does not require detailed geometric input considerations for the system. As a consequence, the modelling will not provide accurate information about local flow phenomena. Neglecting the physical geometry also dramatically decreases the total number of elements per volume within the domain and, therefore, the modelling is less intensive computationally. Modelling via the porous media concept has been the primary approach that has been used to incorporate complexities like chemical reactions and to simulate very large scale systems.

5.1.1 Closure Model

The porous model uses the same control equations as the other models in Chapter 3 and 4, but needs extra input called a closure model. Also called a permeability model, it is commonly used to evaluated various issues of multiphase flow through porous media (Atta, Roy et al. 2007) and is based on averaged parameters for modeling pressure drops

throughout the porous media. The most famous closure model is the Ergun equation, a detail expression for which was presented in Chapter 2, Section 2.8.

5.1.2 Geometry Model and Boundary Conditions

A porous model is applied to simulate the flow in the spherical packed bed. A 3D geometry model was built for a porous model, as shown in Figure 5.1. The diameter of the column was same as that used in the experiments, with a 38.1 mm (1.5") ID with the length of 135 mm long to save computational time.

The middle 100 mm length was is treated as a porous zone with porosity of 0.4. Above and under the porous zone, there were two empty zones with a length of 17.5mm, also identical to the experiments. The empty zone was to enable more homogeneous distribution of the liquid before entering the porous zone. The mesh is shown in Figure 5.2 and had a total of 3.1×10^5 elements.

Several simulation cases were performed, and the simulation conditions followed the experimental conditions described in Chapter 3. Boundary conditions in porous zone of the simulations are presented in Table 5.1; the viscous resistance and inertial resistance coefficients were calculated using the Equations 2.9 and 2.10.

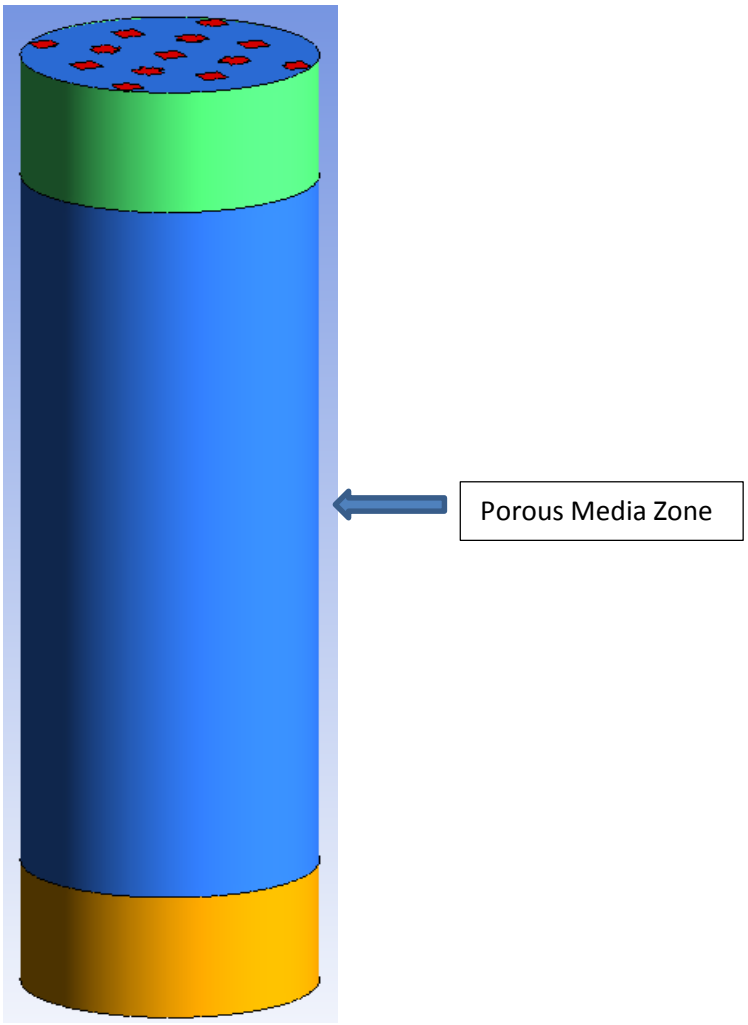

Figure 5.1 Geometry of the simulations.

Table 5.1 Boundary conditions of the simulations.

Simulation parameters	
Porosity	0.4
Viscous resistance coefficient	8.79×10^{6}
Inertial resistance coefficient	3340

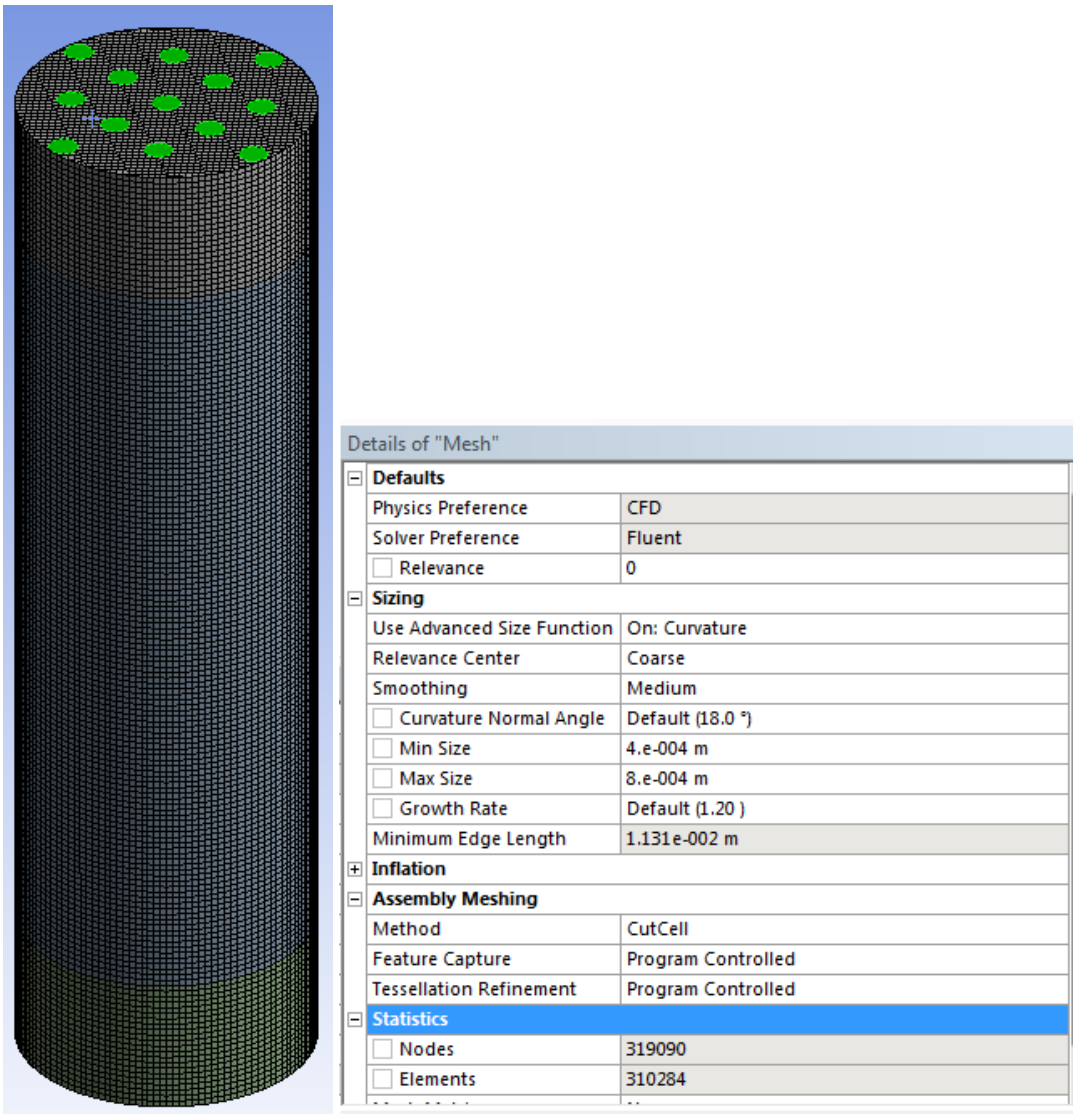

Details of "Mesh"

Defaults	
Physics Preference	CFD
Solver Preference	Fluent
Relevance	0
Sizing	
Use Advanced Size Function	On: Curvature
Relevance Center	Coarse
Smoothing	Medium
Curvature Normal Angle	Default (18.0 °)
Min Size	4.e-004 m
Max Size	8.e-004 m
Growth Rate	Default (1.20)
Minimum Edge Length	1.131e-002 m
Inflation	
Assembly Meshing	
Method	CutCell
Feature Capture	Program Controlled
Tessellation Refinement	Program Controlled
Statistics	
Nodes	319090
Elements	310284

Figure 5.2 Mesh geomerty and details for the simulations.

5.1.3 Results based on the Ergun Equation

Figure 5.3 compares the pressure drops from experimental results and simulation results based on the Ergun model as the closure model. Although they are in reasonable agreement, a relatively large difference exists between the experimental data and simulation results, with Ergun model results always smaller than the experimental results. The reason for this difference may be a result of the fact that that the Ergun model is for

single phase flow; it does not account for the effects of the two-phase flow and counter-current gas-liquid flows.

5.2 Modified Closure Model

The results in Chapter 3 showed that the pressure drops with spherical packing was influenced by both gas and liquid flows. Hence, a closure model other than that based on the Ergun model may be needed to be assessed if better agreement between experimental and model pressure drops are to be developed. In fact, published research has assessed modifications to the Ergun equation to generate better correspondence between experimental and simulation data (Specchia and Baldi 1977, Szady and Sundaresan 1991), this model by changing the values of Ergun's constants. However, this arbitrary approach has no sound scientific basis for counter-current, multi-phase flow. Hence, an alternative to simply changing these constants was investigated.

In the Ergun model pressure drops are a function of particle diameter, void fraction of the bed (porosity), gas phase velocity, density and viscosity, but no factors or dependencies are associated with the liquid phase. Previous research has broached this issue (Ellenberger and Krishna 1999) in which it was reasoned that, if the flow also contains a liquid, the void fraction should be changed because the amount of liquid in the flow is actually related to liquid holdup. To account for liquid holdup, the void fraction can be expressed as:

$$\varepsilon' = \varepsilon - h_o$$

where ε' is modified void fraction, ε is initial void fraction and h is associated with operating liquid holdup .

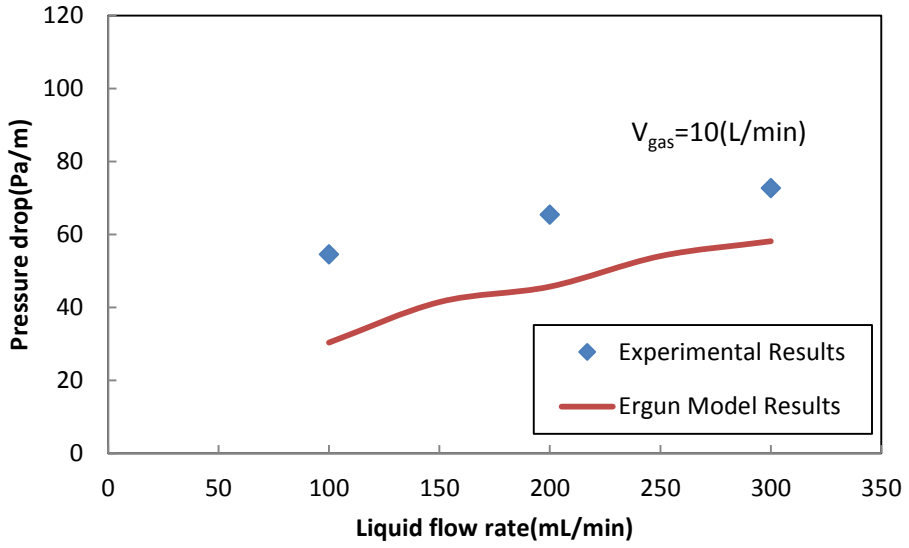

(a)V_{water} = 200 (mL/min)

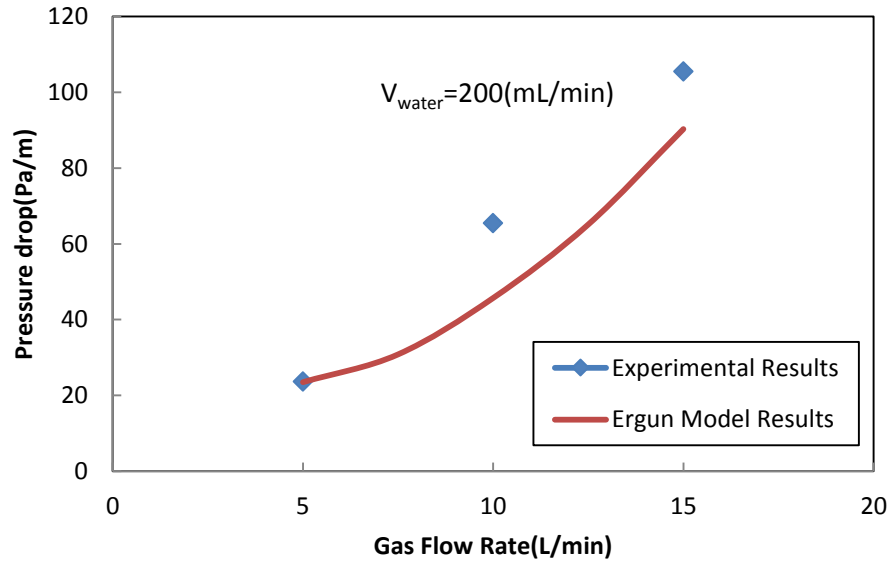

(b) V_{gas}=10(L/min)

Figure 5.3 Comparison of experimental and simulated pressure drops at (a)Vwater = 200 (mL/min) (b) Vgas=10(L/min).

With the modification, the Ergun equation would become:

$$\frac{|\Delta p|}{L} = \frac{150\mu}{D_p^2}\frac{(1-\varepsilon')^2}{\varepsilon'^3}v_\infty + \frac{1.75\rho}{D_p}\frac{(1-\varepsilon')}{\varepsilon'^3}v_\infty^2 \quad (5.1)$$

However, the value of h has to be either measured or calculated for the closure model. Fortunately, research has been performed (Saez and Carbonell 1985) in which datasets for liquid holdup and pressure drop were analyzed over a wide range of flow rates to determine the dependency of relative permeability on the saturation for each phase in co-current, multi-phase flow. The hypothesis was that liquid relative permeability is a function of reduced saturation (δ_l) and can be represented by a ratio of effective volume of flow of the liquid phase-to-the available volume of flow, as in:

$$\delta_l = \frac{\varepsilon_l - \varepsilon_l^0}{\varepsilon - \varepsilon_l^0} \quad (5.2)$$

where ε_l^0 is the static liquid holdup and more details see (Atta, Roy et al. 2007). Additionally, gas phase relative permeability was correlated to be a function of the gas phase saturation, giving the empirical relations:

$$k_l = \delta_l^{2.43} \quad (5.3)$$

$$k_g = s_g^{4.80} \quad (5.4)$$

where $s_g = 1 - \frac{\varepsilon_l^0}{\varepsilon}$

Then, the static liquid holdup (ε_l^0) can be calculated by:

$$\varepsilon_l^0 = \frac{1}{(20+0.9E_o^*)} \quad (5.5)$$

where $E_o^* = \frac{\rho_l g d_p^2 \varepsilon^2}{\sigma_l (1-\varepsilon)^2}$

Hence, equation 5.5 shows the liquid holdup is a function of particle diameter, bed porosity, liquid density and liquid surface tension. In addition, the results in Chapter 3 related to the use of Billet's empirical model (Billet, 1984) shows that liquid holdup should be dependent on liquid velocities.

Hence, based on the data for the spherical ball packing in Chapter 3, and in agreement with use of Billets empirical model, the following dependency of liquid holdup is proposed: :

$$h_o = 0.3Fr_L^{0.25} \tag{5.6}$$

where $Fr_L = \frac{15*U_L^2}{g\varepsilon^{4.65}}$. U_L is the liquid inlet velocity m/s, g is the gravity m/s^2, ε is the void fraction of the bed. Therefore, the modified Ergun model for our studies can be written as:

$$\frac{|\Delta p|}{L} = \frac{150\mu}{D_p^2}\frac{(1-\varepsilon+0.3Fr_L^{0.25})^2}{(\varepsilon-0.3Fr_L^{0.25})^3}v_\infty + \frac{1.75\rho}{D_p}\frac{(1-\varepsilon+0.3Fr_L^{0.25})}{(\varepsilon-0.3Fr_L^{0.25})^3}v_\infty^2 \tag{5.7}$$

Figure 5.4 compares liquid holdups calculated using the modified Ergun model and the results of the simulations discussed in Chapter 3 for the spherical ball packing. Very good agreement between these models for liquid holdup is noted.

Table 5.2 New resistance coefficient of the simulation.

Liquid mass flow rate (mL/min)	Viscous resistance coefficient	Inertial resistance Coefficient
100	3.23×10^7	1.04×10^4
200	5.87×10^7	1.78×10^4
300	1.61×10^8	4.52×10^4

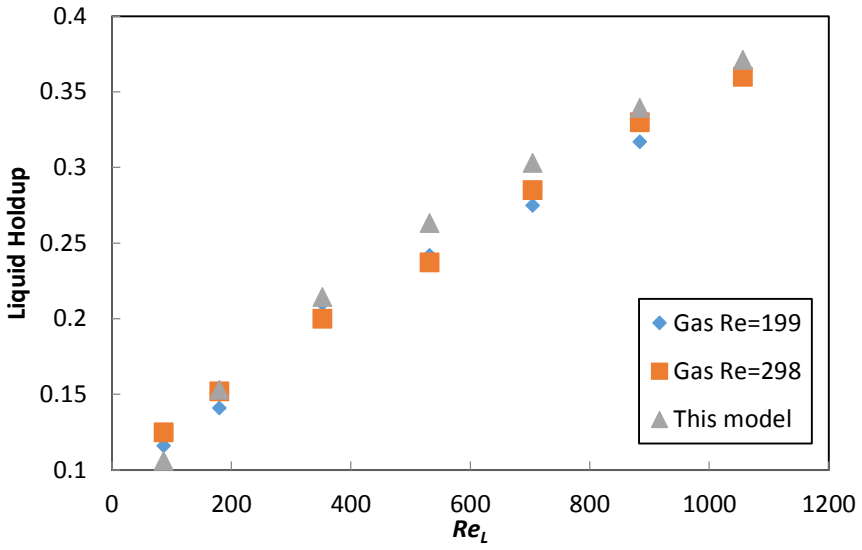

Figure 5.4 Comparison of modified Ergun model that considered liquid holdup model and the simulation results of Chapter 3 for spherical ball packing with changes in the liquid Reynolds numbers.

5.3 Results of a New Closure Model

The change of the void fraction will change the coefficient of equation 5.7. By using the modified viscous and inertial resistance coefficients shown in Table 5.2, in conjunction with the modified Ergun model, it was then possible to compare the pressure drop results calculated from a closure model with those from the experiments, as shown in Figure 48. Now, differences between results from experimental tests and the modified Ergun closure model have decreased to an overall 8% instead of the 40% that is displayed in Figure 5.5. Hence, the modified Ergun equation effectively eliminated the errors in calculation that were associated with not including two phase flow in the packed bed using spherical ball packing.

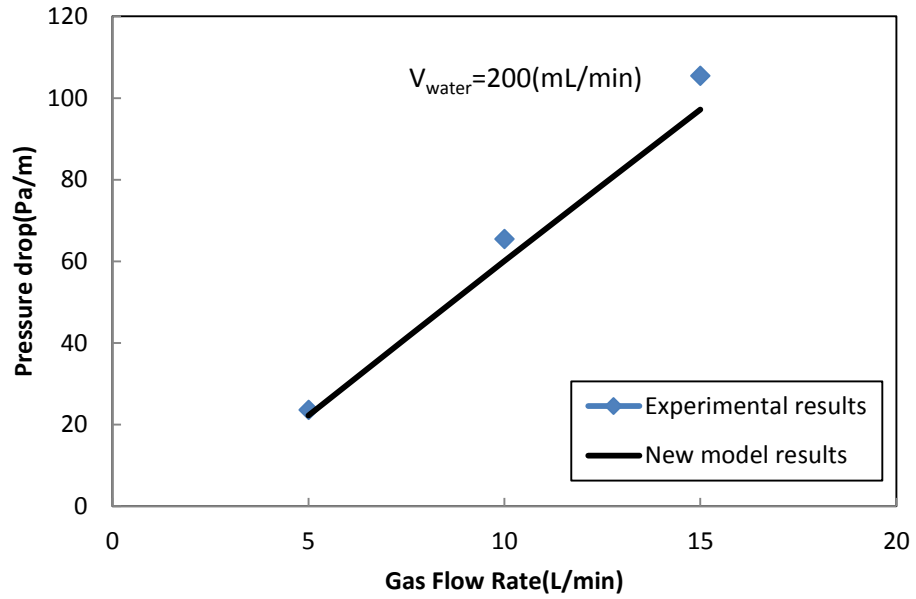

(a)V_{water} = 200 (mL/min)

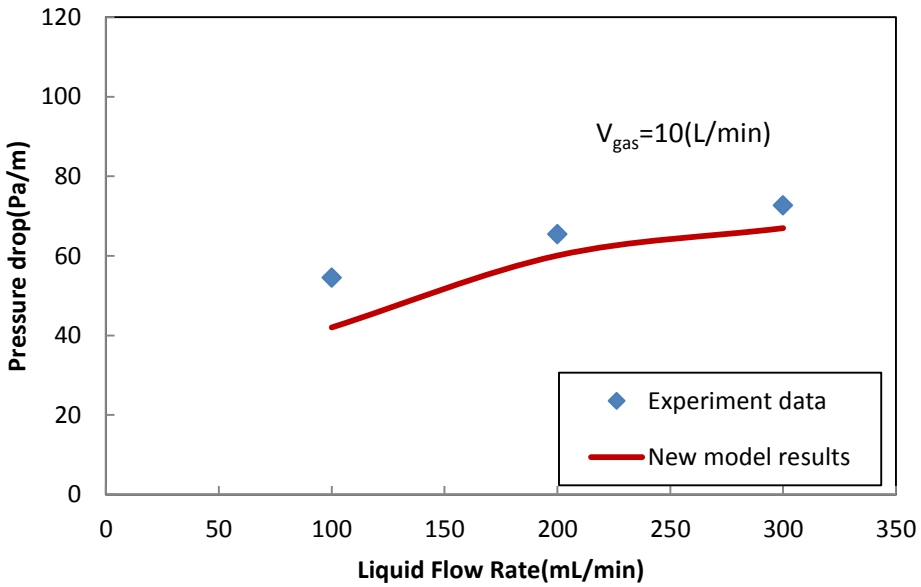

(b) V_{gas}=10(L/min)

Figure 5.5 Comparison of experimental and simulated pressure drops under the new closure model using a modified Ergun equation: (a)V_{water} = 200 (mL/min) (b) V_{gas}=10(L/min).

5.4 Conclusions

Although macro-scale modelling cannot provide detailed characterization of the hydrodynamics in a packed bed reactor, it is less computationally intensive and provides insight in pressure drops associated with the liquid and gas phases. Hence, a porous model for spherical ball packing was assessed which included a closure model that required modification of the Ergun equation to account for the presence of gas and liquid phases in the reactor. This modified Ergun equation included replacing the porosity by the actual pore volume within the packing, which included liquid holdup as an important influence on pressure drops. Additionally, an equation was developed which enabled the prediction of liquid holdup versus the liquid Reynolds number and the results of using this equation were in very good agreement with the results of 3D CFD simulation.

CHAPTER 6. CONCLUSIONS AND FUTURE WORK

There is a scientific consensus on the climate change and global warming, and there is an increasing concern on CO_2 capture and sequestration to mitigate climate change and global warming. Post-combustion CO_2 capture is one of the most promising potential technologies to be commercialized in the near future. One of the obstacles that hurdle the scale up of this process, however, is the large size of the CO_2 absorber due to the relatively low CO_2 absorption kinetics and the lack of knowledge on the hydrodynamics in the packed bed. The hydrodynamic characterizations such as wetted area, film thickness, liquid holdup, liquid distribution and gas-liquid interaction are essential parameters affecting the chemical reaction rate.

To that end, numerical simulation was performed in this dissertation to study the hydrodynamics in the packed bed. A comprehensive meso-scale 3D CFD model was built for gas-liquid under counter currently flow in a spherical ball packing bed and a structured packing bed, and the model was verified by comparing its predictions to laboratory scale experimental data and already existing empirical models. This newly developed 3D CFD was found useful to improve our current understanding of the mechanisms of hydrodynamics in a packed bed reactor. The following summarizes specific outcomes from this thesis.

(1) In the spherical ball packing bed and the structured packing bed, an increase in the *We* number values led to a more uniform liquid distribution. However, the flow regime in the bed with spherical ball packing was mainly film flow when *We* number was greater

than 0.547, with further increases of *We* to 1.51, the trickle flow was observed and the flow regime in the structured packing was trickle flow at *We* number greater than 2.21. Liquid is easier to spread in the structured packing bed.

(2) Liquid holdup was found to be more affected by liquid flow rate, and the gas flow rate had no significant influence for spherical ball packing and structured packing bed. For both spherical ball packing bed and structured packing bed, the pressure drop increased with an increase in both the gas flow and liquid flow rates. The gas flow rate affected the pressure drop in the structured packing bed only when the flow condition changed from film flow to trickle flow creating a sharp pressure drop.

(3) The transient 3-D liquid-gas counter flow system for both the spherical ball packing and the structured packing bed was numerically simulated and the transient behavior of important parameters (wetted area, liquid distribution, gas liquid interaction in the interface, and film thickness) were obtained. One of important new findings is: gas and liquid interaction occurred at their interface through entrainment; it became stronger with an increase in *Re* numbers. When this interaction becomes stronger, it will split the liquid and leading to formation of droplets (which will create a negative performance of the packing beds). The film thickness in structured packing bed was much thinner than that in the spherical ball packing bed, and it increased with an increase in the liquid flow rate. Gas flow rate had no significant effect on building the film layer thickness, but it makes the liquid film not stable. Such instabilities will increase the mass transfer area between the two phases.

(4) The liquid distributor affected behavior of flow in both beds, while increasing the number of inlets did not always enhance the wetted areas or liquid holdups. The effect of liquid inlet on the wetted area was numerically evaluated by changing the liquid inlet number from 1 to 13. As a result, the inlet number of four achieved the highest wetted area and the best liquid holdup. The effect of surface tension had an insignificant influence on pressure drop and liquid holdup; however, lower surface tension helped to increase the wetted area and creating a thinner film thickness, which is a favorable performance condition for the packed bed reactors.

(5) Ergun model used in the porous model was examined and found not to be suitable for counter-current multi-phase flow simulation. The Ergun equation, therefore, was modified by replacing the porosity by the actual pore volume to accurately include performance of the liquid holdup into account. As a result, the modified Ergun equation predicted liquid holdup more accurately.

Future Work:

(1) To understand the relationship between the CO_2 absorption-rate with the hydrodynamic characterization parameters, the reaction mechanism of CO_2 absorption needs to be added to the current meso-scale CFD model. To that end, kinetic data of CO_2 absorption with popular amine solvent such as MEA has been well developed, so the user defined functions (UDF) can be used to add the reaction kinetics to the CFD model. Since the CO_2 is absorbed in this model, the gas (CO_2) flow rate will decrease along its flow path (upward), and the solvent carbon loading may increase along its flow path (downward), slightly affecting the physical properties (such as surface tension and viscosity of the solvent) which will influence the hydrodynamics in the structured

packing bed. This interaction between the chemical reaction and hydrodynamics need to be further investigated.

(2) The meso-scale model which is computationally intensive was proven to be capable of simulating details of the hydrodynamic behavior in the packing bed. On the other hand, porous model (which is less computationally intensive) can simulate the performance of a large scale setup system if a suitable closure model for structured packing bed is developed.

(3) If scaling relationships and/or scaling laws which can relate the performance of micro-scale, meso-scale and macro-scale models were developed, micro-scale (laboratory scale) model can be used to validate the numerical model which can optimize the performance of the macro-scale packed bed reactors. Combination of the scale and numerical modeling can help accelerate R&D effort to identify a highly efficient and effective packed bed reactor system and the optimized operational conditions.

Nomenclature

a	Permeability
$1/a$	Viscous resistance coefficient
a_p	Specific surface area $m^2 m^{-3}$
a_k	Volume fraction in k-th phase
A	Constant in the viscous term of the Ergun type equation
B	Constant in the inertial term of the Ergun type equation
C_2	Inertial resistance coefficient
Dp	Particle diameter, m
d_p'	Particle diameter including surface liquid, m
d	Thickness of the phase inlet, m
ε	Void fraction of bed
ε_k	Volum fraction of k phase
ε_g	Hold up of g phase
ε'	Modified void fraction with liquid phase
ε_l^o	Static liquid holdup
E_o^*	Modified EÖtvos number, $E_o^* = \frac{\rho_l g d_p^2 \varepsilon^2}{\sigma_l (1-\varepsilon)^2}$

f_p	friction factor of a single particle
F	Drag force
F_g	Drag force on the g phase per unit volume, $kgm^{-2}s^{-2}$
$F_{k,R}$	Interphase between K and R phases
Fr_L	Froude number $Fr_L = \frac{15*U_L^2}{g\varepsilon^{4.65}}$
g	Gravity, 9.8 m s^{-2}
Ga_g	Galieo number of the gas phase
h_0	Liquid hold-up
k	Free surface curvature
k_g	Relative permeability of g phase
l	Bed height, m
$\overline{n}$	Unit normal vector
Re	Reynolds number fluid
Re_p	Reynolds number based on the particle diameter
Re_g	Reynolds number of the gas phase
Δp	Pressure drop, pa/m
Δp_{dry}	Pressure drop through an unirrigated (dry)bed Pa/m
Δp_{irr}	Pressure drop through an irrigated bed Pa/m

U_k Cell velocity of k-th phase

We Weber number

t Time, s

v Velocity, m s^{-1}

V_∞ Superficial velocity upstream of the bed entrance, m/s

V Liquid and gas flow rate

ρ_k Density of k-th phase, kg m^{-3}

μ Dynamic viscosity, pa·s

σ Surface tension

Subscripts

g Gas phase

L Liquid phase

References

Abdolkarimi, V. (2013). "Hydrodynamics modeling of a bench scale trickle bed reactor using CFD." Petroleum & Coal **55**(3): 188-195.

Aferka, S., A. Viva, E. Brunazzi, P. Marchot, M. Crine and D. Toye (2011). "Tomographic measurement of liquid hold up and effective interfacial area distributions in a column packed with high performance structured packings." Chemical engineering science **66**(14): 3413-3422.

Atta, A., S. Roy and K. Nigam (2007). "Prediction of pressure drop and liquid holdup in trickle bed reactor using relative permeability concept in CFD." Chemical Engineering Science **62**(21): 5870-5879.

Atta, A., S. Roy and K. D. Nigam (2007). "Investigation of liquid maldistribution in trickle-bed reactors using porous media concept in CFD." Chemical engineering science **62**(24): 7033-7044.

Attou, A. and G. Ferschneider (1999). "A two-fluid model for flow regime transition in gas–liquid trickle-bed reactors." Chemical Engineering Science **54**(21): 5031-5037.

Bai, H., J. r. Theuerkauf, P. A. Gillis and P. M. Witt (2009). "A coupled DEM and CFD simulation of flow field and pressure drop in fixed bed reactor with randomly packed catalyst particles." Industrial & Engineering Chemistry Research **48**(8): 4060-4074.

Balusu, P. S. and B. Mohanty (2011). "CFD Simulation of Multiphase Flow in Trickle Bed Reactor." International Journal of Computer Applications in Engineering Sciences **1**(4).

Barigou, M. (2004). "Particle tracking in opaque mixing systems: an overview of the capabilities of PET and PEPT." Chemical Engineering Research and Design **82**(9): 1258-1267.

Basden, M., R. B. Eldridge, J. Farone, E. Feng, D. S. Hussey and D. L. Jacobson (2013). "Liquid Holdup Profiles in Structured Packing Determined via Neutron Radiography." Industrial & Engineering Chemistry Research **52**(48): 17263-17269.

Battista, J., A. Muzen, M. Cassanello and U. Böhm (2003). "Flow Regime Transitions in Trickle‐bed Reactors with Structured Packings." The Canadian Journal of Chemical Engineering **81**(3‐4): 802-807.

Boyer, C., A.-M. Duquenne and G. Wild (2002). "Measuring techniques in gas–liquid and gas–liquid–solid reactors." Chemical Engineering Science **57**(16): 3185-3215.

Brackbill, J., D. B. Kothe and C. Zemach (1992). "A continuum method for modeling surface tension." Journal of computational physics **100**(2): 335-354.

CABLE, M. (2009). "An evaluation of turbulence models for the numerical study of forced and natural convective flow in Atria."

Calis, H., J. Nijenhuis, B. Paikert, F. Dautzenberg and C. Van Den Bleek (2001). "CFD modelling and experimental validation of pressure drop and flow profile in a novel structured catalytic reactor packing." Chemical Engineering Science **56**(4): 1713-1720.

Chen, L., F. Liu, S. N. Heather, Z. Fan and K. Liu (2014). "Coal Char-fueled Chemical Looping Combustion Use Different Iron-Based Oxygen Carriers." Energy Procedia **63**: 73-79.

Chen, L., Y. Zhang, F. Liu and K. Liu (2015). "Development of a Cost-Effective Oxygen Carrier from Red Mud for Coal-Fueled Chemical-Looping Combustion." Energy & Fuels **29**(1): 305-313.

Chen, Z., D. Yates, J. K. Neathery and K. Liu (2012). "The effect of fly ash on fluid dynamics of CO 2 scrubber in coal-fired power plant." Chemical Engineering Research and Design **90**(3): 328-335.

Christensen, E. D. and R. Deigaard (2001). "Large eddy simulation of breaking waves." Coastal engineering **42**(1): 53-86.

Chu, C. and K. Ng (1989). "Model for pressure drop hysteresis in trickle‐beds." AIChE journal **35**(8): 1365-1369.

Chung, T. S., D. Patiño-Echeverri and T. L. Johnson (2011). "Expert assessments of retrofitting coal-fired power plants with carbon dioxide capture technologies." Energy Policy **39**(9): 5609-5620.

Craster, R. V. and O. K. Matar (2009). "Dynamics and stability of thin liquid films." Reviews of Modern Physics **81**(3): 1131-1198.

Darcy, H. (1856). Les fontaines publiques de la ville de Dijon: exposition et application, Victor Dalmont.

De Brito, M. H., U. Von Stockar, A. M. Bangerter, P. Bomio and M. Laso (1994). "Effective mass-transfer area in a pilot plant column equipped with structured packings and with ceramic rings." Industrial & engineering chemistry research **33**(3): 647-656.

Dixon, A. G. (2012). Computational Fluid Dynamics Analysis of Two-Phase Flow in a Packed Bed Reactor, WORCESTER POLYTECHNIC INSTITUTE.

Drahoš, J., J. Zahradnik, M. Punčochář, M. Fialova and F. Bradka (1991). "Effect of operating conditions on the characteristics of pressure fluctuations in a bubble column." Chemical Engineering and Processing: Process Intensification **29**(2): 107-115.

Ed, D. P., T. . from www.esrl.noaa.gov/gmd/ccgg/trends/.

Elkins, C. J. and M. T. Alley (2007). "Magnetic resonance velocimetry: applications of magnetic resonance imaging in the measurement of fluid motion." Experiments in Fluids **43**(6): 823-858.

Ellenberger, J. and R. Krishna (1999). "Counter-current operation of structured catalytically packed distillation columns: pressure drop, holdup and mixing." Chemical Engineering Science **54**(10): 1339-1345.

Ergun, S. (1952). Chem. Eng. Prog. **48**: 89.

Fan, Z., L. Chen, F. Liu and K. Liu (2015). "Analytical Evaluation of CaO-CO2 Loop for CO2 Removal." CIESC Journal.

Feron, P. H. (2010). "Exploring the potential for improvement of the energy performance of coal fired power plants with post-combustion capture of carbon dioxide." International Journal of Greenhouse Gas Control **4**(2): 152-160.

Figueroa, J. D., T. Fout, S. Plasynski, H. McIlvried and R. D. Srivastava (2008). "Advances in CO2 capture technology—The U.S. Department of Energy's Carbon Sequestration Program." International Journal of Greenhouse Gas Control **2**(1): 9-20.

Force, C. A. T. (2009). "Advanced Post-Combustion CO2 Capture."

Freund, H., J. Bauer, T. Zeiser and G. Emig (2005). "Detailed simulation of transport processes in fixed-beds." Industrial & engineering chemistry research **44**(16): 6423-6434.

Frohn, A. and N. Roth (2000). Dynamics of droplets, Springer Science & Business Media.

Fu, D., L. Wei and S. Liu (2013). "Experiment and model for the surface tension of carbonated MEA–MDEA aqueous solutions." Fluid Phase Equilibria **337**: 83-88.

Gao, G., L. Zhang, X. Li and H. Sui (2011). "CFD simulation of film flow and gas/liquid counter-current flow on structured packing." Transactions of Tianjin University **17**(3): 194-198.

Ghosh, T. (2013). "Modeling of an Air-based Density Separator."

Ginzburg, I. and G. Wittum (2001). "Two-phase flows on interface refined grids modeled with VOF, staggered finite volumes, and spline interpolants." Journal of Computational Physics **166**(2): 302-335.

Gladden, L. F. and P. Alexander (1996). "Applications of nuclear magnetic resonance imaging in process engineering." Measurement Science and Technology **7**(3): 423.

Götz, J., K. Zick, C. Heinen and T. König (2002). "Visualisation of flow processes in packed beds with NMR imaging: determination of the local porosity, velocity vector and local dispersion coefficients." Chemical Engineering and Processing: Process Intensification **41**(7): 611-629.

Green, C. W. (2006). Hydraulic characterization of structured packing via X-ray computed tomography, ProQuest.

Groff, M. K., S. J. Ormiston and H. M. Soliman (2007). "Numerical solution of film condensation from turbulent flow of vapor–gas mixtures in vertical tubes." International Journal of Heat and Mass Transfer **50**(19–20): 3899-3912.

Gualito, J., F. Cerino, J. Cardenas and J. Rocha (1997). "Design method for distillation columns filled with metallic, ceramic, or plastic structured packings." Industrial & engineering chemistry research **36**(5): 1747-1757.

Gueyffier, D., J. Li, A. Nadim, R. Scardovelli and S. Zaleski (1999). "Volume-of-fluid interface tracking with smoothed surface stress methods for three-dimensional flows." Journal of Computational Physics **152**(2): 423-456.

Gunjal, P. R., M. N. Kashid, V. V. Ranade and R. V. Chaudhari (2005). "Hydrodynamics of Trickle-Bed Reactors: Experiments and CFD Modeling." Industrial & Engineering Chemistry Research **44**(16): 6278-6294.

Gunjal, P. R., V. V. Ranade and R. V. Chaudhari (2003). "Liquid distribution and RTD in trickle bed reactors: experiments and CFD simulations." The Canadian Journal of Chemical Engineering **81**(3‐4): 821-830.

Guo, X., Y. Sun, R. Li and F. Yang (2014). "Experimental investigations on temperature variation and inhomogeneity in a packed bed CLC reactor of large particles and low aspect ratio." Chemical Engineering Science **107**: 266-276.

Haroun, Y., D. Legendre and L. Raynal (2010). "Direct numerical simulation of reactive absorption in gas–liquid flow on structured packing using interface capturing method." Chemical Engineering Science **65**(1): 351-356.

Haroun, Y., L. Raynal and P. Alix (2014). "Prediction of effective area and liquid hold-up in structured packings by CFD." Chemical Engineering Research and Design **92**(11): 2247-2254.

Heidari, A. and S. H. Hashemabadi (2013). "Numerical evaluation of the gas–liquid interfacial heat transfer in the trickle flow regime of packed beds at the micro and meso-scale." Chemical Engineering Science **104**: 674-689.

Henley, E. J., J. D. Seader and D. K. Roper (2011). Separation process principles, Wiley.

Hirt, C. W. and B. D. Nichols (1981). "Volume of fluid (VOF) method for the dynamics of free boundaries." Journal of computational physics **39**(1): 201-225.

Hoffmann, A., I. Ausner, J.-U. Repke and G. Wozny (2005). "Fluid dynamics in multiphase distillation processes in packed towers." Computers & chemical engineering **29**(6): 1433-1437.

Horowitz, G., A. Cukierman and M. Cassanello (1997). "Flow regime transition in trickle beds packed with particles of different wetting characteristics—check-up on new tools." Chemical engineering science **52**(21): 3747-3755.

Hosseini, S. H., S. Shojaee, G. Ahmadi and M. Zivdar (2012). "Computational fluid dynamics studies of dry and wet pressure drops in structured packings." Journal of Industrial and Engineering Chemistry **18**(4): 1465-1473.

Iliuta, I. and F. Larachi (2001). "Mechanistic model for structured-packing-containing columns: irrigated pressure drop, liquid holdup, and packing fractional wetted area." Industrial & engineering chemistry research **40**(23): 5140-5146.

Iliuta, I., C. F. Petre and F. Larachi (2004). "Hydrodynamic continuum model for two-phase flow structured-packing-containing columns." Chemical Engineering Science **59**(4): 879-888.

Ismail, I., J. Gamio, S. A. Bukhari and W. Yang (2005). "Tomography for multi-phase flow measurement in the oil industry." Flow Measurement and Instrumentation **16**(2): 145-155.

Jafari, A., P. Zamankhan, S. Mousavi and K. Pietarinen (2008). "Modeling and CFD simulation of flow behavior and dispersivity through randomly packed bed reactors." Chemical Engineering Journal **144**(3): 476-482.

Jiang, Y., M. Khadilkar, M. Al‐Dahhan and M. Dudukovic (2002). "CFD of multiphase flow in packed‐bed reactors: I. k‐Fluid modeling issues." AIChE Journal **48**(4): 701-715.

Johnston, P. M., J.-X. Zhu, H. I. de Lasa and H. Zhang (1999). "Effect of distributor designs on the flow development in downer reactor." AIChE Journal **45**(7): 1587-1592.

Jones, D., D. Bhattacharyya, R. Turton and S. E. Zitney (2011). "Optimal design and integration of an air separation unit (ASU) for an integrated gasification combined cycle (IGCC) power plant with CO2 capture." Fuel Processing Technology **92**(9): 1685-1695.

Kapteijn, F., J. J. Heiszwolf, T. v. Nijhuis and J. A. Moulijn (1999). "Monoliths in multiphase catalytic processes: aspects and prospects." Cattech **3**(1): 24-41.

Kaskes, B., D. Vervloet, F. Kapteijn and J. R. van Ommen (2014). "Numerical validation of a simplified engineering approach for heat transfer in a closed-cross-flow structured tubular reactor." Industrial & Engineering Chemistry Research **53**(42): 16579-16585.

Krieg, D., J. Helwick, P. Dillon and M. McCready (1995). "Origin of disturbances in cocurrent gas‐liquid packed bed flows." AIChE Journal **41**(7): 1653-1666.

Kuzeljevic, Z. (2010). "Hydrodynamics of trickle bed reactors: Measurements and modeling."

Labourasse, E., D. Lacanette, A. Toutant, P. Lubin, S. Vincent, O. Lebaigue, J.-P. Caltagirone and P. Sagaut (2007). "Towards Large Eddy Simulation of isothermal two-phase flows: governing equations and a priori tests." International journal of multiphase flow **33**(1): 1-39.

Latifi, M., S. Rode, N. Midoux and A. Storck (1992). "The use of microelectrodes for the determination of flow regimes in a trickle-bed reactor." Chemical engineering science **47**(8): 1955-1961.

Letzel, H., J. Schouten, R. Krishna and C. Van den Bleek (1997). "Characterization of regimes and regime transitions in bubble columns by chaos analysis of pressure signals." Chemical engineering science **52**(24): 4447-4459.

Levec, J., K. Grosser and R. Carbonell (1988). "The hysteretic behavior of pressure drop and liquid holdup in trickle beds." AIChE journal **34**(6): 1027-1030.

Levec, J., A. Saez and R. Carbonell (1986). "The hydrodynamics of trickling flow in packed beds. Part II: Experimental observations." AIChE journal **32**(3): 369-380.

Li, X., H. Zhang, X. Gao, R. Zhang and H. Li (2012). "Hydrodynamic Simulations of Seepage Catalytic Packing Internal for Catalytic Distillation Column." Industrial & Engineering Chemistry Research **51**(43): 14236-14246.

Lin, T.-J., R.-C. Juang, Y.-C. Chen and C.-C. Chen (2001). "Predictions of flow transitions in a bubble column by chaotic time series analysis of pressure fluctuation signals." Chemical engineering science **56**(3): 1057-1065.

Liu, F. (2013). CERIUM OXIDE (CeO2) PROMOTED OXYGEN CARRIER DEVELOPMENT AND SCALE MODELING STUDY FOR CHEMICAL LOOPING COMBUSTION. Doctor of Philosophy (PhD), University of Kentucky.

Liu, F., L. Chen, J. K. Neathery, K. Saito and K. Liu (2014). "Cerium oxide promoted iron-based oxygen carrier for chemical looping combustion." Industrial & Engineering Chemistry Research **53**(42): 16341-16348.

Liu, F., K.Saito and K. Liu (2015). Scale-Up of Chemical Looping Combustion. Progress in Scale Modeling, Volume II. K. Saito, A. Ito, Y. Nakamura and K. Kuwana, Springer International Publishing**:** 239-248.

Liu, F., T. Li, Y. Zhang, J. K. Neathery, K. Liu and K. Saito (2012). Characterization and Kinetic Study of Ilmenite for Chemical Looping Combustion. Spring Technical Meeting of the Central States Section of the Combustion Institute. Dayton, OH.

Liu, F., Y. Zhang, L. Chen, D. Qian, J. K. Neathery, K. Saito and K. Liu (2013). "Investigation of a Canadian Ilmenite as an Oxygen Carrier for Chemical Looping Combustion." Energy & Fuels **27**(10): 5987-5995.

Llamas, J.-D., C. Pérat, F. Lesage, M. Weber, U. D'Ortona and G. Wild (2008). "Wire mesh tomography applied to trickle beds: A new way to study liquid maldistribution." Chemical Engineering and Processing: Process Intensification **47**(9): 1765-1770.

Lopes, R. J. and R. M. Quinta-Ferreira (2007). Multiphase CFD Modeling of Trickle-Bed Reactor Hydrodynamics. Proceedings of the World Congress on Engineering and Computer Science (WCECS 2007). San Francisco, USA.

Lopes, R. J. G. and R. M. Quinta-Ferreira (2009). "CFD modelling of multiphase flow distribution in trickle beds." Chemical Engineering Journal **147**(2–3): 342-355.

Lopes, R. J. G. and R. M. Quinta-Ferreira (2009). "Turbulence modelling of multiphase flow in high-pressure trickle-bed reactors." Chemical Engineering Science **64**(8): 1806-1819.

Lu, L., J. Xu, W. Ge, Y. Yue, X. Liu and J. Li (2014). "EMMS-based discrete particle method (EMMS–DPM) for simulation of gas–solid flows." Chemical Engineering Science **120**: 67-87.

Luo, S., H. Li, W. Fei and Y.-d. Wang (2009). "Liquid Film Characteristics on Surface of Structured Packing." Chinese Journal of Chemical Engineering **17**(1): 47-52.

Maćkowiak, J. (1991). "Pressure drop in irrigated packed columns." Chemical Engineering and Processing: Process Intensification **29**(2): 93-105.

Maharaj, L., J. Pocock and B. K. Loveday (2007). "The effect of distributor configuration on the hydrodynamics of the teetered bed separator." Minerals Engineering **20**(11): 1089-1098.

Mahr, B. and D. Mewes (2007). "CFD modelling and calculation of dynamic two-phase flow in columns equipped with structured packing." Chemical Engineering Research and Design **85**(8): 1112-1122.

Mathias, P. M., S. Reddy, A. Smith and K. Afshar (2013). "Thermodynamic analysis of CO 2 capture solvents." International Journal of Greenhouse Gas Control **19**: 262-270.

Min, J. K. and I. S. Park (2011). "Numerical study for laminar wavy motions of liquid film flow on vertical wall." International Journal of Heat and Mass Transfer **54**(15–16): 3256-3266.

Moslemian, D., N. Devanathan and M. Dudukovic (1992). "Radioactive particle tracking technique for investigation of phase recirculation and turbulence in multiphase systems." Review of scientific instruments **63**(10): 4361-4372.

Mousazadeh, F., H. van Den Akker and R. F. Mudde (2013). "Direct numerical simulation of an exothermic gas-phase reaction in a packed bed with random particle distribution." Chemical Engineering Science **100**: 259-265.

Niegodajew, P., D. Asendrych, S. Drobniak and W. Elsner (2013). "Numerical modelling of CO2 desorption process coupled with phase transformation and heat transfer in CCS installation." Journal of Power Technologies **93**(5): 354-361.

Niegodajew, P., D. Asendrych, M. Marek and S. Drobniak (2014). Modelling liquid redistribution in a packed bed. Journal of Physics: Conference Series, IOP Publishing.

Olsson, E. and G. Kreiss (2005). "A conservative level set method for two phase flow." Journal of computational physics **210**(1): 225-246.

Olujić, Ž. (1999). "Effect of column diameter on pressure drop of a corrugated sheet structured packing." Chemical Engineering Research and Design **77**(6): 505-510.

Owens, S. A., M. R. Perkins, R. B. Eldridge, K. W. Schulz and R. A. Ketcham (2013). "Computational Fluid Dynamics Simulation of Structured Packing." Industrial & Engineering Chemistry Research **52**(5): 2032-2045.

Padurean, A., C.-C. Cormos and P.-S. Agachi (2012). "Pre-combustion carbon dioxide capture by gas–liquid absorption for Integrated Gasification Combined Cycle power plants." International Journal of Greenhouse Gas Control **7**: 1-11.

Panday, P. K. (2003). "Two-dimensional turbulent film condensation of vapours flowing inside a vertical tube and between parallel plates: a numerical approach." International Journal of Refrigeration **26**(4): 492-503.

Pangarkar, K., T. J. Schildhauer, J. R. van Ommen, J. Nijenhuis, F. Kapteijn and J. A. Moulijn (2008). "Structured Packings for Multiphase Catalytic Reactors." Industrial & Engineering Chemistry Research **47**(10): 3720-3751.

Petre, C. F., F. Larachi, I. Iliuta and B. Grandjean (2003). "Pressure drop through structured packings: Breakdown into the contributing mechanisms by CFD modeling." Chemical Engineering Science **58**(1): 163-177.

Propp, R. M., P. Colella, W. Y. Crutchfield and M. S. Day (2000). "A numerical model for trickle bed reactors." Journal of Computational Physics **165**(2): 311-333.

Ranade, V. V., R. V. Chaudhari and P. R. Gunjal Trickle Bed Reactors - Reactor Engineering and Applications, Elsevier.

Ranade, V. V., R. V. Chaudhari and P. R. Gunjal (2011). Chapter 2 - Hydrodynamics and Flow Regimes. Trickle Bed Reactors. V. V. Ranade and R. V. C. R. Gunjal. Amsterdam, Elsevier**:** 25-75.

Ranade, V. V., R. V. Chaudhari and P. R. Gunjal (2011). Chapter 4 - Flow Modeling of Trickle Beds. Trickle Bed Reactors. V. V. Ranade and R. V. C. R. Gunjal. Amsterdam, Elsevier**:** 117-169.

Raynal, L., C. Boyer and J. P. Ballaguet (2004). "Liquid holdup and pressure drop determination in structured packing with CFD simulations." The Canadian Journal of Chemical Engineering **82**(5): 871-879.

Raynal, L. and A. Royon-Lebeaud (2007). "A multi-scale approach for CFD calculations of gas–liquid flow within large size column equipped with structured packing." Chemical Engineering Science **62**(24): 7196-7204.

Renardy, Y. and M. Renardy (2002). "PROST: a parabolic reconstruction of surface tension for the volume-of-fluid method." Journal of Computational Physics **183**(2): 400-421.

Rode, S., N. Midoux, M. Latifi and A. Storck (1994). "Hydrodynamics and liquid—solid mass transfer mechanisms in packed beds operating in cocurrent gas—liquid downflow: an

experimental study using electrochemical shear rate sensors." Chemical engineering science **49**(9): 1383-1401.

Sachdev, S., S. Pareek, B. Mahadevan and A. Deshpande (2012). Modeling and Simulation of Single Phase Fluid Flow and Heat Transfer in Packed Beds. COMSOL Conference, Bangalore.

Saez, A. and R. Carbonell (1985). "hydrodynamic parameters for gas‐liquid cocurrent flow in packed beds." AIChE Journal **31**(1): 52-62.

Said, W., M. Nemer and D. Clodic (2011). "Modeling of dry pressure drop for fully developed gas flow in structured packing using CFD simulations." Chemical Engineering Science **66**(10): 2107-2117.

Saito, K. and M. A. Finney (2014). "Scale Modeling in Combustion and Fire Research (特集 燃焼現象のスケール効果と模型実験)." 日本燃焼学会誌 = Journal of the Combustion Society of Japan **56**(177): 194-204.

Saito, K., A. Ito, Y. Nakamura and K. Kuwana (2014). Progress in Scale Modeling, Volume II: Selections from the International Symposia on Scale Modeling, ISSM VI (2009) and ISSM VII (2013), Springer.

Saito, K. and F. Williams (2015). Scale Modeling in the Age of High-Speed Computation. Progress in Scale Modeling, Volume II, Springer International Publishing**:** 1-18.

Saroha, A. K., K. Nigam, A. K. Saxena and V. Kapoor (1998). "Liquid distribution in trickle‐bed reactors." AIChE journal **44**(9): 2044-2052.

Satterfield, C. N. (1975). "Trickle‐bed reactors." AIChE Journal **21**(2): 209-228.

Schwidder, S. and K. Schnitzlein (2012). "A new model for the design and analysis of trickle bed reactors." Chemical Engineering Journal **207–208**(0): 758-765.

Sebastia-Saez, D., S. Gu, P. Ranganathan and K. Papadikis (2013). "3D modeling of hydrodynamics and physical mass transfer characteristics of liquid film flows in structured packing elements." International Journal of Greenhouse Gas Control **19**(0): 492-502.

Shetty, S. A. and R. L. Cerro (1995). "Spreading of Liquid Point Sources over Inclined Solid Surfaces." Industrial & Engineering Chemistry Research **34**(11): 4078-4086.

Shi, M. G. and A. Mersmann (1985). "Effective interfacial area in packed columns." German chemical engineering **8**(2): 87-96.

Sidi-Boumedine, R. and L. Raynal (2005). "Influence of the viscosity on the liquid hold-up in trickle-bed reactors with structured packings." Catalysis Today **105**(3): 673-679.

Souadnia, A. and M. Latifi (2001). "Analysis of two-phase flow distribution in trickle-bed reactors." Chemical Engineering Science **56**(21): 5977-5985.

Specchia, V. and G. Baldi (1977). "Pressure drop and liquid holdup for two phase concurrent flow in packed beds." Chemical Engineering Science **32**(5): 515-523.

Spliethoff, H. (2010). Power Generation from Solid Fuels, Springer-Verlag Berlin Heidelberg.

Srinivasan, V. (2006). "A numerical study of a new spray applicator."

Srinivasan, V., A. J. Salazar and K. Saito (2011). "Modeling the disintegration of modulated liquid jets using volume-of-fluid (VOF) methodology." Applied Mathematical Modelling **35**(8): 3710-3730.

Stapf, S. and S.-I. Han (2006). NMR imaging in chemical engineering, John Wiley & Sons.

Stikkelman, R. M., J. de Graauw, Z. Olujic, H. Teeuw and J. A. Wesselingh (1989). Chem. Eng. Technol. **12**: 445.

Stikkelman, R. M. and J. A. Wesselingh (1987). Inst. Chem. Eng. Symp. Ser. **104**: B155.

Sundaresan, S. (1994). "Liquid distribution in trickle bed reactors." Energy & fuels **8**(3): 531-535.

Szady, M. J. and S. Sundaresan (1991). "Effect of boundaries on trickle‐bed hydrodynamics." AIChE journal **37**(8): 1237-1241.

Tkaczyk, P. and H. Morvan (2011). "Film Thickness Prediction in an Annular Two-Phase Flow Around C-shaped Bend." The Journal of Computational Multiphase Flows **3**(1): 27-40.

Tong, Z., A. Marek, W. Hong and J.-U. Repke (2013). "Experimental and numerical investigation on gravity-driven film flow over triangular corrugations." Industrial & Engineering Chemistry Research **52**(45): 15946-15958.

Toye, D., M. Crine and P. Marchot (2005). "Imaging of liquid distribution in reactive distillation packings with a new high-energy X-ray tomograph." Measurement Science and Technology **16**(11): 2213.

Tsai, R. E., A. F. Seibert, R. B. Eldridge and G. T. Rochelle (2011). "A dimensionless model for predicting the mass-transfer area of structured packing." AIChE Journal **57**(5): 1173-1184.

Urseanu, M., J. Boelhouwer, H. Bosman and J. Schroijen (2004). "Induced pulse operation of high-pressure trickle bed reactors with organic liquids: hydrodynamics and reaction study." Chemical Engineering and Processing: Process Intensification **43**(11): 1411-1416.

Van Baten, J., J. Ellenberger and R. Krishna (2001). "Radial and axial dispersion of the liquid phase within a KATAPAK-S® structure: experiments vs. CFD simulations." Chemical Engineering Science **56**(3): 813-821.

van Baten, J. M. and R. Krishna (2001). "Liquid-phase mass transfer within KATAPAK-S® structures studied using computational fluid dynamics simulations." Catalysis Today **69**(1–4): 371-377.

Vincent, S., J. Larocque, D. Lacanette, A. Toutant, P. Lubin and P. Sagaut (2008). "Numerical simulation of phase separation and a priori two-phase LES filtering." Computers & Fluids **37**(7): 898-906.

Watson, R., H. Rodhe, H. Oeschger and U. Siegenthaler (1990). "Greenhouse gases and aerosols." Climate change: the IPCC scientific assessment **1**: 17.

Welch, S. W. and J. Wilson (2000). "A volume of fluid based method for fluid flows with phase change." Journal of computational physics **160**(2): 662-682.

Wen, X., Y. Shu, K. Nandakumar and K. Chuang (2001). "Predicting liquid flow profile in randomly packed beds from computer simulation." AIChE journal **47**(8): 1770-1779.

Wilson, I. D. (2004). Gas-liquid contact area of random and structured packing, The University of Texas at Austin.

Wu, Y., M. R. Khadilkar, M. H. Al-Dahhan and M. P. Duduković (1996). "Comparison of Upflow and Downflow Two-Phase Flow Packed-Bed Reactors with and without Fines: Experimental Observations." Industrial & Engineering Chemistry Research **35**(2): 397-405.

Xu, Y. Y., S. Paschke, J. U. Repke, J. Q. Yuan and G. Wozny (2009). "Computational Approach to Characterize the Mass Transfer between the Counter‐Current Gas‐Liquid Flow." Chemical engineering & technology **32**(8): 1227-1235.

Yang, L., N. K. Akafuah, T. Li, B. Nienberg, G. Iler and K. Saito (2015). "Performance Evaluation of an Internal Heat Exchanger Used in the Automobile Air Conditioning Systems." Research Journal of Modeling and Simulation **25**: 33.

Yu, H. (2013). "Carbon Capture and Storage: A Challenging Approach for Mitigation of Global Warming." Journal of Clean Coal and Energy **2**(3): 23-24.

Zhang, C., W. Zhang, N. Lin, Y. Tang, C. Zhao, J. Gu, W. Lin, X. Chen and A. Qiu (2013). "A two-phase flow model coupling with volume of fluid and immersed boundary methods for free surface and moving structure problems." Ocean Engineering **74**(0): 107-124.

Zhang, H., H. Weng and A. Martin (2014). "Simulation of Flow-tube Oxidation on the Carbon Preform of PICA." AIAA Paper **1209**: 2014.

Zhang, Y., F. Liu, L. Chen, C. Han, L. R. Richburg, J. K. Neathery and K. Liu (2013). "Investigation of the Water Vapor Influence on the Performance of Iron-, Copper-, and Nickel-Based Oxygen Carriers for Chemical Looping Combustion." Energy & Fuels **27**(9): 5341-5351.

Zhao, L. and R. Cerro (1992). "Experimental characterization of viscous film flows over complex surfaces." International journal of multiphase flow **18**(4): 495-516.

H. Zhang. High Temperature Flow Solver for Aerothermodynamics Problems. PhD thesis, The University of Kentukcy, Lexington, KY, 2015.

Vita

Li Yang

Born in Shaan Xi Province, China

Education:

September 2003-July 2007 B.S. Thermal Engineering and Power Generation

September 2007-July 2010 M.S. Fluid Machinery and Engineering

Certificate:

Lean Systems Student Certificate

Graduate Certificate: Computational Fluid Dynamics (CFD)

Publications

Journals:

Yang Li, Nelson K. A. Tianxiang L., Brent N., Gary Il.and Kozo Saito; "Performance Evaluation of an Internal Heat Exchanger Used in the Automobile Air Conditioning Systems" Research Journal of Modeling and Simulation. DOI:10.12966/rjms.02.03.2015

Z. Song, J. Chen, **Li Yang**; "Heat Transfer Enhancement in Tubular Heater of Stirling Engine for Waste Heat Recovery from Flue Gas Using Steel Wool" Applied Thermal Engineering. DOI:10.1016/j.applthermaleng.2015.05.028

Yang Li, Chen Ning, Liu Fang, Xu Haichao;"New Method of Temperature Decrement in Coal Mines" Journal of Coal Mine Machinery. 1003-0794(2008)06-0140-04.

Liu, F.; Song Z.C.; **Yang Li**; Li J.; "Study of Temperature Distribution in Cement Rotary Kilns" Energy for Metallurgical Industry, 2009, 28(5), pp.21-25.

Liu, F.; **Yang Li**; Song Z.C.; Li J.; "Influence of Excess-air Coefficient and Coal Feeding on the Temperature Distribution in Cement Rotary Kilns," Light Metal, 2010(1):20-24,27.

Liu, F.; Song Z.C.; **Yang Li**; Li J.; "Influence of Speed and Piston Stroke on Performance of Air-power Engine" Industry and Mine Automation, 2009, 35(9), pp.38-40.

Yang Li, Fang Liu, Tianxiang Li, Kunlei Liu, Kozo Saito*; "CFD Simulations on hydraulic characteristics of liquid film in A Counter-Current Multiphase Flow System" to be submitted.

Yang Li, Fang Liu, Zhengchang song, Kunlei Liu, Kozo Saito*; "CFD Simulations on hydraulic characteristics of liquid film in A Structured packing bed" to be submitted.

Presentations/Proceedings:

Yang Li, Fang Liu, Tianxiang Li, Kunlei Liu, Kozo Saito*; "CFD Simulations of Capturing CO2 in A Counter-Current Multiphase Flow System". The 9th U. S. National Combustion institute Meeting. Cincinnati, OH. May 2015.